

# 國立交通大學

電子工程學系 電子研究所碩士班

## 碩士論文

利用 Si/SiGe 堆疊式結構提升非均質矽鍺奈米線  
靈敏度之特性研究

The enhancement of the sensitivity for  
non-homogeneous SiGe nanowire by Si/SiGe stack  
structure

研究生：劉重顯

指導教授：張國明 教授

中華民國九十九年八月

利用 Si/SiGe 堆疊式結構提升非均質矽鍺奈米線靈敏度之  
特性研究

The enhancement of the sensitivity for non-homogeneous  
SiGe nanowire by Si/SiGe stack structure

研 究 生：劉重顯

Student : Chung-Hsien Liu

指導教授：張國明博士

Advisor : Dr. Kow-Ming Chang

國立交通大學

電子工程學系 電子研究所碩士班

碩 士 論 文

A Thesis

Submitted to Department of Electronics Engineering & Institute of Electronics College of  
Electrical and Computer Engineering  
National Chiao Tung University  
in partial Fulfillment of the Requirements  
for the Degree of  
Master

in

Industrial Technology R & D Master Program on  
Microelectronics and Nano Sciences

August 2010

Hsinchu, Taiwan, Republic of China

中華民國九十九年八月

# 利用 Si/SiGe 堆疊式結構提升非均質矽鍺奈米線靈敏度 之特性研究

學生：劉重顯

指導教授：張國明 教授

國立交通大學

電子工程學系 電子研究所碩士班

摘要

近幾年來，矽奈米線在生物感測上的應用都被廣泛的研究和探討，也被視為最具潛力的元件之一。本實驗室團隊也成功的製作出矽鍺奈米線，並證實矽鍺奈米線具有生物的感測特性。在本論文中，主要是在於 P 型矽鍺奈米線的探討以及堆疊式結構上的研究，藉由半導體製程的技術，將矽鍺奈米線製作於 spacer 的位置，接著藉由結構上的改變和矽鍺比例上的不同，製作出具有不同寬度和不同濃度的矽鍺奈米線，最後再藉由氧化上的處理，讓矽鍺奈米線中的鍺析出，使原本均質的矽鍺奈米線變成非均質的矽鍺奈米線，並證明寬度較小且濃度較高的非均質的矽鍺奈米線有較好的靈敏度。因此本論文所研究出的矽鍺奈米線，能在生物感測元件上的應用有更好的提升。

# The enhancement of the sensitivity for non-homogeneous SiGe nanowire by Si/SiGe stack structure

Student : Chung-Hsien Liu

Advisor : Dr. Kow-Ming Chang

National Chiao Tung University

Department of Electronics Engineering & Institute of Electronics

## ABSTRACT

Recently, Si nanowire is generally investigated and discussed in bio-sensor applications. It is considered as one of the promising candidate for sensing devices. In our previous research, we successfully demonstrated the SiGe nanowire and we confirmed that it presented bio-sensor characteristic. In this thesis, it focused on the investigation of P-type SiGe nanowire and Si/SiGe stack structure process. First, SiGe nanowires were fabricated by sidewall spacer formation, which was compatible to VLSI technology. Second, we changed SiGe stack structure and Si/Ge ratio to fabricate SiGe nanowires, which were different widths and concentrations. Finally, we oxidized SiGe nanowires to precipitate Ge, and then we transformed homogenous structure into non-homogeneous structure. We confirm that non-homogeneous structure presented the better sensitivity. In our results, SiGe nanowires presented the better application in bio-sensor devices.

## 誌 謝

首先要感謝 張國明教授在這兩年中的指導，讓我在學業上能有所精進，老師也常常分享自己在求學經過所遇到的問題以及生活上的經驗，所以老師教導我們不僅僅是在學業上，甚至在做人的道理我們也都學到很多，所以很感謝老師用心的教導。

其次我要感謝實驗室的學長、同學、學弟們與指導或協助我完成論文及實驗的陳巨峰學長、王育彬學長、鄭文魁學長、謝政廷學弟以及吳金濤學弟，很感謝你們在實驗上的指導，讓我在研究論文時可以學到很多的專業知識，且在研究上能有一個很好的方向。另外要特別感謝同屆的同學們，因為有大家的互相鼓勵以及幫忙，讓我在做實驗的時候能解決很多問題，最後能順利完成論文。

此外要感謝國家奈米元件實驗室(NDL)與交通大學奈米中心(NCTU - NFC)提供良好的實驗環境使我順利完成研究，並感謝所有的工程師、技術員以及客服人員們，因為有你們的幫忙，才能使我的研究順利。

最後要感謝的是我的家人們以及女朋友，因為有你們的支持以及體諒，我才能全心全力的放在學業上，並能順利的完成學業，謝謝你們。

# Contents

Abstract(Chinese).....	I
Abstract(English).....	II
Acknowledgement.....	III
Contents.....	IV
Figure Captions.....	VII
<b>Chapter 1</b> -----	<b>1</b>
<b>Introduction</b> -----	<b>1</b>
1.1 Overview of nanowire sensors-----	1
1.2 Silicon nanowire fabrication -----	2
1.2.1 Bottom-up approaches of SiNW fabrication -----	2
1.2.2 Top-down approaches of SiNW fabrication-----	4
1.3 Applications of SiNW sensors-----	5
1.3.1 pH sensor -----	5
1.3.2 DNA sensor-----	6
1.3.3 Gas detection -----	6
1.3.4 Virus detection -----	7
1.4 Other materials of nanowire sensors-----	8
1.4.1 Metal oxide nanowire sensor-----	8
1.4.2 Conducting polymer nanowire sensor-----	9
1.4.3 Metal nanowire sensor -----	10

1.5	Sensitivity -----	11
1.6	Ge condensation technology -----	12
1.7	The oxidation mechanism of SiGe -----	13
<b>Chapter 2</b>	<b>-----</b>	<b>15</b>
<b>Experiment</b>	<b>-----</b>	<b>15</b>
2.1	Process flow -----	15
2.2	Functionalization-----	17
2.3	Measurement of electric characteristics-----	17
2.4	Define the sensitivity S -----	18
<b>Chapter 3</b>	<b>-----</b>	<b>19</b>
<b>The Characteristics of SiGe/Si Stacked Structures</b>	<b>-----</b>	<b>19</b>
3.1	Motive of the experiment -----	19
3.2	The different stacked structures with different Ge concentrations-	20
3.2.1	Comparing with different stacked structures -----	21
3.2.2	Comparing with different Ge concentrations -----	21
3.2.3	Combining different stacked structures and Ge concentrations	22
3.3	Electrical response after dripping APTMS and BS3 -----	22
3.4	The Sensitivity of SiGe nanowire with no treatment -----	22
3.4.1	The sensitivity of different Ge density with the same width --	23
3.4.2	The sensitivity of the same width with different Ge densities-	24
3.5	Summary of the characteristics of SiGe/Si stacked structure -----	25

## **Chapter 4----- 26**

### **The Treatment of Oxidation for SiGe/Si Stacked Structure**

#### **----- 26**

4.1 The Introduction of Oxidation Treatment ----- 26

4.2 The Influence of SiGe Nanowire with proportion of Nitrogen and  
Oxygen ----- 27

4.3 The Performance of Stacked Structures after Oxidation----- 27

4.4 The Sensitivity of SiGe nanowire after the treatment of Oxidation 28

4.5 The comparison between N<sub>2</sub> 100% and N<sub>2</sub> 0% ----- 30

4.6 The Raise of Sensitivity After N<sub>2</sub> 13% of Oxidation----- 31

4.7 The oxidation of stacked structure with different times ----- 32

## **Chapter 5----- 34**

## **Conclusions ----- 34**

## **Chapter 6----- 36**

## **Future Works ----- 36**

## **Reference----- 75**

# Figure Captions

## Chapter 1

- Fig.1-1 Numerical simulation result of the relationship between the response time ( $t_s$ ) and the detectable concentration ( $\rho_0$ ) of a DNA sensor[3] ----- 37
- Fig.1-2 The proposed growth model of nanowires. (A) Nucleation - 37
- Fig.1-3 (a) Silicon-rich region of the Fe-Si binary phase diagram. -- 38
- Fig.1-4 (a) Schematic illustration of vapor-liquid-solid nanowire --- 38
- Fig.1-5 Schematic view of the NW transfer steps by trilayer NIL on The imprinted *SU8/SiO<sub>2</sub>/PMMA* structure----- 39
- Fig.1-6 (a)–(d) Key fabrication flow, (f) top view of the device structure, and(e) cross-sectional view along the dashed line A to B in (f)----- 39
- Fig.1-7 (A) Schematic illustrating the conversion of a NWFET into NW nanosensors for pH sensing.(B) Real-time detection of the conductance for an APTESmodified SiNW for pHs from 2 to 9 (C)Plot of the conductance versus pH (D)The conductance of unmodified SiNW(red) versus pH. The dashed green curve is a plot of the surface charge density for silica as a function of pH ----- 40
- Fig.1-8 Modification scheme of the SiNW surface for the DNA----- 40
- Fig.1-9 Real-time detection of DNA. (a) Conductance of a p-type SiNW modified with DNA probes (CCT AAT AAC AAT)

- versus time. (b) Conductance of the same p-type SiNW shown in (a). (c) Conductance of an n-type SiNW modified with the same DNA probes as in (a) and (b) ----- 41
- Fig.1-10 (a) The setup of the gas sensing system; (b) The response of the thin-film device to NO<sub>2</sub>(red curve) and NH<sub>3</sub> (blue curve); (c) The response of 130 nm NW device to NO<sub>2</sub> and NH<sub>3</sub>; (d) The response of 75 nm NW device to NO<sub>2</sub> and NH<sub>3</sub>----- 41
- Fig.1-11 Nanowire-based detection of single viruses. (*Left*) Schematic shows two nanowire devices Specific binding of a single virus to the receptors on nanowire 2 produces a conductance change (*Right*) characteristic of the surface charge of the virus only in nanowire 2 ----- 42
- Fig.1-12 Selective detection of single viruses. (*C*) Conductance (*Upper*) and optical (*Lower*) data recorded simultaneously vs. time for a single silicon nanowire device after introduction of influenza A solution ----- 42
- Fig.1-13 (A) I-Vd curves of In<sub>2</sub>O<sub>3</sub> nanowire sensors before and after exposure to 1% NH<sub>3</sub>.(Inset) Energy band diagrams of heavily doped In<sub>2</sub>O<sub>3</sub> and NH<sub>3</sub> molecules. (B) I-Vd curves of In<sub>2</sub>O<sub>3</sub> nanowire sensors before and after exposure to 1% NH<sub>3</sub>. (Inset) Energy band diagrams of lightly doped In<sub>2</sub>O<sub>3</sub> and NH<sub>3</sub> molecules[31]----- 43
- Fig.1-14 Electrical responses of an unmodified polymer nanowire (A) to 100 nM biotin-DNA (single stranded) and avidin-embedded polypyrrole (200 nm) nanowires to 1 nM (B) and 100 nM (C)

biotin-DNA. The responses were recorded on two separate polypyrrole-avidin nanowires[37] ----- 43

Fig.1-15 (A) Schematic of CdTe-Au-CdTe nanowire field-effect transistor. (B) Schematic illustration of surface receptors modified CdTe-Au-CdTe nanowire FET for the detection of DNA[41] ----- 44

Fig.1-16 CdTe-Au-CdTe nanowire sensor detecting ssDNA-(II) at different concentrations[41] ----- 44

Fig.1-17 Simulated conductance values as a function of the surface potential for the 200-nm-wide and 50-nm-wide wires[42] -- 45

Fig.1-18 Ternary phase diagram for the Si-Ge-O system at 1000 K and 1 bar, calculated based on the thermochemical data[45]----- 45

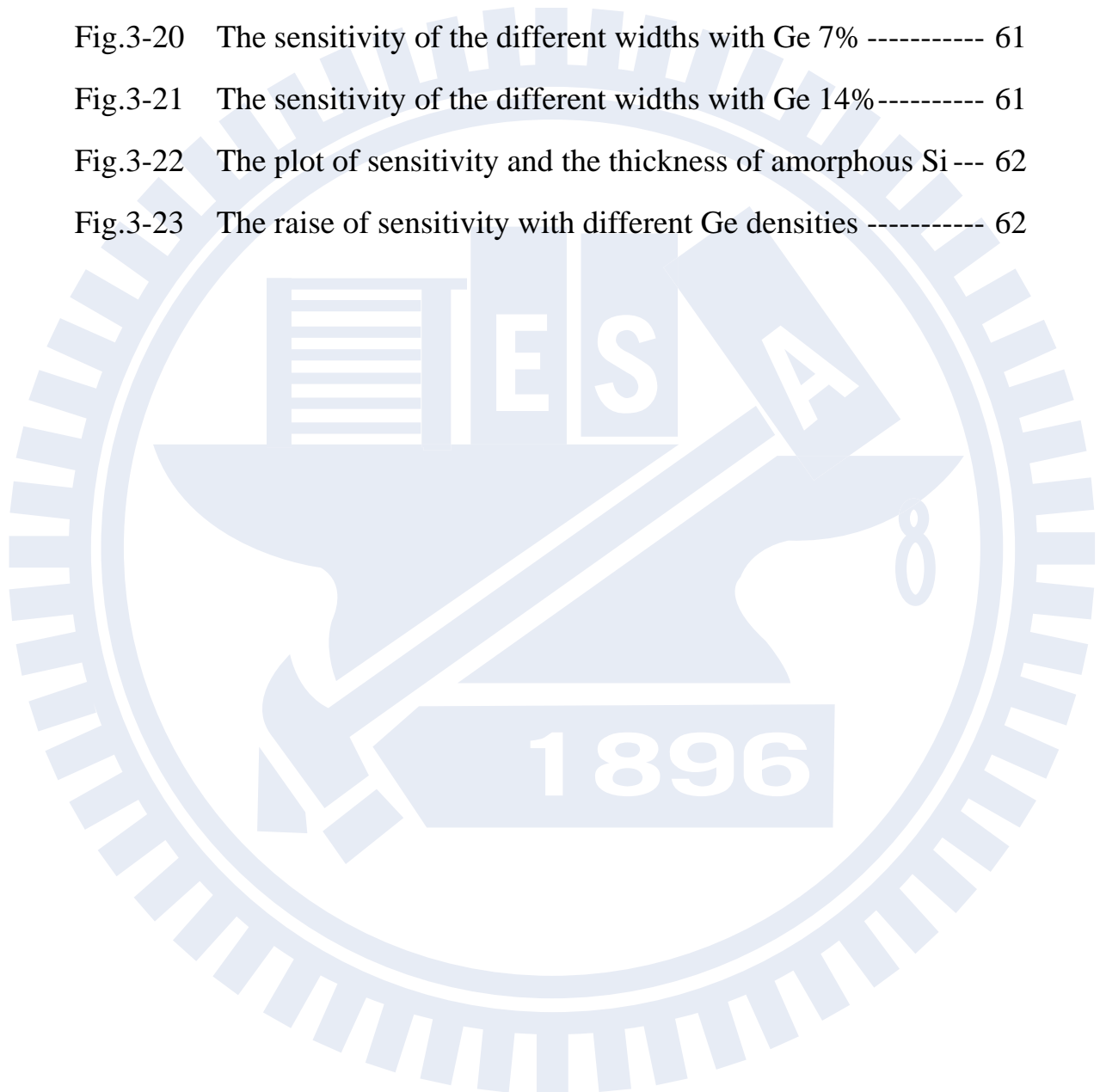
## Chapter 2

Fig.2- 1	SiO <sub>2</sub> grew 5000Å on Si substrate-----	46
Fig.2- 2	Mask#1:Etch SiO <sub>2</sub> 3000Å -----	46
Fig.2- 3	Deposit amorphous Si on SiO <sub>2</sub> -----	47
Fig.2- 4	Deposit amorphous SiGe on amorphous Si -----	47
Fig.2- 5	Mask#2:Define nanowire on the sidewall -----	48
Fig.2- 6	Mask#3:Etch unwanted sidewall nanowire -----	48
Fig.2- 7	Implant Boron-fluoride(BF <sub>2</sub> <sup>49+</sup> ) into SiGe nanowires-----	49
Fig.2- 8	Deposit Al 5000Å on the devices-----	49
Fig.2- 9	Mask#4: Define the Al contact position -----	50
Fig.2- 10	The device view from top position -----	50
Fig.2- 11	The modification of surface by APTMS and linked by BS3	51

## Chapter 3

Fig.3-1	The oxidation of stacked structures under different combination of Nitrogen and Oxygen for three minutes -----	51
Fig.3-2	SEM images of amorphous Si 200Å and 7% of Ge concentration -----	52
Fig.3-3	SEM images of amorphous Si 200Å and 14% of Ge concentration -----	52
Fig.3-4	SEM images of amorphous Si 200Å and 20% of Ge concentration -----	53
Fig.3-5	SEM images of amorphous Si 400Å and 7% of Ge concentration -----	53
Fig.3-6	SEM images of amorphous Si 400Å and 14% of Ge concentration -----	54
Fig.3-7	SEM images of amorphous Si 600Å and 7% of Ge concentration -----	54
Fig.3-8	SEM images of amorphous Si 600Å and 14% of Ge concentration -----	55
Fig.3-9	I-V curve with different stacked structures on Ge 7% -----	55
Fig.3-10	I-V curve with different Ge concentrations on $\alpha$ -Si 200Å ---	56
Fig.3-11	I-V curve with different Ge concentrations on $\alpha$ -Si 400Å ----	56
Fig.3-12	I-V curve with different Ge concentrations on $\alpha$ -Si 600Å ---	57
Fig.3-13	I-V curve with combining structures and Ge density -----	57
Fig.3-14	The conductance with combining structures and Ge density	58
Fig.3-15	The conductance with no treatment in 200Å 7% -----	58

Fig.3-16	The Sensitivity of with no treatment in 200Å 7%-----	59
Fig.3-17	The conductance with no treatment in 400Å 7%-----	59
Fig.3-18	The conductance with no treatment in 600Å 7%-----	60
Fig.3-19	The sensitivity of different Ge densities with the same width	60
Fig.3-20	The sensitivity of the different widths with Ge 7% -----	61
Fig.3-21	The sensitivity of the different widths with Ge 14%-----	61
Fig.3-22	The plot of sensitivity and the thickness of amorphous Si---	62
Fig.3-23	The raise of sensitivity with different Ge densities -----	62



## Chapter 4

Fig.4-1	I-V curve with oxidation on 200Å 14% -----	63
Fig.4-2	I-V curve with oxidation on 400Å 14% -----	63
Fig.4-3	I-V curve with oxidation on 200Å 14% -----	64
Fig.4-4	I-V curve with oxidation on 400Å 14% -----	64
Fig.4-5	The sensitivity of the treatment of oxidation on 200Å 7% ---	65
Fig.4-6	The sensitivity of the treatment of oxidation on 200Å 14% -	65
Fig.4-7	The sensitivity of the treatment of oxidation on 400Å 7% ---	66
Fig.4-8	The sensitivity of the treatment of oxidation on 400Å 14% -	66
Fig.4-9	The sensitivity of the treatment of oxidation on 600Å 7% ---	67
Fig.4-10	The sensitivity of the treatment of oxidation on 600Å 14% -	67
Fig.4-11	The EDS analysis in 600Å 14% -----	68
Fig.4-12	The comparison between N <sub>2</sub> 100%, N <sub>2</sub> 0% and N <sub>2</sub> 13% ----	68
Fig.4-13	The raise of sensitivity fixed on Si <sub>0.93</sub> Ge <sub>0.07</sub> -----	69
Fig.4-14	The percentage change of Si <sub>0.93</sub> Ge <sub>0.07</sub> after APTMS modified	69
Fig.4-15	The raise of sensitivity fixed on Si <sub>0.86</sub> Ge <sub>0.14</sub> -----	70
Fig.4-16	The percentage change of Si <sub>0.86</sub> Ge <sub>0.14</sub> after APTMS modified	70
Fig.4-17	The raise of sensitivity fixed on amorphous Si 200Å -----	71
Fig.4-18	The raise of sensitivity fixed on amorphous Si 400Å -----	71
Fig.4-19	The raise of sensitivity fixed on amorphous Si 600Å -----	72
Fig.4-20	The raise of sensitivity with all stacked structures -----	72
Fig.4-21	The percentage change of all structures after APTMS modified -----	73
Fig.4-22	The treatment of time on 400Å 7% -----	73



# Chapter 1

## Introduction

### 1.1 Overview of nanowire sensors

The application of nanowires had been the topic of significant recent research[1-2], and nanowire had attracted much interest as essential building blocks for functional electronics devices because of its potential applications in nanoelectronics[3-5] and highly sensitive biosensor[6-7]. An important feature of nanowire is the large surface-to-volume ratio, which was crucial for ultrasensitive detection of chemical or biological species. In view of this unique feature, physical properties of nanowire were greatly influenced by surface adsorption of chemical species or biomolecules, such as electrical or optical signal.

We well knew that most of researches were focus on nanowire-based sensors in field-effect-transistor(FET), in which a single nanowire or nanowire array was bridged between source and drain. The advantage of nanowire FET sensor were label-free, real-time, direct electrical readout and high device packing density, which were also the advantage in nanowire bio-sensors. We compared to planar sensors, like chemical field-effect transistor(CHEMFET) and ion-sensitive field –effect(ISFET). According to other researches, the nanowire-based sensors exhibited the

fastest response and the highest detection limit. In Fig. 1-1[8], we obviously found out that the detection limit of nanowire-based sensors was three to four orders higher than planar sensors.

There were lots of nanowire-based chemical sensors, including silicon nanowires, polymer nanowires, metal-oxide nanowire, metal nanowire and nanotube. Among these, silicon nanowire was the most promising candidates for bio-sensing applications.

Silicon nanowire (SiNW) is one of the most interesting 1-D nanostructures. In some researches, we well knew that SiNW could be easily integrated with other electronic devices and communication circuit. The silicon oxide could effectively passivate surface dangling bond, which was the silanol groups(Si-OH). The silanol chemistry provided surface functionalization, and ready to detect particular analytes.

## **1.2 Silicon nanowire fabrication**

In generally, silicon nanowire fabrications were divided into bottom-up approach and top-down approach.

### **1.2.1 Bottom-up approaches of SiNW fabrication**

The bottom-up process means that nanostructures are naturally formed on substrate under certain condition. And we know that a lot of bottom-up techniques are developed for nanowire synthesis, which can generally divide to thermal evaporation, laser ablation, and vapor-liquid-solid(VLS).

First, we discuss the method of thermal evaporation. Thermal

evaporation of a mixture of only SiO[9] or Si and SiO<sub>2</sub>[10] was presented as a way of silicon nanowire fabrication. In this paper, Silicon nanowires formed by thermal evaporation were covered by SiO<sub>2</sub> shell owing to the growth mechanism, and the diameter of crystalline or polycrystalline silicon core could be under 20nm. So Lee and co-workers successfully used a oxide-assisted growth model to illustrate the mechanism of Si nanowires. The proposed growth model of nanowires was shown in Fig. 1-2.

Second, we discuss the method of laser ablation. Hu and co-workers[11] used the Fe-Si target and the content of Fe in the target was 10%. The mechanism of the laser ablation was shown in Fig. 1-3, which was found out that Si nanowire synthesis is achieved by laser ablation of a Si<sub>0.9</sub>Fe<sub>0.1</sub> target at temperatures 1200 °C. Laser ablation of the Si<sub>1-x</sub>Fe<sub>x</sub> target produces a vapor of Si and Fe that rapidly condenses into Si-rich liquid Fe-Si nanoclusters, and when the nanoclusters become supersaturated in Si, the coexisting pure Si phase precipitates and crystallizes as nanowires. Ultimately, the growth terminates when the gas flow carries the nanowires out of the hot zone of the furnace.

Finally, we discuss the method of vapor-liquid-solid(VLS). Vapor state synthesis grown nanowires lack a diameter-control mechanism. The catalyst nanoparticle size could control the diameter of nanowires. Wu and co-workers[12] used the Au for metal catalyst. When the concentration of Ge increased in Au, the phase would change to alloy liquid. Thus, with the concentration of Ge saturated in Au, the Ge would

precipitate to form Ge nanowire. The process and phase diagram were shown in Fig. 1-4(a) and (b).

### **1.2.2 Top-down approaches of SiNW fabrication**

Top-down approaches involved lithography patterning and etching process. Most of the VLSI technology belonged to this category because parameters were much easier controlled than VLSI.

Top-down fabrication processes of the SiNWs sensor always involved the electron beam lithography (EBL) [13, 14] technology which was very expensive and time consuming. EBL enabled nano-scale patterning with critical length under 30nm, even 10 was achieved.

In the other way, nanoimprint lithography was a technology with low cost, high throughput, and high resolution. The technique involved direct contact between the template and photoresist on the material of nanowire. And then used lift-off and etching process in following process. Wan and co-workers [15] successfully used the nanoimprint technology to form the gas sensor. The wide nanowire could be changed by the RIE time. The Fig. 1-5 was the nanowire by the nanoimprint technique, and the wide naowire were 75nm and 130nm.

The sidewall spacer formation was another approach to fabricate nanowires. The anisotropic dry etching and conformal deposition on pre-patterned surfave were the significant factor to form the side spacer nanowires. The width and height of spacer nanowires were controlled by the thickness of thin film deposition and anisotropic etching process. Overall, the technique was very versatile and flexible. Lin and

co-workers[16] used the poly-Si spacer to be the channel for thin film transistor, and structure and fabrication flow were shown in Fig. 1-6. Kim and co-workers[17] demonstrated single electron transistor with poly-Si spacer. In upward studies, both of all were showed good controllability and reproducibility of spacer formation technology. In this study, we took advantage of spacer formation to fabricate SiGe nanowire.

### **1.3 Applications of SiNW sensors**

The application of Si nanowire sensors were developed widely in biological and chemistry. And in this section, We would discuss some nanowire sensors, which were placed importance on researches, such as pH sensor, DNA sensor, gas sensor, and virus detection.

#### **1.3.1 pH sensor**

Leiber's group[1] used the bottom-up approach of SiNW fabrication to process the NW nanosensor for pH detection. The device structure and the response were shown in Fig. 1-7. They investigated the response of SiNWs with and without 3-aminopropyltriethoxysilane(APTES) surface modification. We could clearly found out that the conductance of 3-minopropyltriethoxysilane modified SiNWs increase stepwise with discrete changes in pH 2 to 9 and exhibit linear pH dependence. However, unmodified SiNWs showed nonlinear response. At low pH, the  $-NH_2$  group was protonated to  $-NH_3^+$  and formed positive charge on the surface. The positive charge could deplete hole carriers in p-type nanowire and decreased the conductance. In contrast, at high pH,  $-SiOH$  was

deprotonated to  $-\text{SiO}^-$  and formed negative charge on the surface. The negative charge could accumulate hole carriers in p-type nanowire and increased the conductance.

### 1.3.2 DNA sensor

Li and co-workers[18] demonstrate the sensor detection of DNA molecules based on intrinsic charge by using silicon nanowires fabricated by top-down approach. The 3-mercaptopropyltrimethoxysilane(MPTES) by gas-phase reaction in Ar for 4 hours was utilized to modify the surface of nanowire. The CCT-AAT-AAC-AAT DNA linked on the modified surface in Fig. 1-8.

The conductance remains the same as the un-match DNA connected, which is shown in Fig. 1-9(a). However, when SiNW is p-type, the conductance increases as the GGA-TTA-TTG-TTA DNA links, which is shown in Fig. 1-9(b). On the other hand, when SiNW is n-type, the conductance decreases as the GGA-TTA-TTG-TTA DNA links, which is shown in Fig.1-9(c).

### 1.3.3 Gas detection

Wan and co-workers[15] demonstrated a novel SU8/SiO<sub>2</sub>/PMMA trilayer nanoimprint to fabricate the Silicon nanowire(SiNWs) sensor used for gas. The response of the thin-film device to NO<sub>2</sub> and NH<sub>3</sub> was in the Fig. 1-10. The resistance of the NW devices had a dramatic increase which mainly due to the carriers traps formed in RIE process. The Fig.1-10(a) was mechanism of gas sensor. The Fig. 1-10(b)(c)(d)

obviously found that when the NO<sub>2</sub> gas was flowed in, the electrical current abruptly increased due to the holes accumulation. And a opposite trend could be observed for the NH<sub>3</sub> gas detection, which was attributed to the depletion of the NW's channel. The reason[19] was shown in next introduction. When we flowed the NO<sub>2</sub>, NO<sub>2</sub> served as charge accepting molecules and withdraw electrons from the nanowire. The following reaction was happened.



So it resulted in a reduction of electrical conductance.

On the other hand, when we flowed the NH<sub>3</sub>, NH<sub>3</sub> reacted with adsorbed hydrogen ions on the surface of nanowire. The following reaction was happened.



It resulted in overall increase of the electrical conductance.

#### 1.3.4 Virus detection

Leiber and co-workers[20] presented the virus sensors by p-type SiNWs, and most important, they demonstrated the nanowires were modified with different antibody receptors, which was shown in Fig. 1-11. We could find out that modification of different nanowires within the array with receptors specific for different viruses provided a means for simultaneous detection of multiple viruses. And the Fig. 1-12 showed the conductance(upper) and optical(lower) data that was recorded simultaneously. It was parallel collection of conductance, fluorescence, and bright-field data from a single nanowire device. Each discrete

conductance changed corresponds to a single virus binding to and unbinding from nanowire. We also knew other virus researches, such as cancer[21].

## **1.4 Other materials of nanowire sensors**

With lots of researches used Si nanowire, other materials gradually respected in nanowire sensors. Nanowire sensors were fabricated by various materials, such as silicon nanowire, metal nanowire sensor, metal oxide semiconductor nanowire sensor, and polymer nanowire sensor.

### **1.4.1 Metal oxide nanowire sensor**

Metal oxide nanowires had showed great potential to be used as chemical sensors. Many groups successfully demonstrated chemical sensors based on semiconducting metal oxide 1-D nanostructures, including nanotube[22], nanorod[23], nanobelt[24], nanoribbon[25], and nanowire[26]. Various kinds of metal oxide wire-like nanostructures were reported, including ZnO, In<sub>2</sub>O<sub>3</sub>, SnO<sub>2</sub>, Co<sub>3</sub>O<sub>4</sub>, Fe<sub>2</sub>O<sub>3</sub>, TiO<sub>2</sub>, MoO<sub>3</sub>, and V<sub>2</sub>O<sub>5</sub>. Among these, most attention had been focused on ZnO, SnO<sub>2</sub>, and In<sub>2</sub>O<sub>3</sub>.

Fan and Liu[27] successfully developed a field-effect chemical sensor, which was based on ZnO nanowire. And it was applied on the sensors of NO<sub>2</sub> and NH<sub>3</sub>. They used the gate potential to affect the sensitivity, and we obviously found out that when we applied a large negative voltage could desorb gas molecules at surface. And in other

researches, ZnO nanostructures was applied in nanorod, nanotube, and nanowire. And all exhibited high surface-to-volume ratio.

Zhang and co-workers[28] fabricated and tested an  $\text{In}_2\text{O}_3$  nanowire sensor for which a detection limit of  $\sim 5$  ppb was achieved. It explained the detection of a wide range of chemicals with the metal oxide nanowire. And in the other research[29], Zhou's group also fabricated the  $\text{In}_2\text{O}_3$  nanowire. They demonstrated  $\text{NO}_2$  and  $\text{NH}_3$  sensor that was based on a single  $\text{In}_2\text{O}_3$  nanowire and operated at room temperature. The mechanism of gas sensor was introduced in section 1.4.3. The resistance of  $\text{In}_2\text{O}_3$  nanowire changed by six and five orders of magnitude as exposed to diluted  $\text{NO}_2$  and  $\text{NH}_3$ . And they discussed the result in Fig. 1-13, which showed the  $I$ - $V_D$  curves and energy band diagrams of heavily doped and lightly doped  $\text{In}_2\text{O}_3$  nanowire. The response time were 5sec for 100ppm  $\text{NO}_2$  and 10sec for 1%  $\text{NH}_3$ . Thus, they explained the sensing mechanism by experimental observation[30,31].

#### **1.4.2 Conducting polymer nanowire sensor**

The materials of polymer nanowire, such as mechanical flexibility and chemical diversity, leads to some advantages of conducting polymer nanowire(CPNW) sensors. Several methods of polymer nanowire fabrication were electrochemical dip-pen lithography[32], mechanical stretching[33], electro-spinning[34], and template-directed electrochemical synthesis[35]. In sum, CPNW was fabricated by electrochemical polymerization.

In this research[35], functionalization of CPNW could be carried out

before, during, or after polymerization. The polymerization reaction was defined in this research[36]. That is, specific receptor was linked to monomer. Moreover, physical entrapment of receptors was researched in this paper[37]. Ramanatha and co-workers[38] demonstrated that CPNW sensor could be biomolecule-functionlized and label-free DNA detection. In Fig. 1-14 showed that the electrical response of an unmodified nanowire (A) to 100nM biotin-DNA (single stranded) and avidin-embedded polypyrrole (200nm) nanowires to 1nM (B) and 100nM (C) biotin-DNA. The sensitivity  $\frac{\Delta R}{R} = 13\%$  at 1nM biotin-DNA.

We could find out that CPNW may not be biocompatible and postsynthesis assembly remained a problem, because CPNW was mechanically weak and not very reliable.

#### **1.4.3 Metal nanowire sensor**

Many groups were successfully fabricated different kind of metal nanowire with proper plating, electrodeposition parameters, and the help of template. In the research[38], Diahua and co-workers made the metal nanowire from ferromagnetic materials. When the nanowire was magnetized dipole lied along the wire's axis in the view of the inherent shape anisotropy. And the other application of magnetic alignment to segmented metal nanowire was demonstrated by Hargarter and co-workers[39].

Tao and co-workers[40] fabricated Cu nanowire arrays to detect 2,2-bipyridine, adenine, and mercaptopropioni acid(MPA). This letter described an electric-field assisted assembly technique used to position

individual nanowires suspended in a dielectric medium between two electrodes defined lithographically on a  $\text{SiO}_2$  substrate. The conclusion of this letter was that the different surface scattering behavior and adsorbates-nanowire interaction were happened by the conductance modulation.

In another research[41], Wang and co-workers fabricated the CdTe-Au-CdTe hetero junction nanowire DNA sensor and the diagram of this segmented nanowire DNA sensor, which were shown in Fig. 1-15. The sensitivity of the combining of semiconductor and metal was more sensitive to surface charges than metallic nanowire. Otherwise, the Au segment could raise the sensor performance when the single strand DNA linked. The electrical characteristics at different concentrations were shown in Fig. 1-16.

### **1.5 Sensitivity**

The sensitivity for biosensor nanowire was defined to the ratio of the conductance, which was the magnitude of change. The nanowire-based nanowire sensor had the higher sensitivity than conventional sensor. There were two advantage of the nanowire-based nanowire sensor were (1) the surface-to-volume ratio and (2) the contribution of surface from sidewall. The phenomenon[42] was proved in Fig. 1-17. It was shown that the 50-nm-wide nanowire was more sensitive to surface potential, because the surface-to-volume ratio was larger than 200-nm-wide wire.

We considered semiconductor nanowires, like Si and SiGe nanowires. According to this paper[43], we could define a simplified

expression of conductance, conductance, conductance variation, and sensitivity respectively as follow:

$$G_0 = \frac{q\mu N_D \pi d^2}{4L_{NW}}$$

$$\Delta G = \frac{\pi d \mu \sigma}{L_{NW}}$$

$$S = \frac{|\Delta G|}{G} = \frac{4\sigma}{qdN_D}$$

, where d : diameter, length of nanowire :  $L_{NW}$ , uniform doping density :  $N_D$ , and q :  $1.6 \times 10^{-19}C$ .

## 1.6 Ge condensation technology

Oxidation of SiGe was also named Ge condensation because only Si was oxidized during oxidation, and Ge was rejected from pure SiO<sub>2</sub> layer, increasing Ge concentration under oxide layer. This phenomenon is observed in 1980s[44] and received a lot of attention since then owing to the importance of SiGe and Ge for electronic and optoelectronic devices[46]. Conventionally, in order to obtain SiGe film with high Ge concentration and good quality, it was necessary to increase Ge concentration gradually during deposition, resulting in very thick SiGe film which was not practical. Several groups had demonstrated that ultrathin SiGe film with very high Ge concentration and good quality was

attainable by way of Ge condensation.

In our research, we would depend on the Ge condensation technology to implement size reduction and achieved to raise the Ge concentration at interface, which greatly enhanced sensitivity.

## 1.7 The oxidation mechanism of SiGe

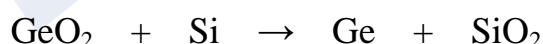
SiGe alloys were attractive materials for semiconductor device fabrication because they exhibited higher carrier mobility than Si and could be thermally oxidized at relatively low temperatures. In many researches[45,46], they were defined the oxidation mechanism of SiGe., which were well explained by the combination of oxidation kinetics and diffusion kinetics in the following expression:



With Gibbs free energy change of  $\Delta G_1 = -732 \text{ KJ/mol O}_2$ .



With Gibbs free energy change of  $\Delta G_2 = -376 \text{ KJ/mol O}_2$ . Combining these two equations, it would get new equation:



With Gibbs free energy change of  $\Delta G_3 = -356 \text{ KJ/mol O}_2$ . According upward equations, When we oxidized the SiGe, the Si and Ge would be oxidized simultaneously. And then well knew that Si was more reactive than Ge. Furthermore, we could explain from  $\Delta G_3$  that any Ge oxidized would eventually be reduced by Si, resulting in pure  $\text{SiO}_2$  and Ge pileup at interface. According to the Fig. 1-18, we obviously realized that as long as the Si existed, no  $\text{GeO}_2$  was formed under equilibrium. And the

research[47,48] was reported, in case that the oxide layer on top of SiGe layer was not very thick, the presence of Ge enhanced the oxidation rate of Si by a factor about 2~3 in wet oxidation and 1.5~2 in dry oxidation. Oxidation rate of SiGe film was correlated to Ge concentration; oxidation rate increased as Ge concentration was higher. This phenomenon was demonstrated for both single crystalline SiGe and polycrystalline SiGe in both wet ambient and dry ambient.

We provided the summary of Si and SiGe oxidation. For Si oxidation, Si interstitials injection was a factor that reduced oxidation rate. However, Si interstitials injection was greatly alleviated with the presence of Ge. In addition, the vacancy flux from oxide to SiGe bulk was reported, which mean more Si atoms diffuse to the interface through vacancy and reacted with oxygen atoms.

# Chapter 2

## Experiment

In this study, the top-down approach was used for SiGe/Si stack nanowires fabrication. We defined SiGe/Si nanowires Which were nanometer scale on the spacer, instead of commonly e-beam lithography.

### 2.1 Process flow

A p-type Si substrate (100) was used in this study. The resistivity of silicon substrate was about 1~10 $\Omega$ -cm.

1. Standard RCA clean and wet oxidation to grow 5000Å thick bottom oxide by *SVCS Furnace system*. The structure is shown in Fig. 2-1.
2. Mask#1: Define active area. *TEL CLEAN TRACK MK-8* and *Canon FPA-3000I 5+stepper lithography system* were employed to transfer pattern onto oxide layer. Then, dry etching 3000Å was carried out with *TEL5000R.I.E system* to form oxide step. It is ready for sidewall spacer formation. The structure is shown in Fig. 2-2.
3. Standard RCA clean,  $\alpha$ -Si layer was deposited on bottom oxide by *Vertical furnace system*. This  $\alpha$ -Si layer deposited 200Å、400Å and

600Å separately for the stack structure. Then,  $\alpha$ -Si served as seed layer for SiGe film deposition. The structure is shown in Fig. 2-3.

4. Standard RCA clean, and then SiGe was deposited by *ANELAVA SiGe UHV-CME*. The structure is shown in Fig. 2-4.
5. Mask#2: Define S/D region and form spacer sidewall. Dry etching was carried out with *TCP9400 SE poly etcher* to define S/D region on the active layer and the SiGe/Si nanowires were defined on the spacer. The structure is shown in Fig. 2-5.
6. Mask#3: Remove unwanted sidewall spacer. TCP 9400 SE poly etcher was employed to remove unwanted spacer, which would have resulted in short circuit between two nanowire devices if not removed. The structure is shown in Fig. 2-6.
7. Boron-fluoride( $\text{BF}_2^{49+}$ ) was implanted into SiGe nanowires by *E500HP implanter*. The implantation dose is focused on  $1 \times 10^{15}$  ions/cm<sup>2</sup> and energy was focused on 50keV. The structure is shown in Fig. 2-7.
8. Annealing in Furnace at 950°C for 30min to activate dopants.
9. 4000Å ~5000Å Aluminum deposited by *AST Peva 600I*. The structure is shown in Fig. 2-8.
10. Mask#4: Define aluminum contact pad. Al pads are formed by wet etching ( $\text{HNO}_3:\text{CH}_3\text{COOH}:\text{H}_3\text{PO}_4:\text{H}_2\text{O}=2:9:50:10$ ). The structure is shown in Fig. 2-9.
11. Aluminum sintering at 400°C in N<sub>2</sub> ambient for 30 min.
12. The device view from top position. The structure is shown in Fig. 2-10.

## 2.2 Functionalization

First, we used amino-propyl-trimethoxy-silane (APTMS) to modify the surface of SiNW. The native oxide was around SiNW, so the APTMS to SiNW oxide surface resulted in a surface terminating in both  $-NH_2$  and  $-SiOH$  groups. The modification was shown in Fig. 2-11. After APTMS modification, the surface of nanowire was terminated by amine groups. In our experiment, amine group was prone to be positive charge. It is like that SiNW had the positive gate bias, so the conductance of P-type SiNW decreased. Next, we used bis-sulfo-succinimidyl substrate (BS3) to bond on the APTMS. BS3 treatment resulted in negative charge, so the conductance of P-type nanowires increased. In this study, we focused on sensitivity ( $S$ ) and conductance with different stack structures.

## 2.3 Measurement of electric characteristics

HP4156A was used in this study to measure the electric characteristics of nanowire sensors. Drain voltage ( $V_D$ ) was from  $-10V$  to  $10V$  and step was  $100mV$ , and back gate voltage ( $V_G$ ) was  $0V$ . The electric measurement of electric characteristics was performed at every stage of surface modification, and the average conductance was then extracted from  $I_D$ - $V_D$  characteristics with  $V_D=4\sim6V$ .

## 2.4 Define the sensitivity S

First, we measured the I-V curve for no treatment devices, and then we defined the current was  $I_0$ . Second, We dripprd the APTES to the surface of SiGe nanowires , and the measured the I-V curve. Then we defined the current was I. The sensitivity was  $S = \left| \frac{I - I_0}{I_0} \right|$ . Thus, we focused on this definition to measure sensitivity.

# Chapter 3

## The Characteristics of SiGe/Si Stacked

### Structures

#### 3.1 Motive of the experiment

According to our group's previous research, we focused on Ge density、annealing temperature and oxidation time. We based on our group's previous research, and then we changed the thickness of amorphous Si, which was the purpose of increasing current. When we increased the thickness of amorphous Si, the thickness of SiGe relatively was thin. However, the amorphous Si had the higher resistance than SiGe, so the thinner SiGe had the high current.

In previous research, we focused on annealing temperature 950°C. Ge would diffuse over 1000°C and sensitivity would decrease because there was not enough energy to repair the defects at 900°C. Hence, we anneal at 950°C in order to obtain better quality and higher sensitivity. We found out the best combination in the experiment. In this section, we only discussed the characteristics of SiGe/Si stack structure with on treatment.

The procedure of experiment was showed in Fig.3-1. We let nanowires of Poly Si,  $\text{Si}_{0.93}\text{Ge}_{0.07}$ ,  $\text{Si}_{0.86}\text{Ge}_{0.14}$  and  $\text{Si}_{0.20}\text{Ge}_{0.80}$  in combination of amorphous Si 200Å, 400Å and 600Å. The treatment of oxidation was  $\text{N}_2$  0%、 $\text{N}_2$  13.3% and  $\text{N}_2$  100% at 900°C for 3min.

The SEM was showed in next introduction. The structure of 200Å 7% imaged Fig.3-2, which showed the width of nanowire was 72nm. The structure of 200Å 14% imaged Fig.3-3, which showed the width of nanowire was 77nm. The structure of 200Å 20% imaged Fig.3-4, which showed the width of nanowire was 65nm. The structure of 400Å 7% imaged Fig.3-5, which showed the width of nanowire was 67nm. The structure of 400Å 14% imaged Fig.3-6, which showed the width of nanowire was 73nm. The structure of 600Å 7% imaged Fig.3-7, which showed the width of nanowire was 70nm. The structure of 600Å 14% imaged Fig.3-8, which showed the width of nanowire was 72.5nm.

### **3.2 The different stacked structures with different Ge concentrations**

In this section, we discussed the structures in this thesis. We used the stacked structures, which was SiGe/Si. The bottom part was amorphous Si with different thicknesses and the top part was SiGe with different Ge concentrations. The following sections were discussed the stacked structures and Ge concentrations separately.

### 3.2.1 Comparing with different stacked structures

In this section, we focused on the stacked structures. The stacked structures were divided into the different depths of amorphous Si, which were 200Å 、400Å and 600Å .The purpose was the amorphous Si with high resist, so the current flowed into the path of SiGe. When the amorphous Si was thick, the current of SiGe nanowire was enhanced. The conclusion was in Fig. 3-9, which was focused on  $\text{Si}_{0.93}\text{Ge}_{0.07}$  .

### 3.2.2 Comparing with different Ge concentrations

In this section, we focused on the different Ge concentrations. The Ge concentrations were divided into 7%, 14% and 20%. We fixed the thickness of amorphous Si on 200Å , and the conclusion was in Fig. 3-10. And then the amorphous Si on 400Å and 600Å were shown in Fig. 3-11 and Fig. 3-12. In this conclusion, we found that whatever the thickness of amorphous Si, only the Ge concentration enhanced the performance of SiGe nanowire devices. If Ge concentration increased, the the performance of SiGe nanowires was increased. The Ge had high mobility, so that the high Ge concentration enhanced high current.

### 3.2.3 Combining different stacked structures and Ge concentrations

In this section, we discussed the different stacked structures with different Ge concentrations. We focused on amorphous Si 200Å 、400 Å and 600 Å with Ge 7% and 14% concentrations. The conclusion was shown in Fig. 3-13. The 600Å 14% had the higher current than others. Because the structure had high Ge concentration and SiGe on the amorphous Si 600Å was relatively thinner than other structures. We showed the conductance of all structures in Fig.3-14 and found out the structure with amorphous Si 600Å and  $\text{Si}_{0.86}\text{Ge}_{0.14}$  had the high conductance.

### 3.3 Electrical response after dripping APTMS and BS3

The APTMS and BS3's bond structures contained positive and negative electricity respectively, Therefore, the conductance would decrease after drip APTMS on p-type SiGe nanowire, but it would be increased when the bonds of BS3 occur after it dripped on APTMS.

### 3.4 The Sensitivity of SiGe nanowire with no treatment

Before the sensitivity, we discussed the conductance with the

structure of 200Å 7%, which was shown in Fig.3-15. We obviously the APTMS decreased and the BS3 increased, because they were positive charge and negative charge. According to the conclusions, we could confirm our nanowire had the characteristic of bio-sensor.

First, we dripped APTMS on SiGe nanowires , and then we found the sensitivity  $S_1 = \frac{I_1 - I_0}{I_0} \times 100$ . Second, we dripped BS 3 on the SiGe nanowire , which was dripped APTMS already, and then we found the sensitivity  $S_2 = \frac{I_2 - I_1}{I_1} \times 100$  ( $I_0$ : dripped water current,  $I_1$ :dripped APTMS current,  $I_2$ :dripped BS3 current).The conclusion was shown in Fig. 3-16. The sensitivity of dripped WATER was 0.644%. The sensitivity of dripped APTMS was -6.54%. The sensitivity of dripped BS3 was 2.49%.The conclusion was that the APTMS was positive charge, so APTMS could accumulate the surface of p-type nanowire. And the BS3 was negative charge, so BS3 could deplete the surface of p-type nanowire.

We also showed the conductance and sensitivity with different stack structures to prove our nanowire with the characteristic of bio-sensor. The 400Å 7% was shown in Fig.3-17. The 600Å 7% was shown in Fig.3-18.

### 3.4.1 The sensitivity of different Ge density with the same width

First, we defined that the sensitivity was the part of dripped APTMS. Thus the sensitivity was  $S_1 = \left| \frac{I_1 - I_0}{I_0} \right| \times 100$ . In the view of the APTMS was

the linker, the APTMS was the important part.

In this section, we had to compare Si nanowire with SiGe nanowire and knew what density of Ge was the best. In the conclusion, we were known that the nanowires with Ge ingredients had the highest sensitivity. So we confirmed that SiGe nanowire was better than the Si nanowire.

In previous research, when Ge density increased, the sensitivity decreased. It was that the higher amount of Ge would increase high vacancies of surface which would not be easy for objects under test to bond and decreased sensitivity. We confirmed the conclusion. It was shown in Fig.3-16, which was focused on amorphous Silicon 200Å. The sensitivity of poly Si was 2.873%. The sensitivity of Ge 7% was 3.019%. The sensitivity of Ge 14% was 5.4%. The sensitivity of Ge 20% was 2.2%. Thus, we focused on the density of Ge were 7% and 14% in next sections.

### **3.4.2 The sensitivity of the same width with different Ge densities**

As the result of previous discussions, we focused on the density of Ge, which were 7% and 14%. Thus in this section, we fixed the Ge density. We had to know what thickness of amorphous Si was the best stacked structure. According to previous research, we assumed that amorphous Si 600Å enhanced the high sensitivity, because the amorphous Si 600 Å held the thin SiGe layer and the high Ge density. In view of the important factors, the stacked structure which was amorphous Si 600 Å

had the high sensitivity. The conclusion which was fixed on Ge 7% was shown in Fig.3-17. The sensitivity of amorphous Si 200Å was 4.379%. The sensitivity of amorphous Si 400Å was 4.487%. The sensitivity of amorphous Si 600Å was 5.845%. And another which was fixed on Ge 14% was shown in Fig.3-18. The sensitivity of amorphous Si 200Å was 4.61%. The sensitivity of amorphous Si 400Å was 5.073%. The sensitivity of amorphous Si 600Å was 7.95%.

### **3.5 Summary of the characteristics of SiGe/Si stacked structure**

In this chapter, we only focused on the characteristics of SiGe/Si stacked structure without any treatment. However, we could clean out the following conclusions. When the thickness of SiGe was narrowed and the Ge density was 14%, the sensitivity was increased at most. In Fig.3-19, we could find that the slope of  $\text{Si}_{0.86}\text{Ge}_{0.14}$  was higher than the slope of  $\text{Si}_{0.93}\text{Ge}_{0.07}$ . It was mean that the high concentration and amorphous Si 600Å could have the high sensitivity with no treatment. And in the Fig.3-20, we would know that the raise of sensitivity between 7% of Ge density and 14% of Ge density. It was shown that the thickness of amorphous was 600Å, which raised about 29.8%, because the narrowed SiGe layer and the high Ge density were in the structure. In the next chapter, we would do some treatments of oxidation to increase sensitivity more.

# Chapter 4

## The Treatment of Oxidation for SiGe/Si Stacked Structure

### 4.1 The Introduction of Oxidation Treatment

In previous research, we produced non-homogeneous structure. With the help of oxidation, we could find the better quality of deposited SiGe layer with oxidation and then high density of Ge would be separated on surface. Besides, base on Auger analysis, we could obviously realize that Ge only remained on the surface of nanowires, and the sensitivity happened to be decreased when Ge's density increased. We assumed that the higher amount of Ge would increase high vacancies of surface which would not easy for objects under test to bond and decreased sensitivity. Above of all, we used the characteristic of SiGe oxidation, the oxidation process with nitrogen could repair the vacancies of surface and improved the quality of oxide in order to increase sensitivity.

In this section, we discussed the treatment of oxidation for SiGe/Si stacked structure. We treated  $N_2/O_2$  ratio for SiGe/Si stacked structure.

We focused on no oxidation, N<sub>2</sub> 0%, N<sub>2</sub> 13.3% and N<sub>2</sub> 100% for 3min and the oxidation temperature was 900°C. In this treatment, we would find the best one to treat different time, which was divided to 3min、5min and 7min.

#### **4.2 The Influence of SiGe Nanowire with proportion of Nitrogen and Oxygen**

To process non-homogeneous structure was the intention of this thesis. We obtained high Ge concentration during oxidation, but the quality was not good enough, because the bonding energy of surface reduced and the sensitivity fell down.

As the conclusions, we tried to add the content of nitrogen during oxidation in order to repair the defects and improve the quality of surface. In previous research, we add content of nitrogen to 13%, 40% and 66.6%, and we testified 13% of nitrogen would be best. However, in this thesis, we would focus on 13% of nitrogen. In addition, we would discuss 100% of nitrogen, which was pure nitrogen. We would compare the repair of pure nitrogen to 13% of nitrogen.

#### **4.3 The Performance of Stacked Structures after Oxidation**

Before the discussion of oxidation, we focused on N<sub>2</sub> 100%, which was that we only flowed nitrogen without oxygen at 900°C. We would compare the oxidation without oxygen to the oxidation with oxygen. Next,

the treatment of oxidation was divided into N<sub>2</sub> 0% and N<sub>2</sub> 13%, which were the ratio of nitrogen and oxygen.

First, we focused on the characteristics which were no oxidation, N<sub>2</sub> 0% and N<sub>2</sub> 100%. In this part, we discussed the performance of SiGe through repair of nitrogen. The conclusion was shown in Fig. 4-1, which was focused on 200Å 14%. And another structure's conclusion was shown in Fig. 4-2, which was 400Å 14%. In the conclusion, we obviously found out the current increased after oxidation and repair of nitrogen. And the current of N<sub>2</sub> 0% was higher than the current of N<sub>2</sub> 100%, because the effect of oxidation was weak. In this condition, it made Ge reject less, so that the current was not obvious.

Second, we would add N<sub>2</sub> 13% to measure the I-V curve. In previous research, we found out that N<sub>2</sub> 13% was the best treatment, so we added the treatment on our stacked structures. We identically exploited 200Å 7% and 400Å 7% to show the conclusion, which was shown in Fig. 4-3 and Fig. 4-4.

#### 4.4 The Sensitivity of SiGe nanowire after the treatment of Oxidation

In this section, we identically dripped APTES and calculated its sensitivity  $S_1 = \left| \frac{I_1 - I_0}{I_0} \right| \times 100$ . We compared the reactions of 200Å 7%, 200Å 14%, 400Å 7%, 400Å 14%, 600Å 7% and 600Å 14%. The conclusion was shown in Fig. 4-5, which was 200Å 7%. However, we could find out that when the width of SiGe nanowire narrowed and the

concentration of Ge went up, the sensitivity raised. And then the 13% of nitrogen increased at most. The sensitivity of 13% of nitrogen was 5.819%. The 200Å 14% was shown in Fig. 4-6, and the sensitivity of 200Å 14% was 8.94% in 13% of nitrogen. The 400Å 7% was shown in Fig. 4-7, and the sensitivity of 400Å 7% was 10.4% in 13% of nitrogen. The sensitivity of 13% of nitrogen was 5.819%. The 400Å 14% was shown in Fig. 4-8, and the sensitivity of 400Å 14% was 12.03% in 13% of nitrogen. The sensitivity of 13% of nitrogen was 5.819%. The 600Å 7% was shown in Fig. 4-9, and the sensitivity of 600Å 7% was 11.679% in 13% of nitrogen. The sensitivity of 13% of nitrogen was 5.819%. The 600Å 14% was shown in Fig. 4-10, and the sensitivity of 600Å 14% was 4.493% in 13% of nitrogen.

We could see that the 13% of nitrogen was the best. Because nitrogen could repair the defects, the concentration of Ge on the surface raised and the quality became better after the oxidation of SiGe nanowire. Further, the width of SiGe nanowire became narrow, so the raise of sensitivity was obvious excluding the structure of 600Å 14%.

We also observed that the 100% of nitrogen was less than pure oxygen. This was because when we added too much nitrogen, the effect of oxidation was weak. In this condition, it made Ge reject less, so that the raise of the sensitivity was not obvious.

In upward conclusions, we found out the sensitivity of 600Å 14% decreased and the sensitivity of 600Å 7% was raised less than the sensitivity of 400Å 14%. Because the process limited, the width of 600Å 14% and 600Å 7% were about 65nm to 70nm. It was mean that the SiGe

layer only was 5nm to 10nm. Thus, when it was through 3min oxidation, it was oxidized all very likely. The nanowire was only poly silicon, so its sensitivity was close to silicon nanowire. We could confirm the conclusion by EDS, Which was shown in Fig. 4-11. We perceived the Ge information was not many. And then, we found that when the Ge density was high, the oxidation rate would increase. It was confirmed in the paper[49], which explained the SiGe oxidation with the different Ge densities. Overall, we could explained this condition due to the process limited, the SiGe oxidation rate was faster than Si oxidation rate and the high Ge density had the fastest oxidation rate.

#### **4.5 The comparison between N<sub>2</sub> 100% and N<sub>2</sub> 0%**

In this section, we would compare 100% of nitrogen to 13% of nitrogen. In previous discussions, we knew that both of 100% of nitrogen and 13% of nitrogen could enhance the sensitivity, so we had to realize which one was the best. In the Fig. 4-12, we obviously found out that the structure of 200Å 7%, which was shown that the 100% of nitrogen increased sensitivity about 28% and the 13% of nitrogen increased sensitivity about 92%. And the structure of 200Å 14% was shown that the 100% of nitrogen increased sensitivity about 18.6% and the 13% of nitrogen increased sensitivity about 99%. This was because when we added too much nitrogen, the effect of oxidation was weak. In this condition, it made Ge reject less, so that the raise of the sensitivity was

not obvious.

#### 4.6 The Raise of Sensitivity After N<sub>2</sub> 13% of Oxidation

We already discussed the 13% of nitrogen, which was the best treatment of oxidation, so we focused this treatment to calculate the raise of sensitivity. We compared every stacked structures including poly Si nanowire.

First, we fixed on Si<sub>0.93</sub>Ge<sub>0.07</sub>. The result was in Fig. 4-13. We obviously obtained that the sensitivity of poly Si raised 62%, the sensitivity of amorphous 200Å raised 93% , the sensitivity of amorphous 400Å raised 119% and the sensitivity of amorphous 600Å only raised 93%. The raise percentage of sensitivity was defined as the next equation.

$$\text{The raise percentage of sensitivity(\%)} = \frac{S_f - S_i}{S_i} \times 100\%$$

S<sub>i</sub> was the sensitivity of SiGe before dipping chemical molecules, S<sub>f</sub> was the sensitivity of SiGe nanowire after dipping chemical molecules. The value showed the percentage change of sensitivity after the APTMS and BS3 modified. The Fig. 4-14 was the percentage change of Si<sub>0.93</sub>Ge<sub>0.07</sub> after APTMS modified.

Excluding the structure of amorphous 600Å , the high concentration of Ge and the narrow width of nanowire was raised the sensitivity at most.

Second, we fixed on Si<sub>0.86</sub>Ge<sub>0.14</sub>. The result was in Fig. 4-15. We obviously obtained that the sensitivity of poly Si raised 62%, the

sensitivity of amorphous 200Å raised 101% , the sensitivity of amorphous 400Å raised 138% and the sensitivity of amorphous 600Å was decreased 33%. The reason of decreased amorphous 600Å was explained in front section. Identically, the high concentration of Ge and the narrow width of nanowire was raised the sensitivity at most. The Fig. 4-16 was the percentage change of  $\text{Si}_{0.86}\text{Ge}_{0.14}$  after APTMS modified. Next, we fixed on amorphous Si, so the Fig. 4-17, Fig. 4-18 and Fig. 4-19 were fixed on amorphous Si 200Å , amorphous Si 400Å and the amorphous Si 600Å . Finally, we combined all the stacked structures to discuss the raise of sensitivity, and we would find the high raise one. The result was shown in Fig. 4-20.

Though upward clean out, we could clearly find that the amorphous Si 400Å tied in 14% of Ge content raised at most, because the structure of 400Å 14% avoided the limiting of amorphous Si 600Å . And the structure of 400Å 14% had the narrowed nanowire and the high concentration of Ge after oxidation with 13% of nitrogen, so the sensitivity could increase 138%. The Fig. 4-21 was the percentage change of all structures after APTMS modified.

#### **4.7 The oxidation of stacked structure with different times**

According to upward conclusions, we focused on the structures of 400Å 7% and 400Å 14% in this discussion. We already knew that the

raise of 400Å 7% with 13% of nitrogen and 3min was 99% and the raise of 400Å 14% with 13% of nitrogen and 3min was 138%. So we tried to increase times, which were 5min and 7min with the same 13% of nitrogen. In Fig. 4-22, we obvious found out that the sensitivity at 3min was the best in the structure of 400Å 7%. And the Fig. 4-23 was the same conclusion with Fig. 4-22. The Fig. 4-23 was the structure of 400Å 14%. Both of all, the oxidation time for 5min and 7min decreased to the same with poly Si nanowire. It was told that when we oxidized 5min and 7min, the nanowire only was poly Si. The SiGe was oxidized all on amorphous Si. In the summary, we clearly knew that the oxidation for 3min and with 13% of nitrogen could increase the sensitivity at most.

# Chapter 5

## Conclusions

We could summarize the following result according to the research from previous experiment:

1. APTES generated bond with BS3 and had the electrical response
2. We successfully fabricated the stacked structures, which were 200Å 7%, 200Å 14%, 200Å 20%, 400Å 7%, 400Å 14%, 600Å 7% and 600Å 14%. The several structures had the electrical response, and we found out the structure of 600Å 14% enhanced the highest sensitivity, because the thickness of SiGe was narrowed and the Ge density was 14%. The conclusion was the same with our prediction.
3. After oxidation, we successfully produced the non-homogeneous structures of SiGe nanowire, and we confirmed that its sensitivity was better than the homogeneous structure.
4. We could increase the density of Ge on the surface of nanowire with the help of oxidation, and sensitivity would increase with the density of Ge.
5. We compared the 100% of Nitrogen to 13% of Nitrogen. The 100% of nitrogen was less than pure oxygen. This was because when we added too much nitrogen, the effect of oxidation was weak. In this condition,

it made Ge reject less, so that the raise of the sensitivity was not obvious. The conclusion was 13% of Nitrogen had more sensitive than the 100% of Nitrogen.

6. We found out that when we added 13% of Nitrogen to oxidation, our stacked structure increased at most, excluding the structure of 600Å 14%. The structure of 400Å 14% could increase higher to 138%. And also found out that the structure of 600Å 14% was so narrow that it only was poly Si after oxidation, so the structure of 400Å 14% had the suitable thickness of amorphous Si and the 14% of Ge density.
7. As for time of oxidation, the 3min with 13% of Nitrogen could increase sensitivity at most.

# Chapter 6

## Future Works

In my research, we find out that the structure 400Å 14% with 13% of nitrogen and oxidation for 3min can increase sensitivity at most. In the future works, we can focus on amorphous 400Å and increase the Ge densities to 30% and 40%. It maybe increase the sensitivity better than 20% of Ge density.

The structure of 400Å 14% is the best structure with oxidation. We can focus on this structure and increase the N<sub>2</sub> ratio from 13% to 100% with 3min oxidation. We possibly find another high sensitivity in the range.

According to previous discussions, we know that the SiGe oxidation is faster than Si oxidation. We can deposit PECVD SiO<sub>2</sub> before oxidation, because the PECVD SiO<sub>2</sub> can control the rate of oxidation. Thus, we possibly let lots of Ge precipitations on the surface.

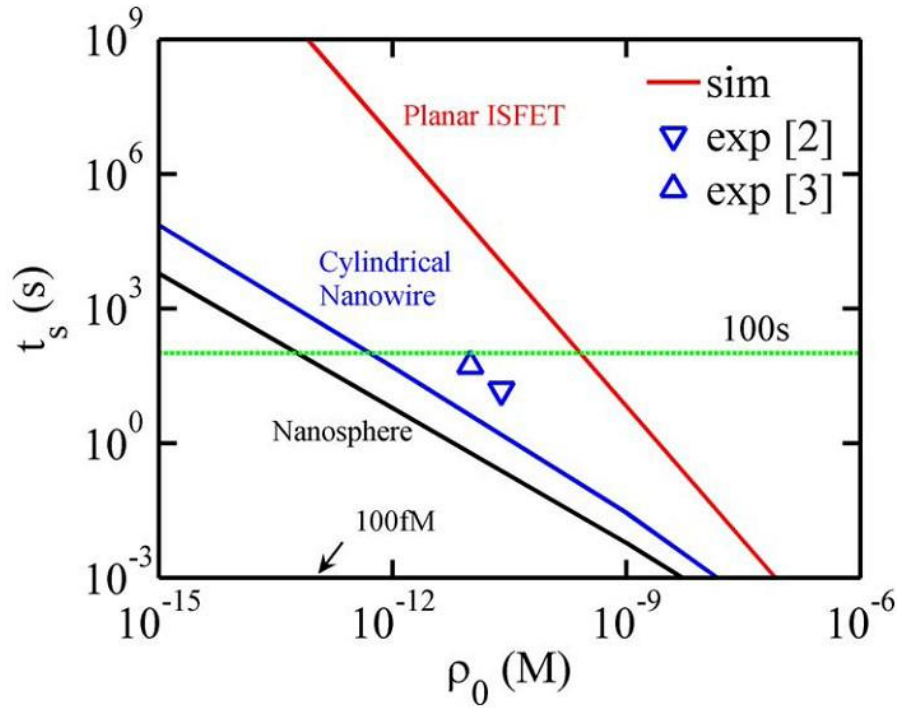


Fig.1- 1 Numerical simulation result of the relationship between the response time ( $t_s$ ) and the detectable concentration ( $\rho_0$ ) of a DNA sensor[3]

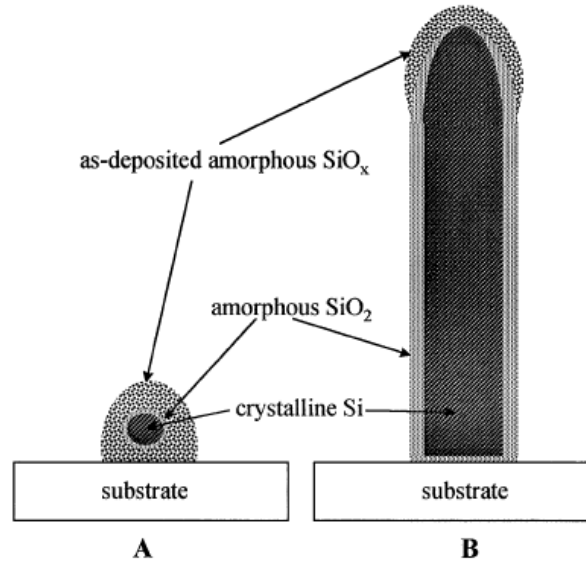


Fig.1- 2 The proposed growth model of nanowires. (A) Nucleation starts when nanoclusters are deposited as an amorphous matrix on a substrate surface. (B) An amorphous oxide sheath is formed as the expelled oxide and free oxygen reach the slower growing edge of the nucleus

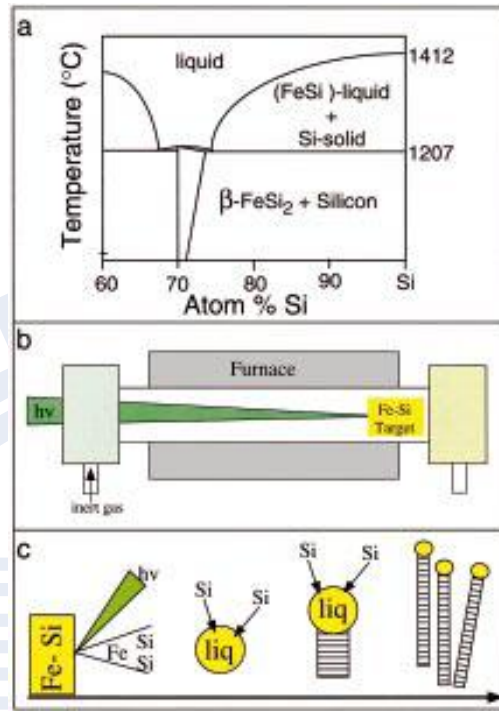


Fig.1- 3 (a) Silicon-rich region of the Fe-Si binary phase diagram. (b) Schematic diagram of the nanowire growth apparatus. (c) Nanowire growth process

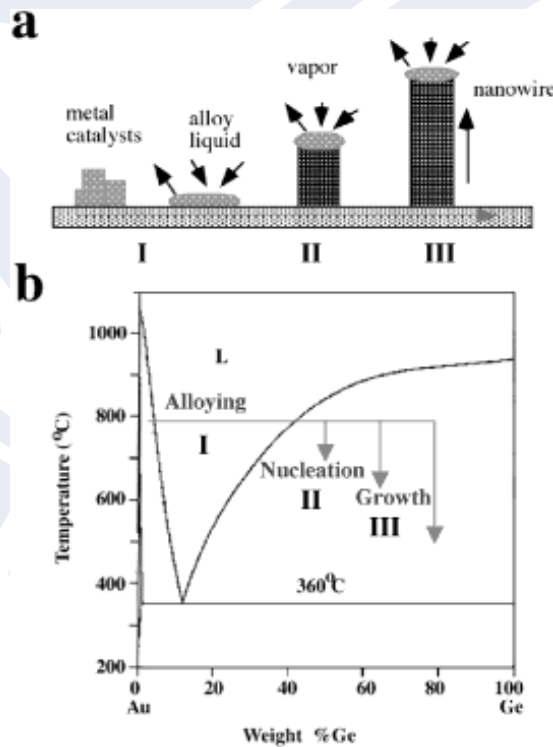


Fig.1- 4 (a) Schematic illustration of vapor-liquid-solid nanowire growth mechanism including three stages.(b) To show the compositional and phase evolution during the nanowire growth process

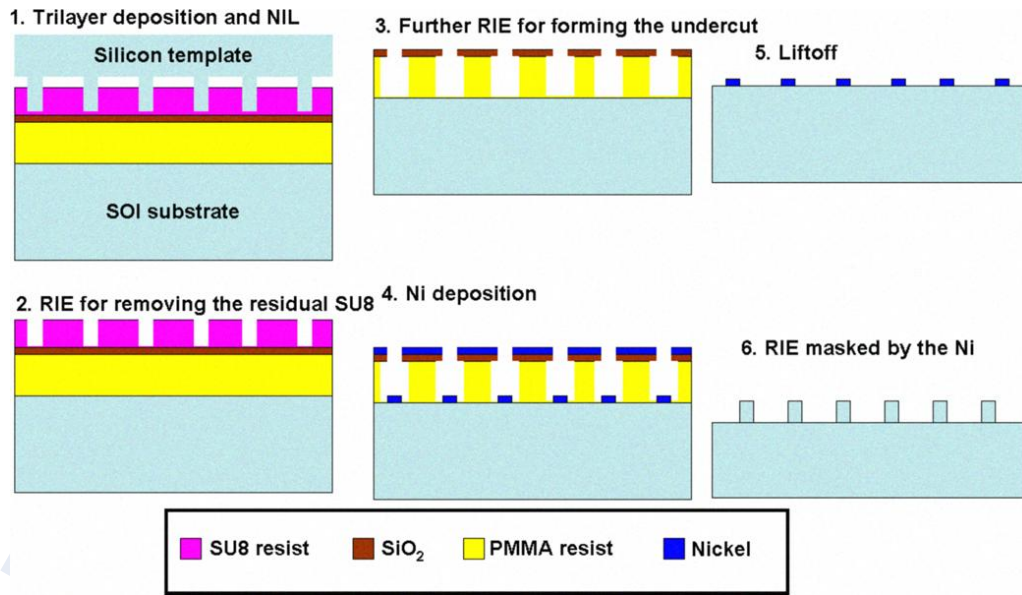


Fig.1- 5 Schematic view of the NW transfer steps by trilayer NIL on The imprinted *SU8/SiO<sub>2</sub>/IPMMA* structure

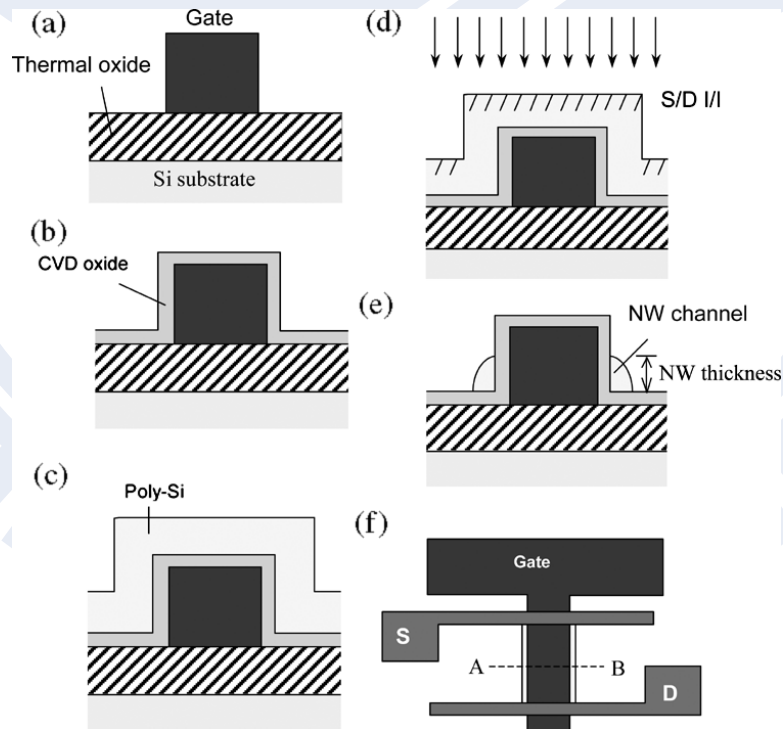


Fig.1- 6 (a)–(d) Key fabrication flow, (f) top view of the device structure, and (e) cross-sectional view along the dashed line A to B in (f)

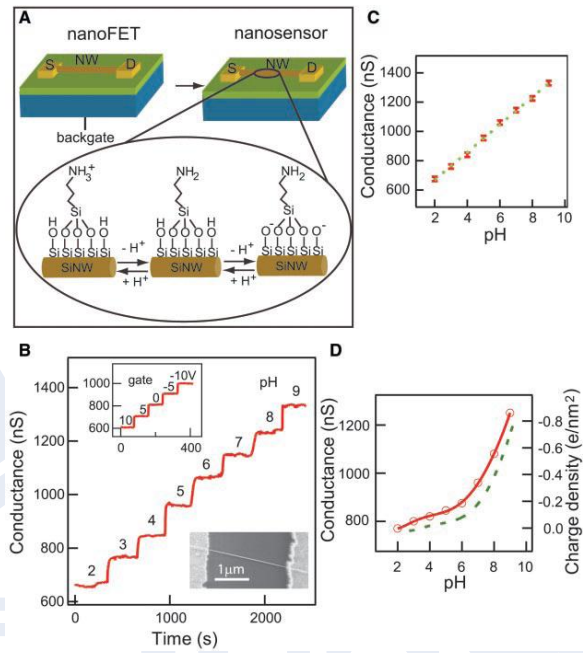


Fig.1- 7 (A) Schematic illustrating the conversion of a NWFET into NW nanosensors for pH sensing.(B) Real-time detection of the conductance for an APTESmodified SiNW for pHs from 2 to 9 (C)Plot of the conductance versus pH (D) The conductance of unmodified SiNW(red) versus pH. The dashed green curve is a plot of the surface charge density for silica as a function of pH

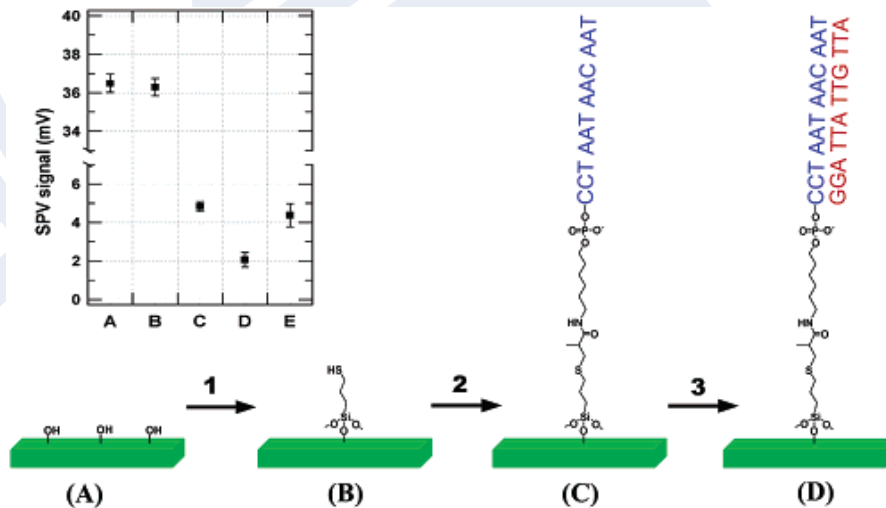


Fig.1- 8 Modification scheme of the SiNW surface for the DNA Detector

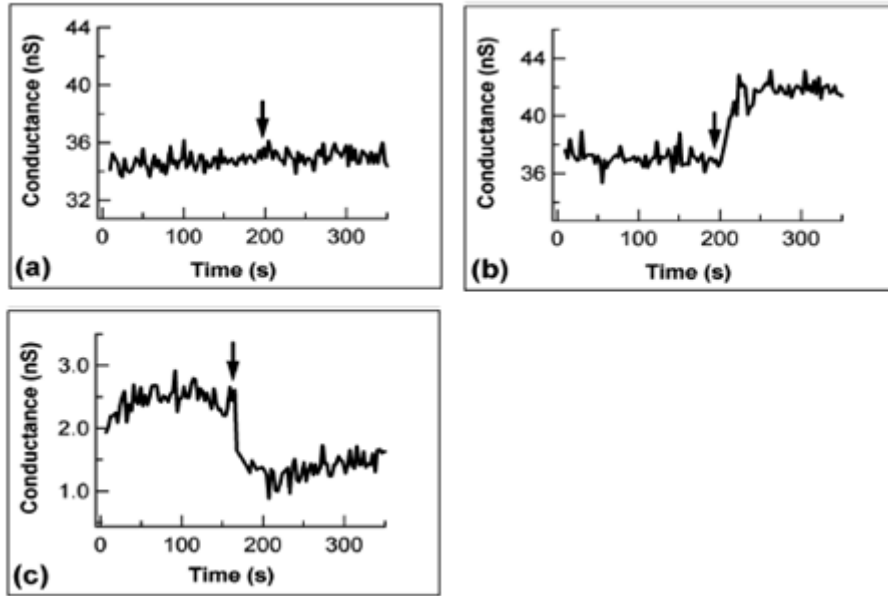


Fig.1- 9 Real-time detection of DNA. (a) Conductance of a p-type SiNW modified with DNA probes (CCT AAT AAC AAT) versus time. (b) Conductance of the same p-type SiNW shown in (a). (c) Conductance of an n-type SiNW modified with the same DNA probes as in (a) and (b)

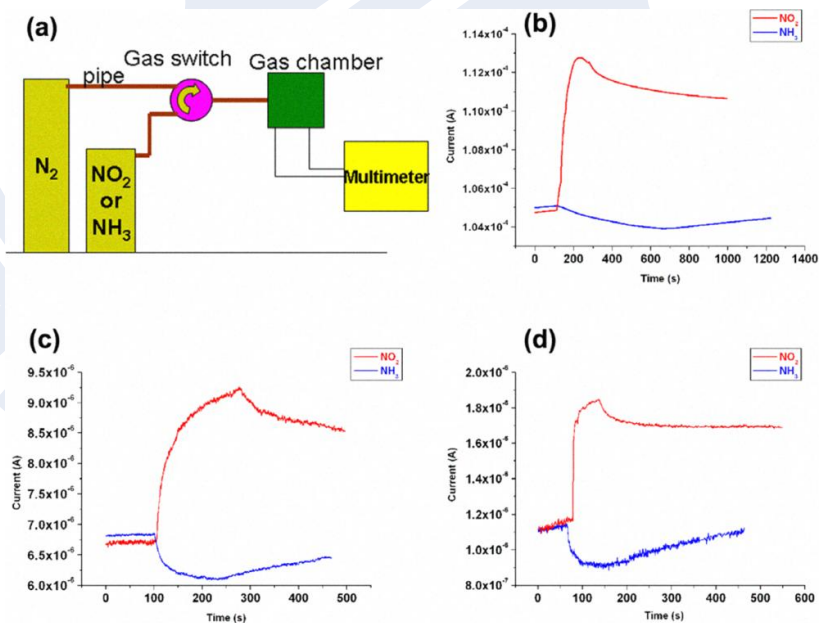


Fig.1- 10 (a) The setup of the gas sensing system; (b) The response of the thin-film device to NO<sub>2</sub>(red curve) and NH<sub>3</sub> (blue curve); (c) The response of 130 nm NW device to NO<sub>2</sub> and NH<sub>3</sub>; (d) The response of 75 nm NW device to NO<sub>2</sub> and NH<sub>3</sub>

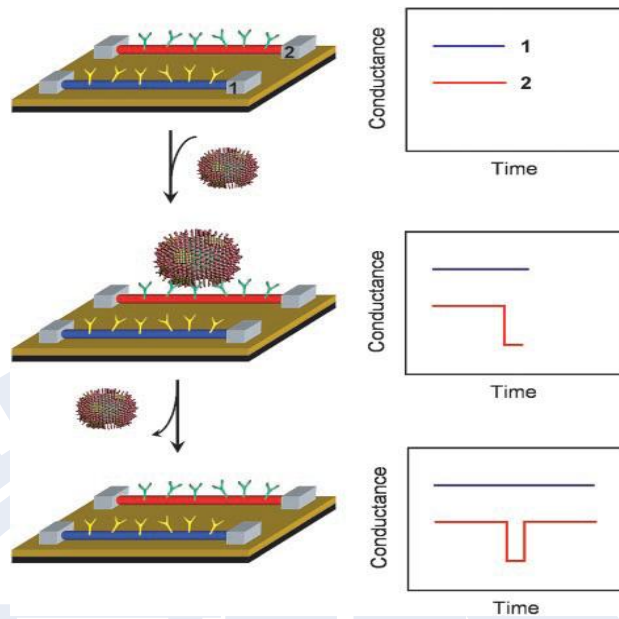


Fig.1- 11 Nanowire-based detection of single viruses. (*Left*) Schematic shows two nanowire devices Specific binding of a single virus to the receptors on nanowire 2 produces a conductance change (*Right*) characteristic of the surface charge of the virus only in nanowire 2

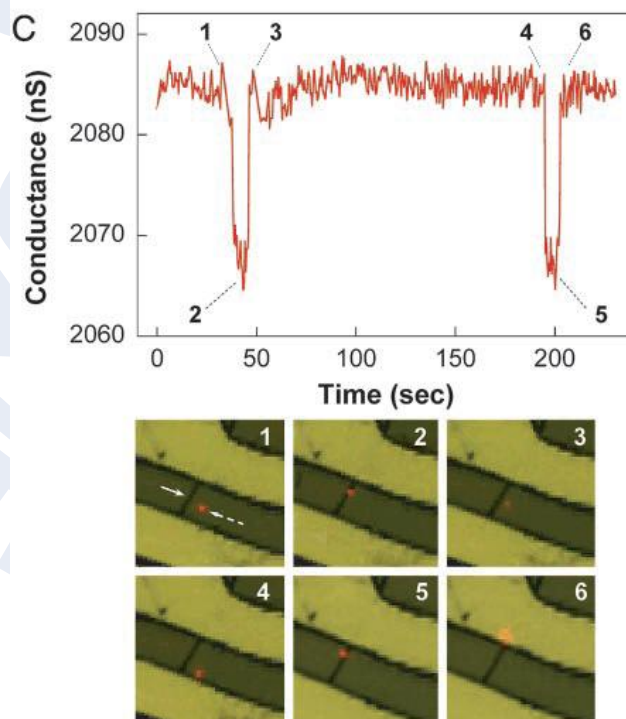


Fig.1- 12 Selective detection of single viruses. (C) Conductance (*Upper*) and optical (*Lower*) data recorded simultaneously vs. time for a single silicon nanowire device after introduction of influenza A solution

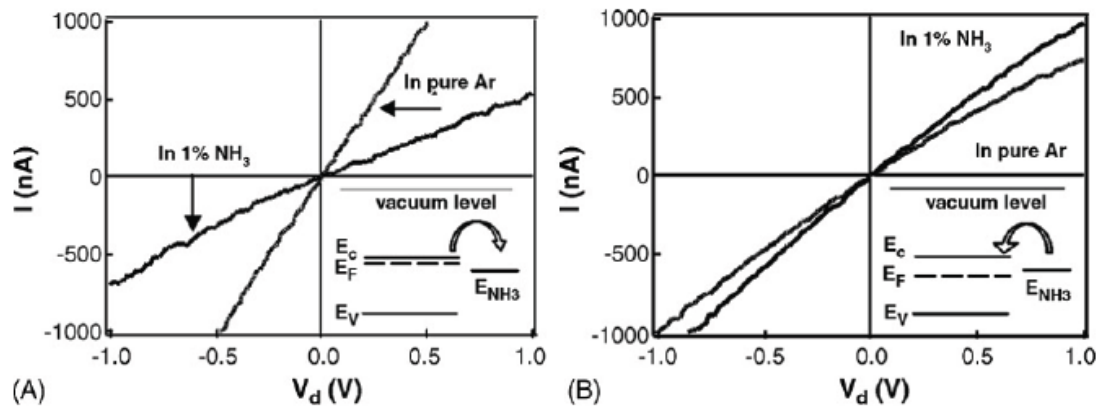


Fig.1- 13 (A) I-Vd curves of In<sub>2</sub>O<sub>3</sub> nanowire sensors before and after exposure to 1% NH<sub>3</sub>. (Inset) Energy band diagrams of heavily doped In<sub>2</sub>O<sub>3</sub> and NH<sub>3</sub> molecules. (B) I-Vd curves of In<sub>2</sub>O<sub>3</sub> nanowire sensors before and after exposure to 1% NH<sub>3</sub>. (Inset) Energy band diagrams of lightly doped In<sub>2</sub>O<sub>3</sub> and NH<sub>3</sub> molecules[31]

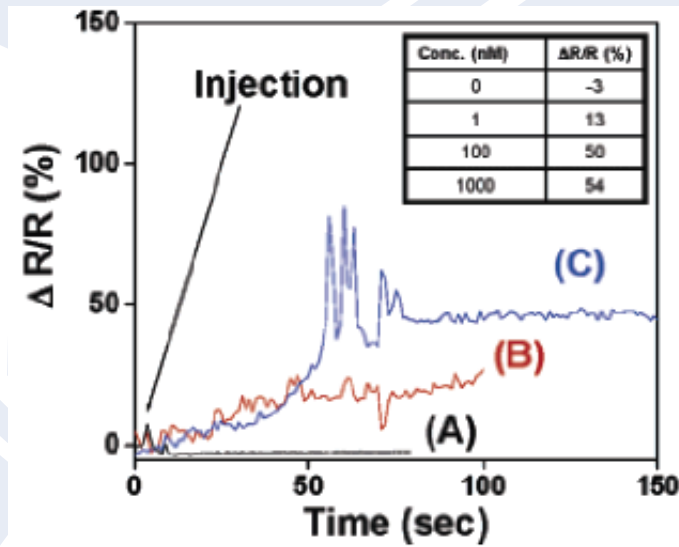


Fig.1- 14 Electrical responses of an unmodified polymer nanowire (A) to 100 nM biotin-DNA (single stranded) and avidin-embedded polypyrrole (200 nm) nanowires to 1 nM (B) and 100 nM (C) biotin-DNA. The responses were recorded on two separate polypyrrole-avidin nanowires[37]

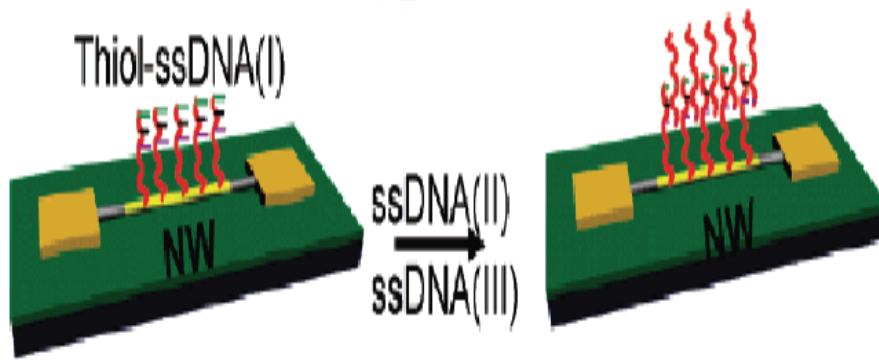


Fig.1- 15 (A) Schematic of CdTe-Au-CdTe nanowire field-effect transistor. (B) Schematic illustration of surface receptors modified CdTe-Au-CdTe nanowire FET for the detection of DNA[41]

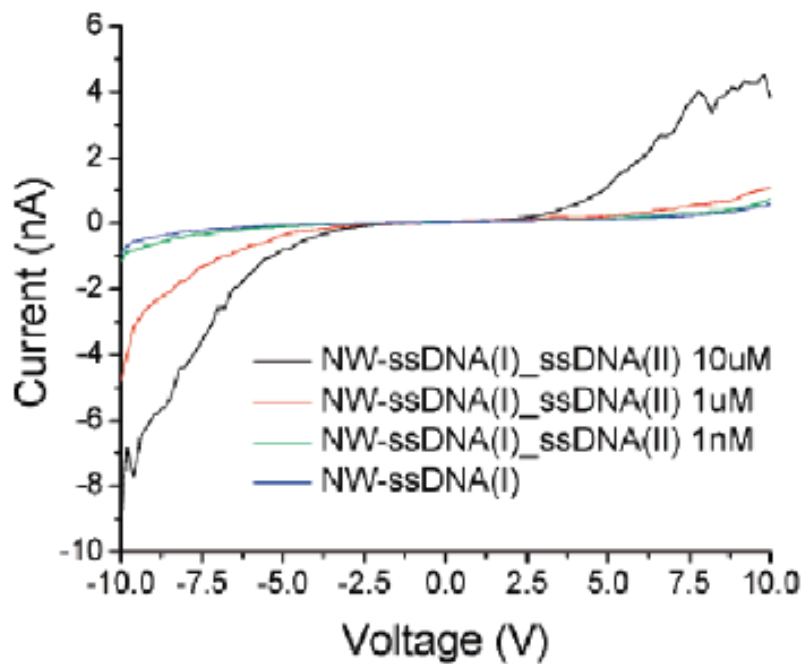


Fig.1- 16 CdTe-Au-CdTe nanowire sensor detecting ssDNA-(II) at different concentrations[41]

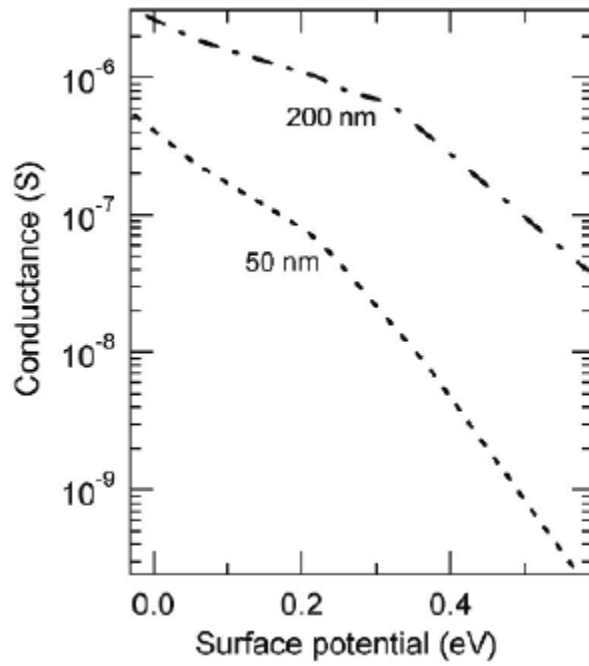


Fig.1- 17 Simulated conductance values as a function of the surface potential for the 200-nm-wide and 50-nm-wide wires[42]

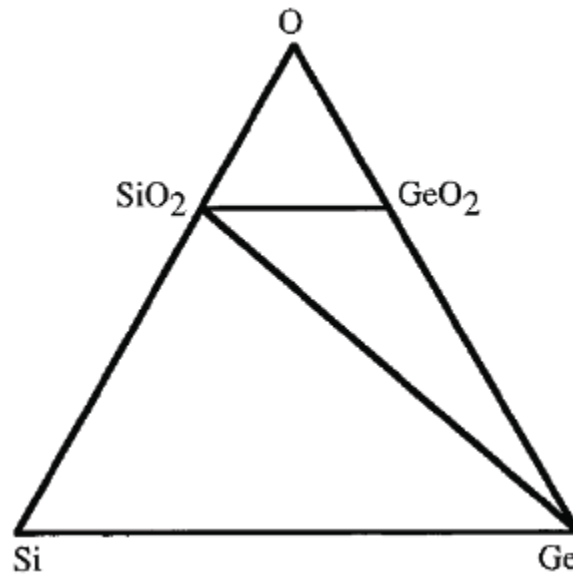


Fig.1- 18 Ternary phase diagram for the Si–Ge–O system at 1000 K and 1 bar, calculated based on the thermochemical data[45]

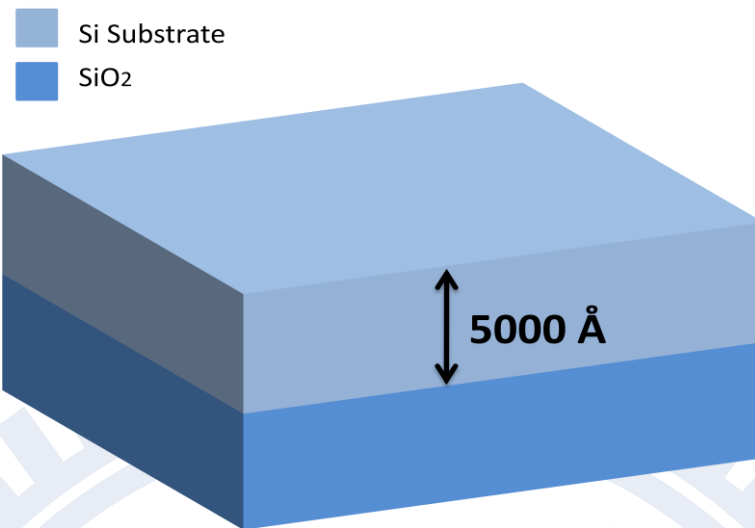


Fig.2- 1 SiO<sub>2</sub> grew 5000Å on Si substrate

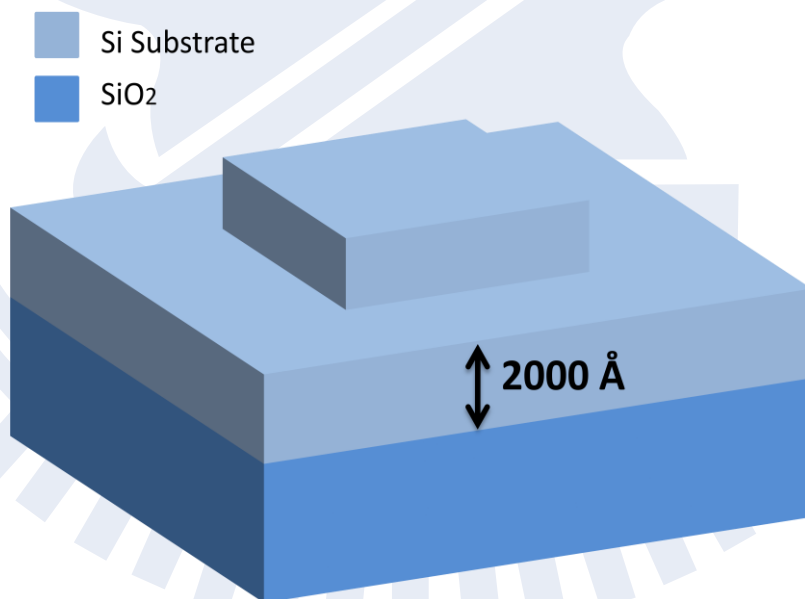


Fig.2- 2 Mask#1:Etch SiO<sub>2</sub> 3000Å

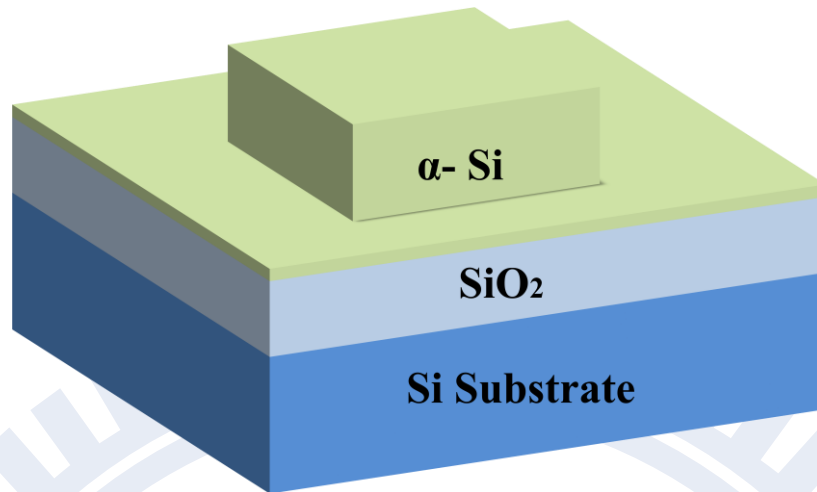


Fig.2- 3 Deposit amorphous Si on SiO<sub>2</sub>

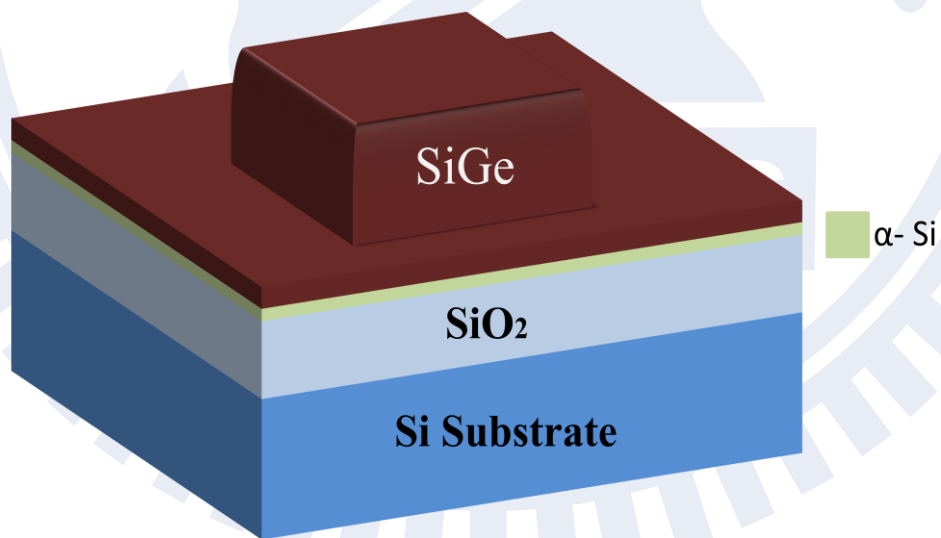


Fig.2- 4 Deposit amorphous SiGe on amorphous Si

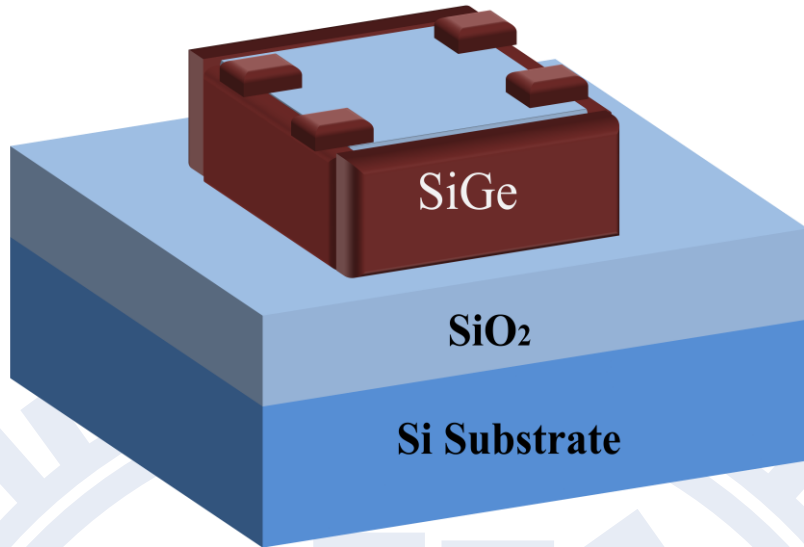


Fig.2- 5 Mask#2:Define nanowire on the sidewall

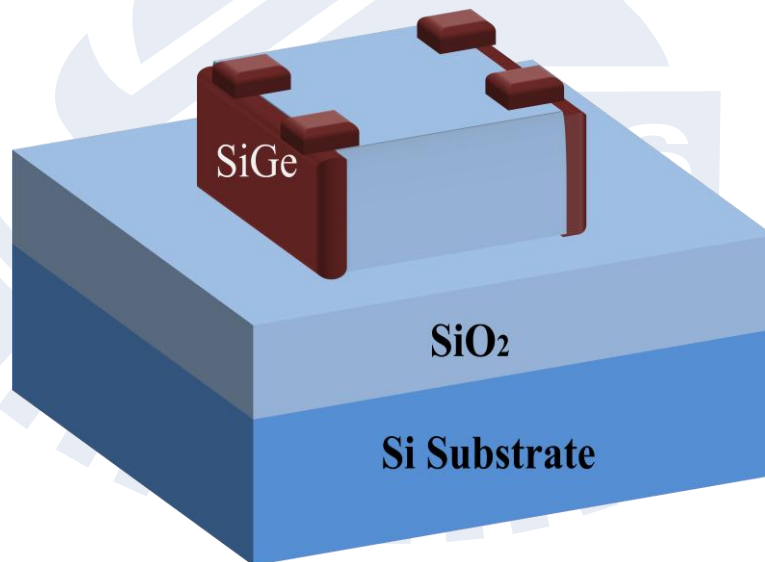


Fig.2- 6 Mask#3:Etch unwanted sidewall nanowire

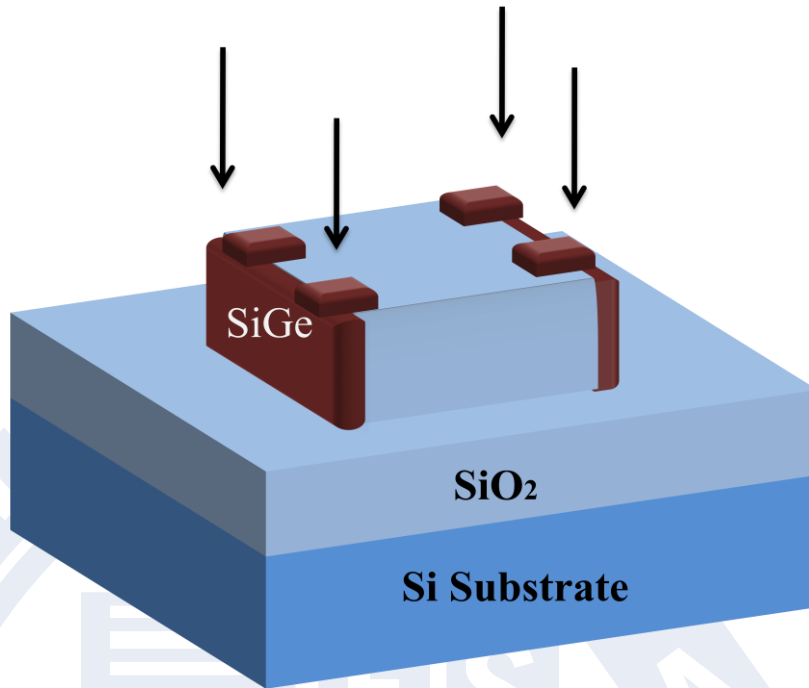


Fig.2- 7 Implant Boron-fluoride( $\text{BF}_2^{49+}$ ) into SiGe nanowires

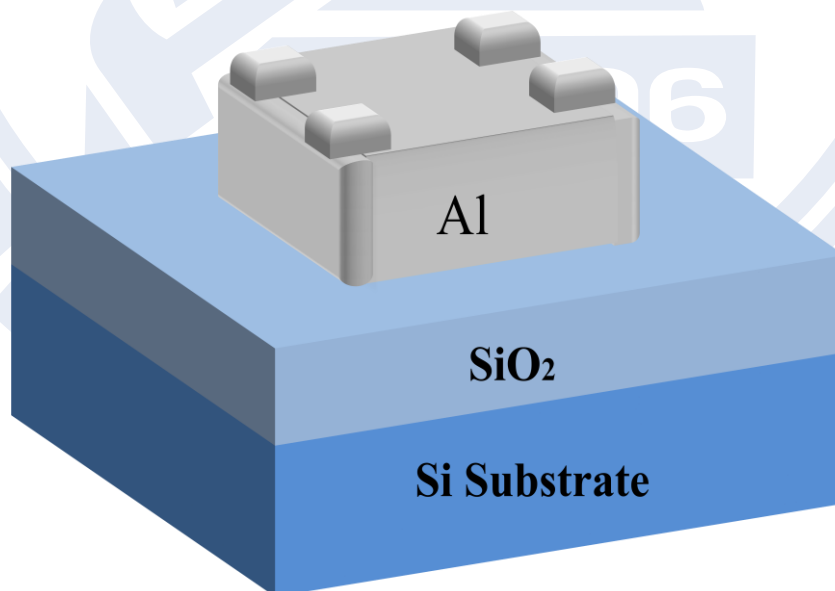


Fig.2- 8 Deposit Al 5000Å on the devices

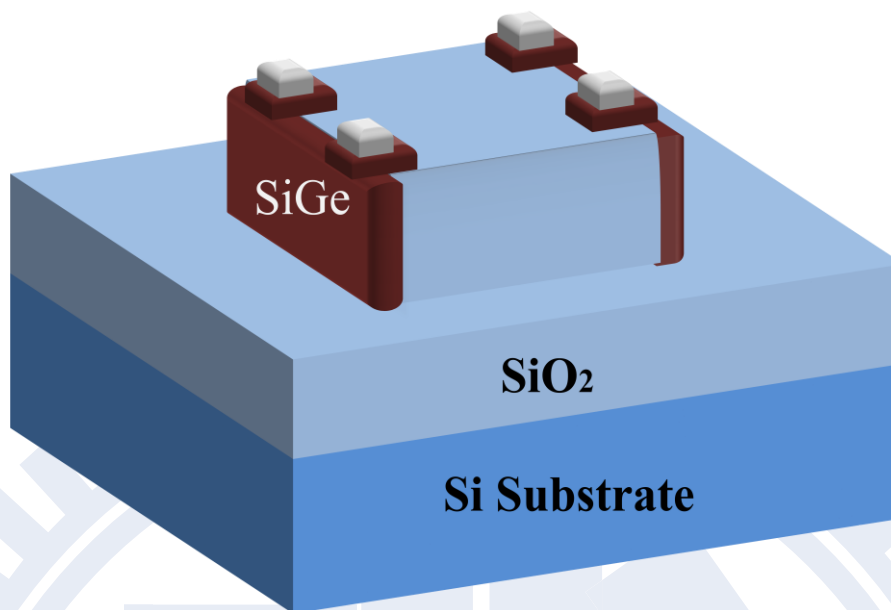


Fig.2- 9 Mask#4: Define the Al contact position

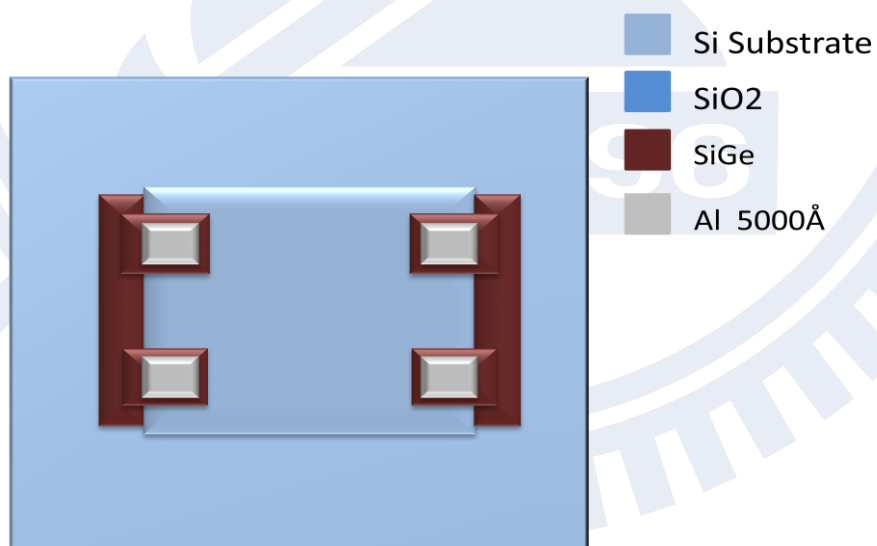


Fig.2- 10 The device view from top position

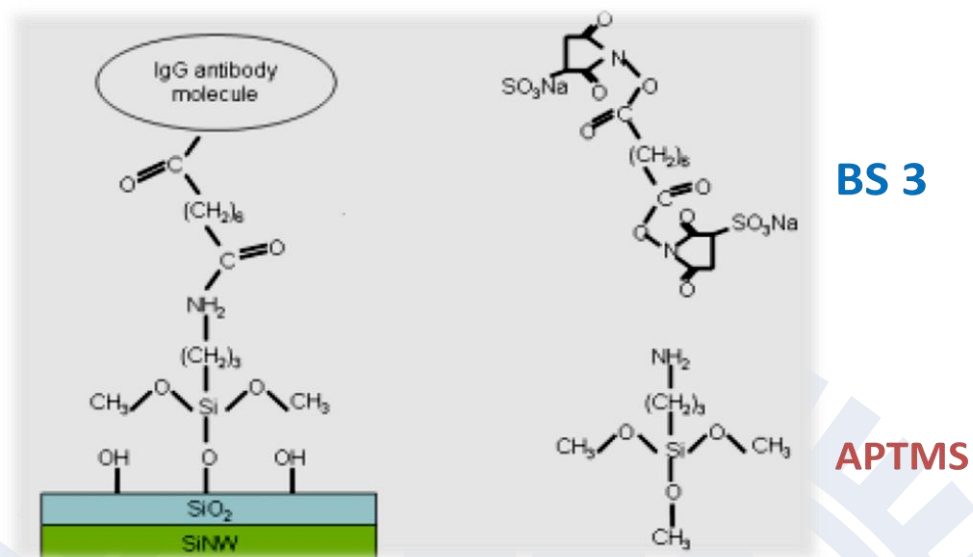


Fig.2- 11 The modification of surface by APTMS and linked by BS3

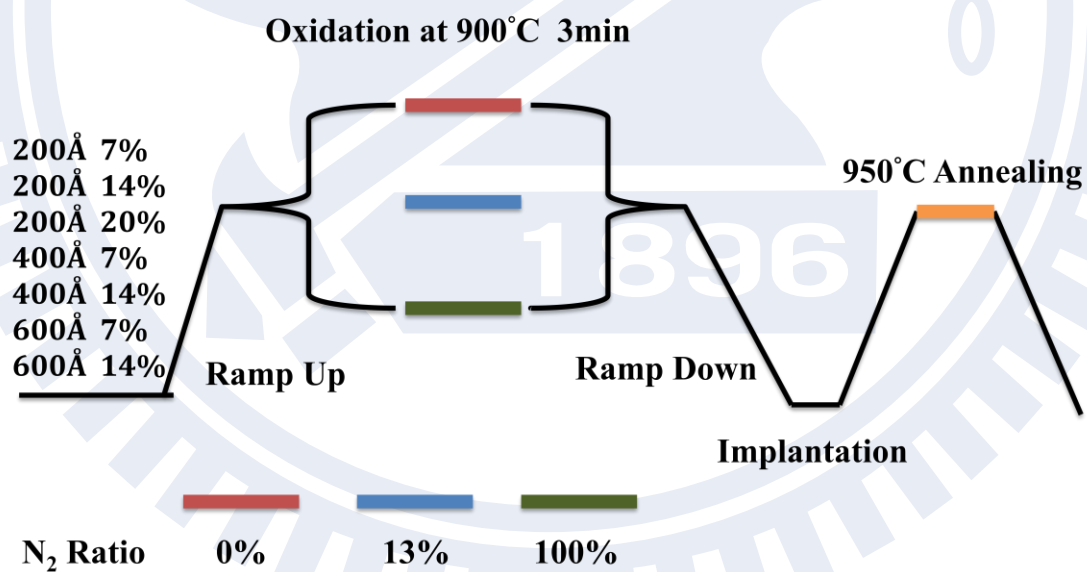


Fig.3- 1 The oxidation of stacked structures under different combination of Nitrogen and Oxygen for three minutes

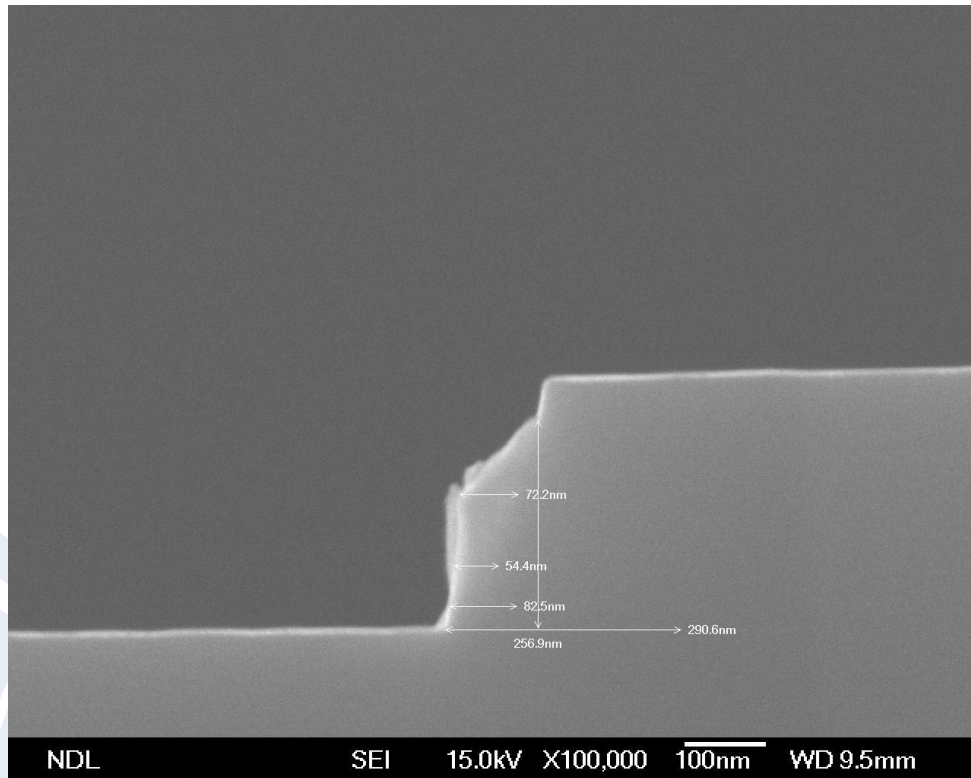


Fig.3- 2 SEM images of amorphous Si 200Å and 7% of Ge concentration

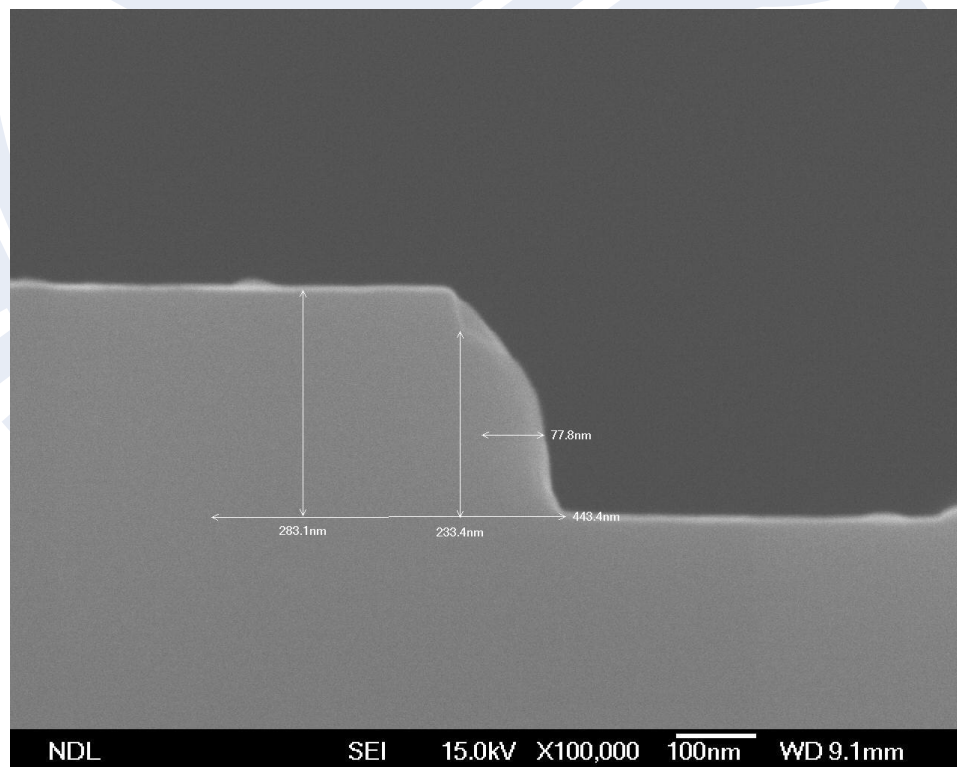


Fig.3- 3 SEM images of amorphous Si 200Å and 14% of Ge concentration

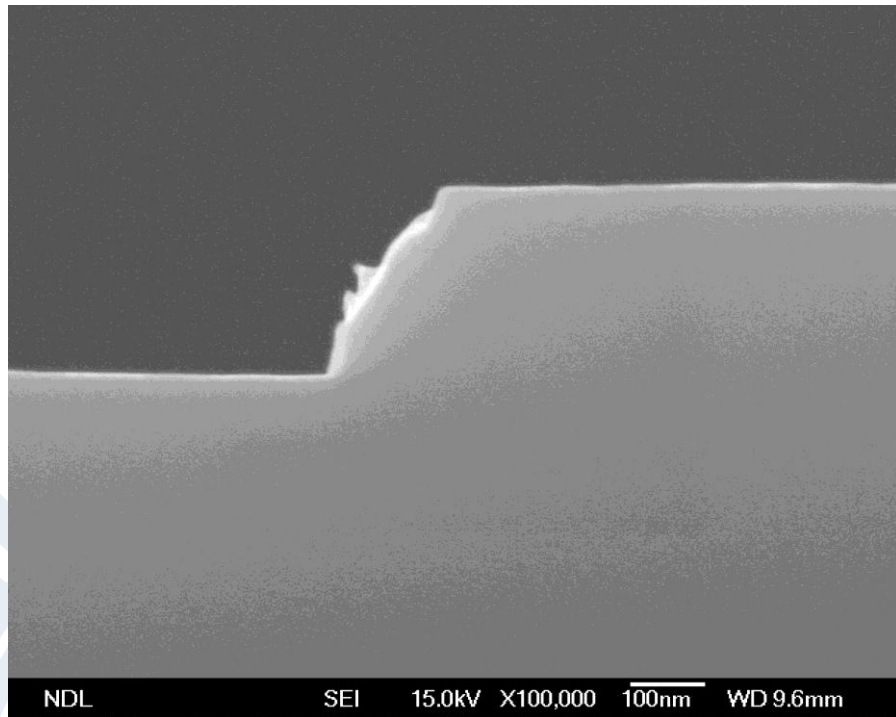


Fig.3- 4 SEM images of amorphous Si 200Å and 20% of Ge concentration

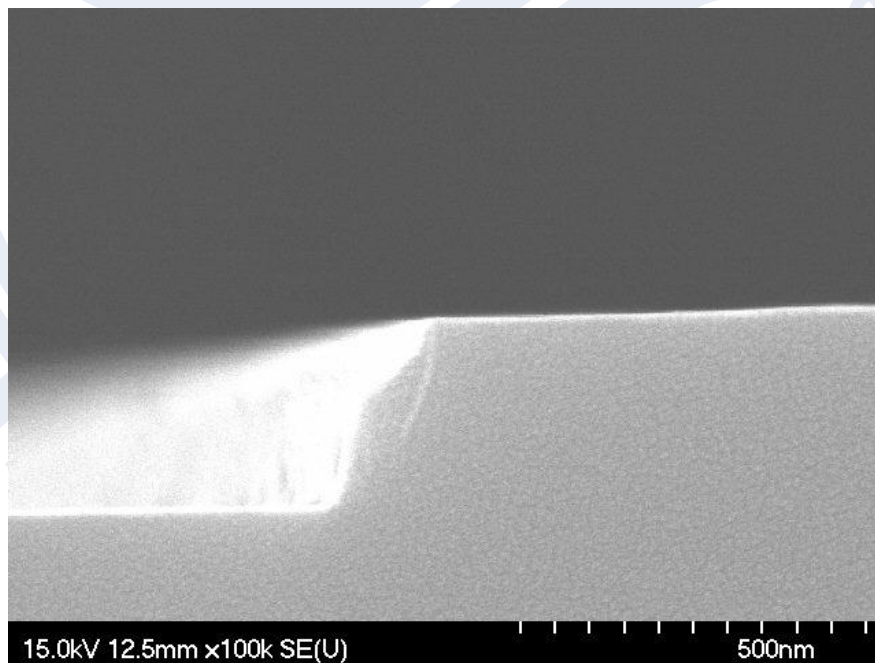


Fig.3- 5 SEM images of amorphous Si 400Å and 7% of Ge concentration

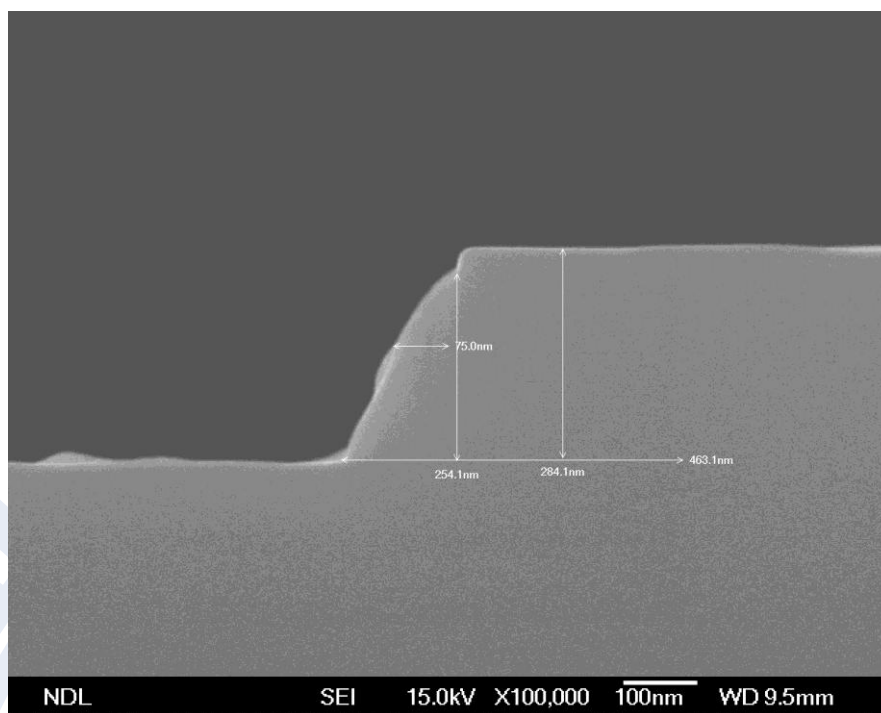


Fig.3- 6 SEM images of amorphous Si 400Å and 14% of Ge concentration

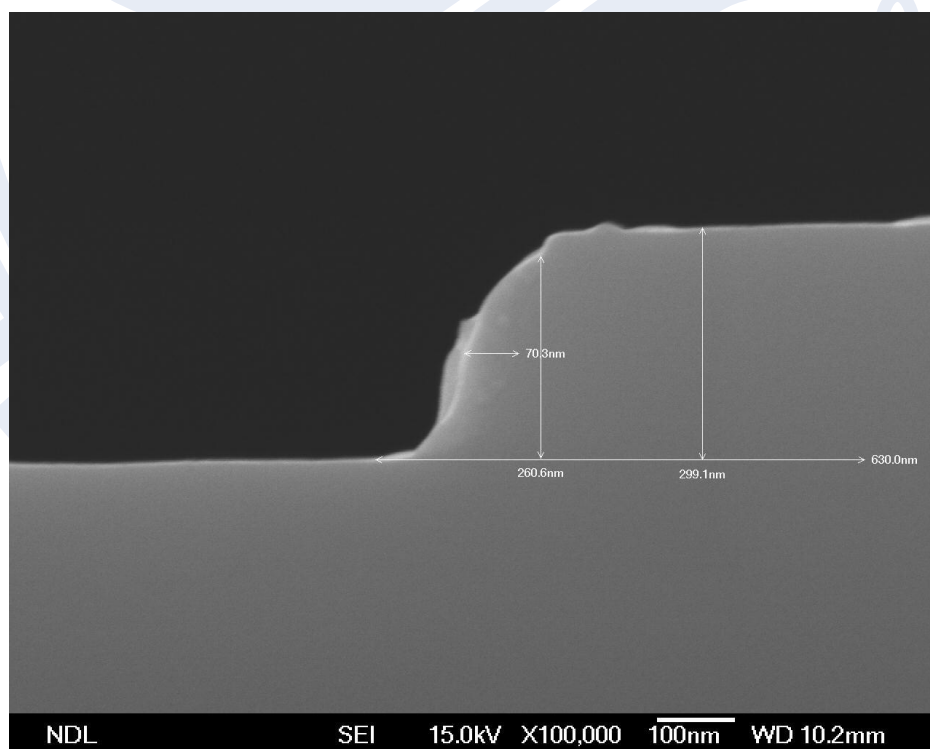


Fig.3- 7 SEM images of amorphous Si 600Å and 7% of Ge concentration

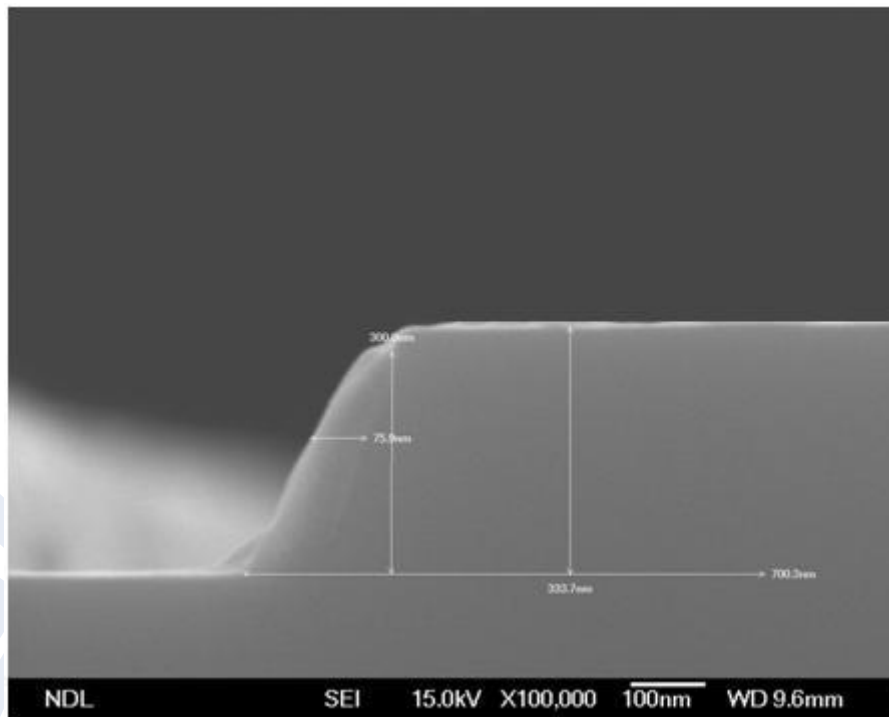


Fig.3- 8 SEM images of amorphous Si 600Å and 14% of Ge concentration

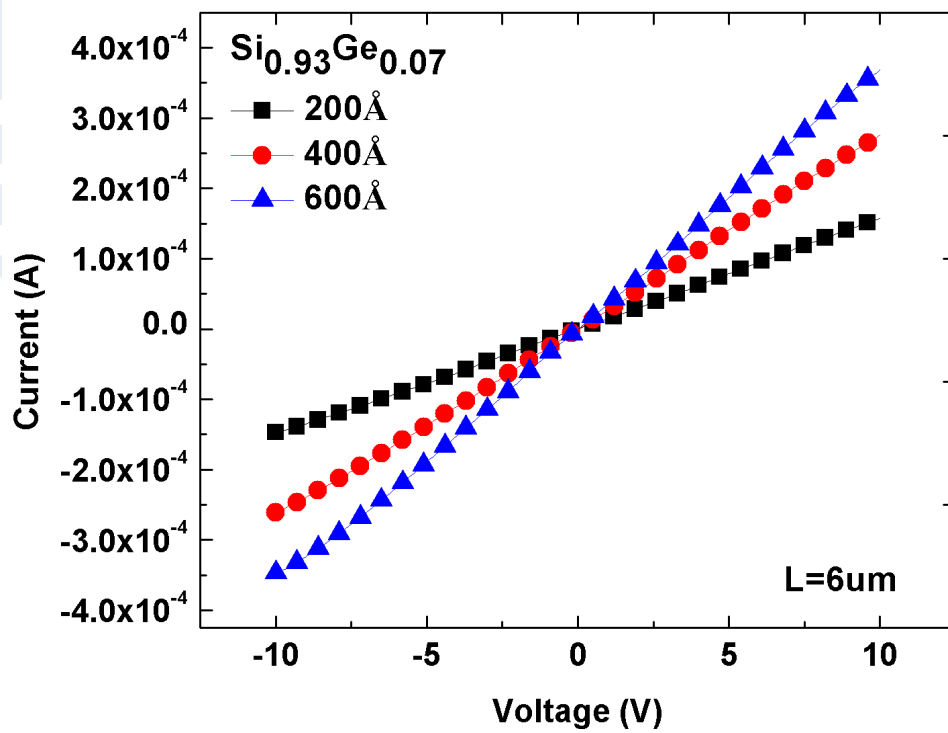


Fig.3- 9 I-V curve with different stacked structures on Ge 7%

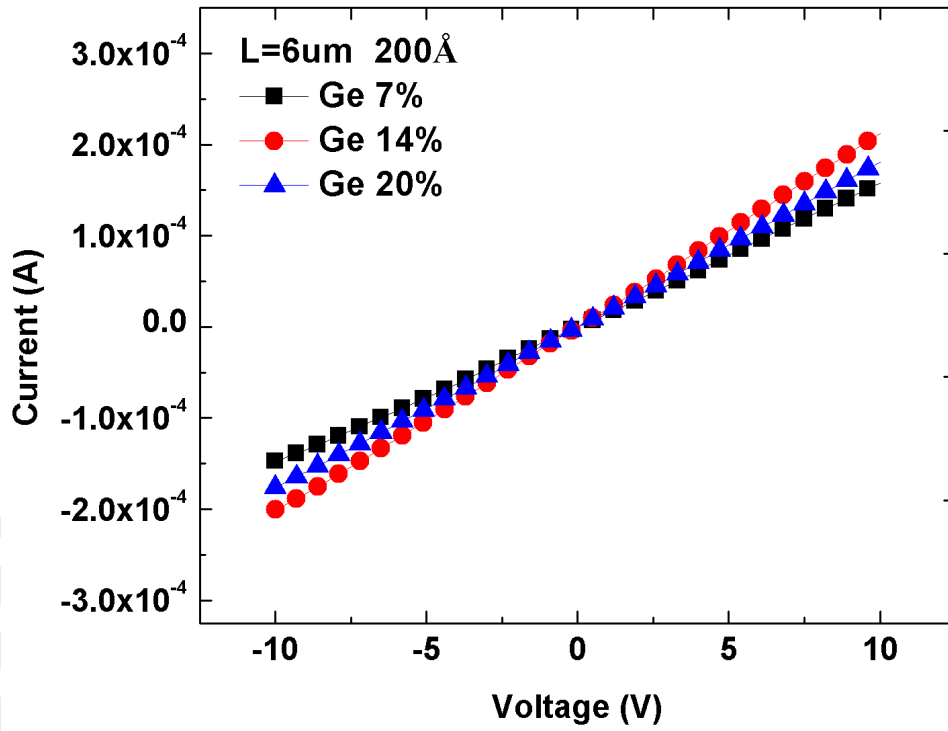


Fig.3- 10 I-V curve with different Ge concentrations on  $\alpha$ -Si  $200\text{\AA}$

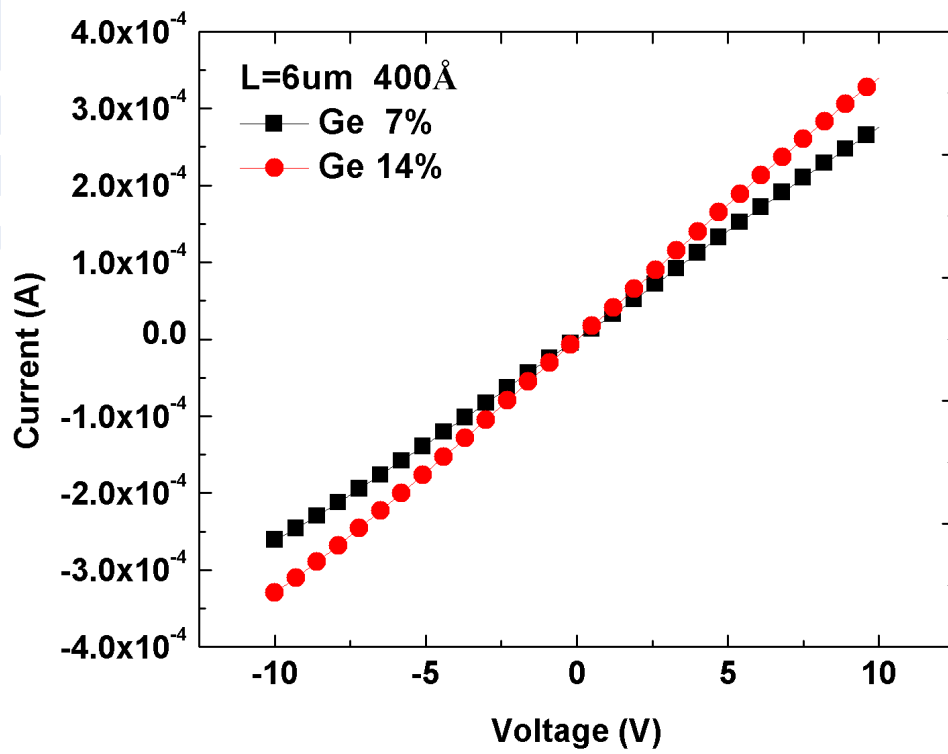


Fig.3- 11 I-V curve with different Ge concentrations on  $\alpha$ -Si  $400\text{\AA}$

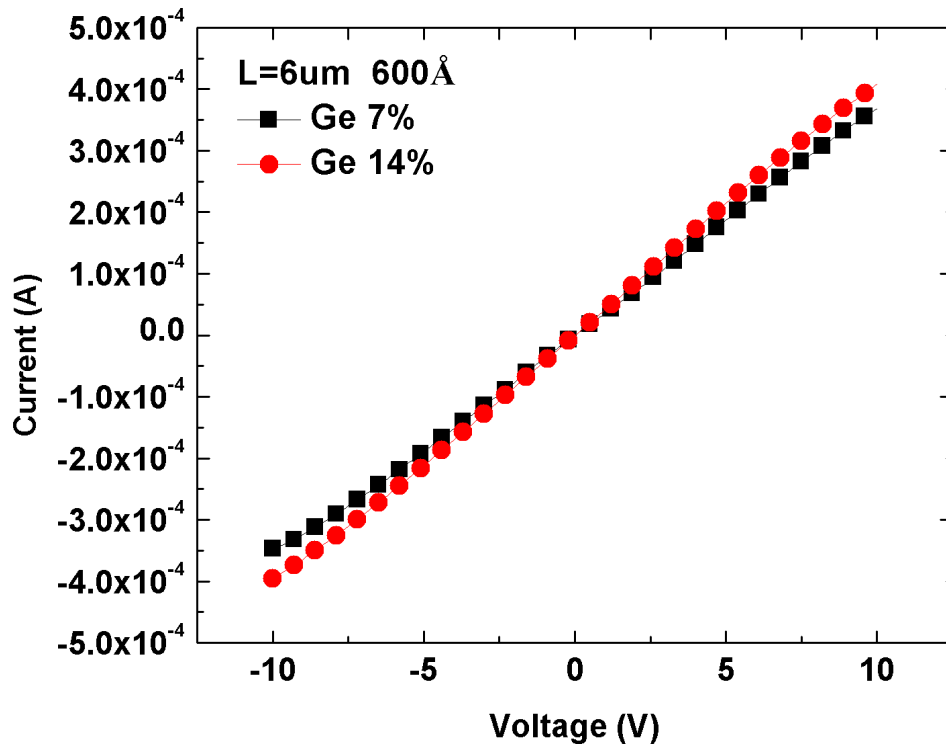


Fig.3- 12 I-V curve with different Ge concentrations on  $\alpha$ -Si  $600\text{\AA}$

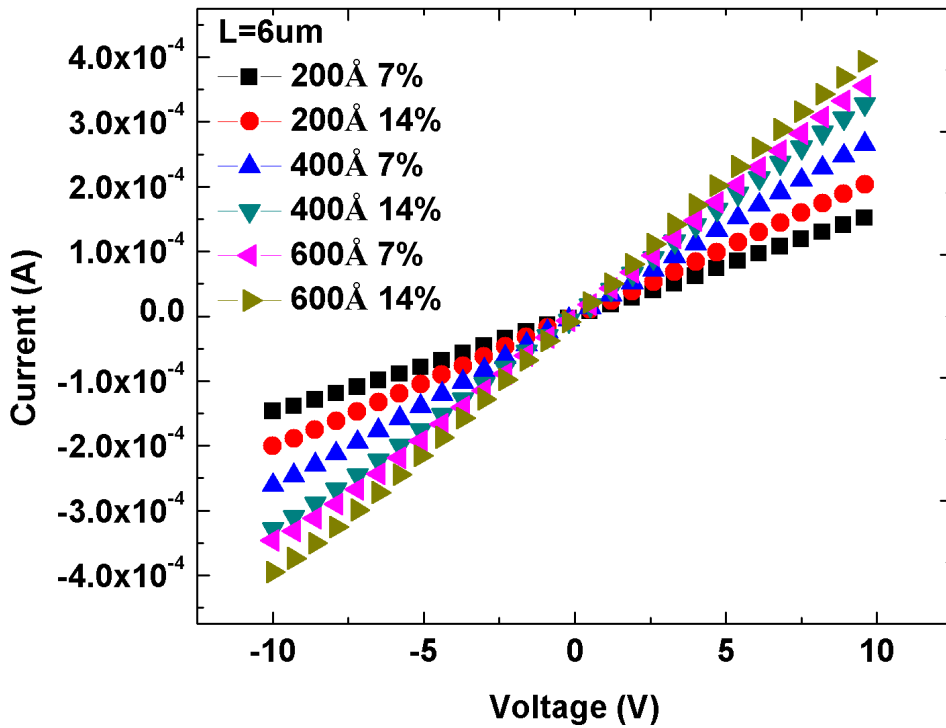


Fig.3- 13 I-V curve with combining structures and Ge density

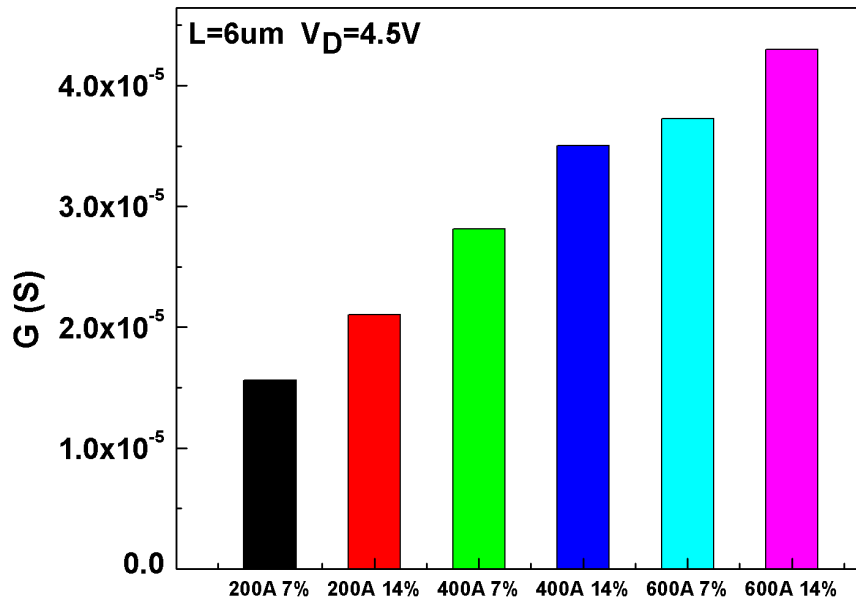


Fig.3- 14 The conductance with combining structures and Ge density

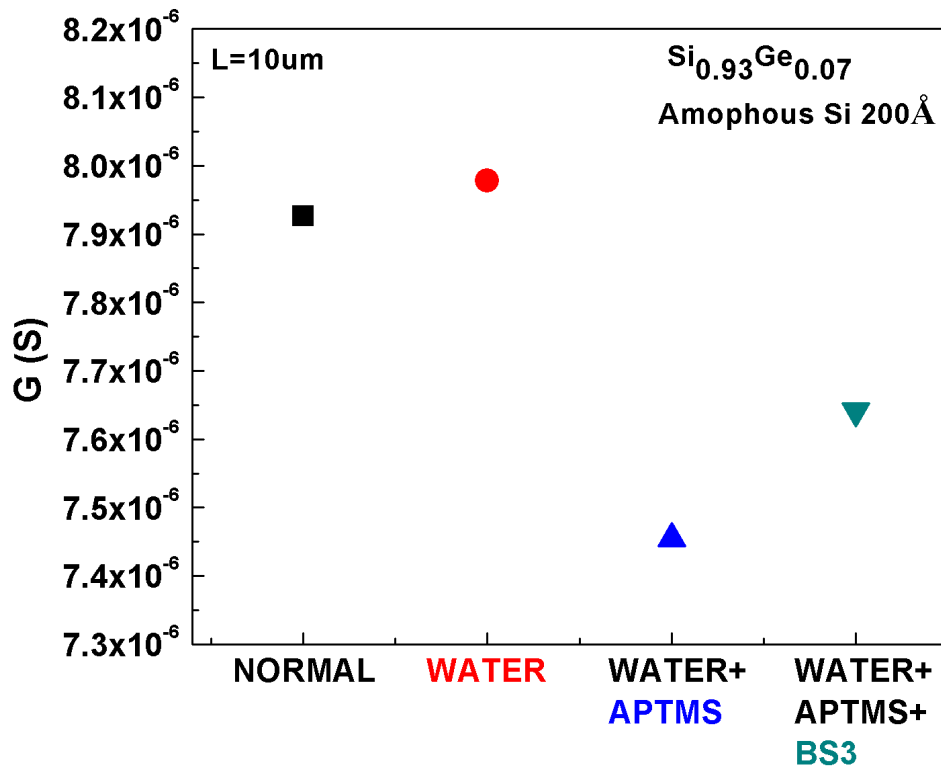


Fig.3- 15 The conductance with no treatment in 200Å 7%

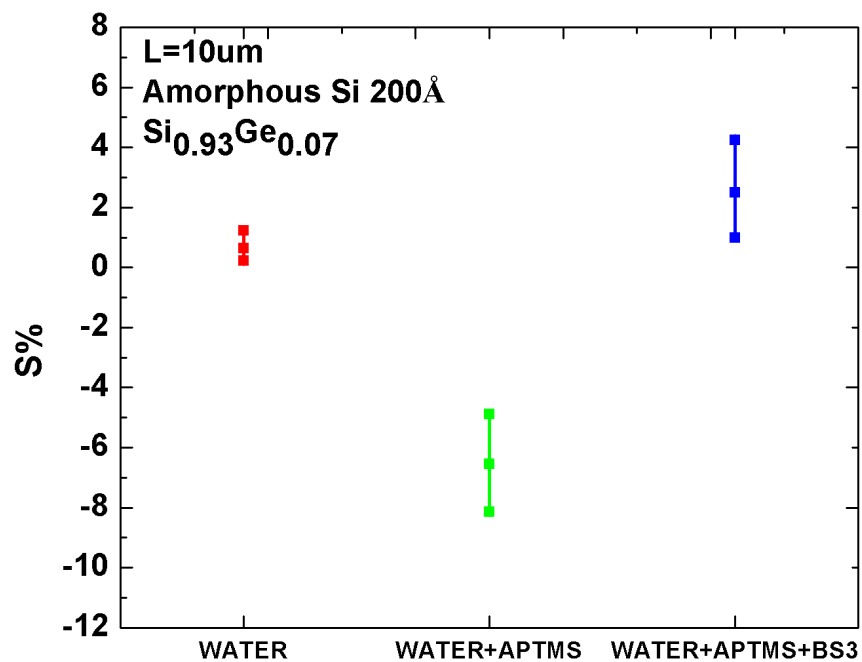


Fig.3- 16 The Sensitivity of with no treatment in  $200\text{\AA}$  7%

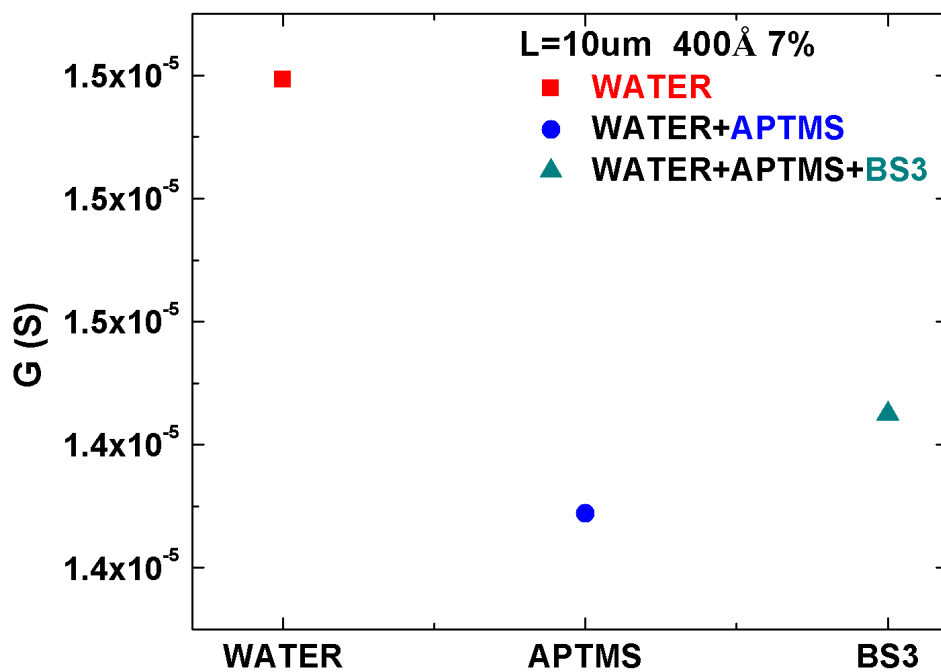


Fig.3- 17 The conductance with no treatment in  $400\text{\AA}$  7%

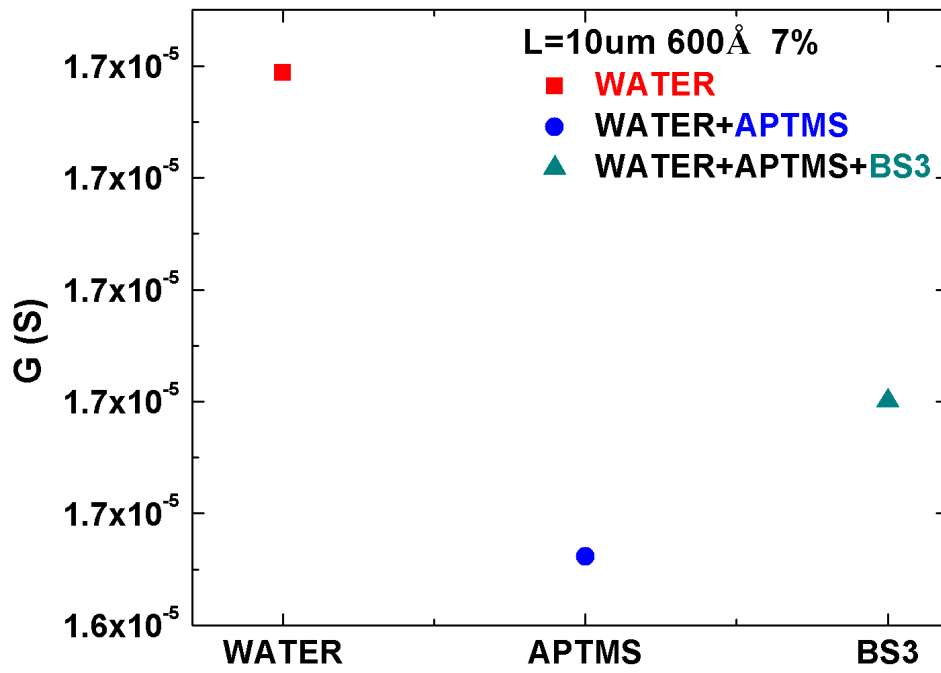


Fig.3- 18 The conductance with no treatment in  $600\text{\AA}$  7%

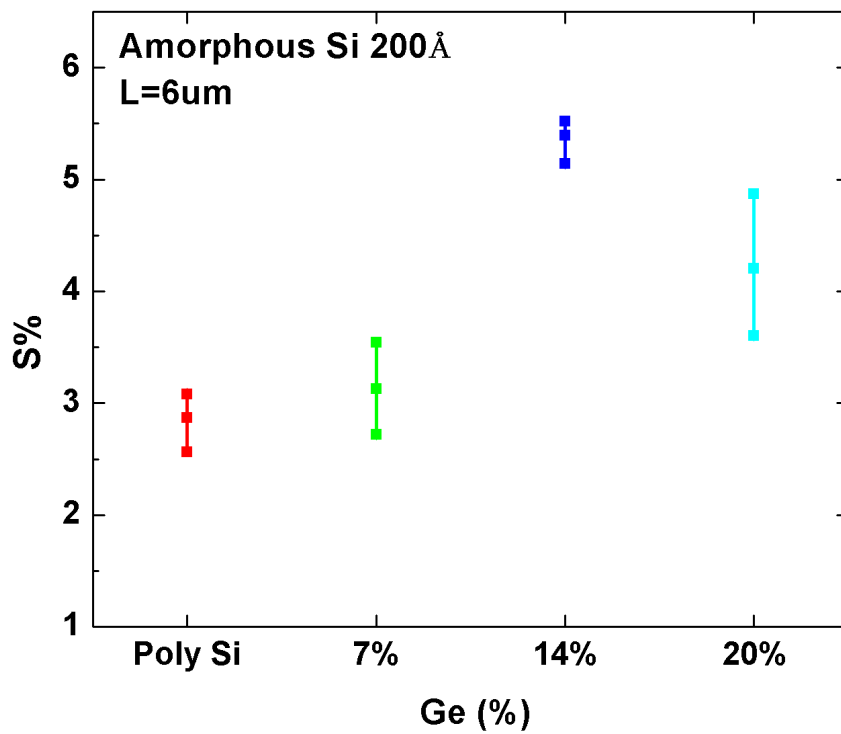


Fig.3- 19 The sensitivity of different Ge densities with the same width

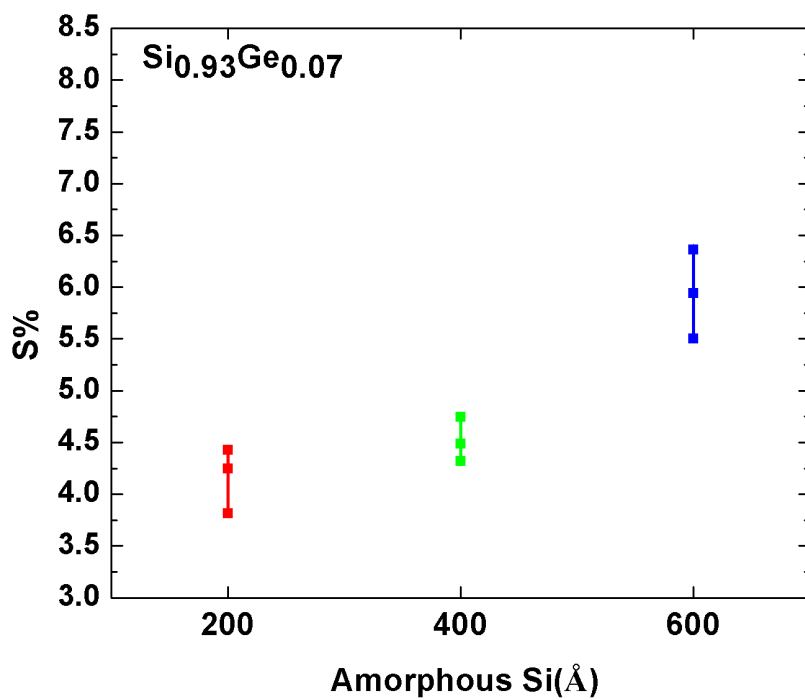


Fig.3- 20 The sensitivity of the different widths with Ge 7%

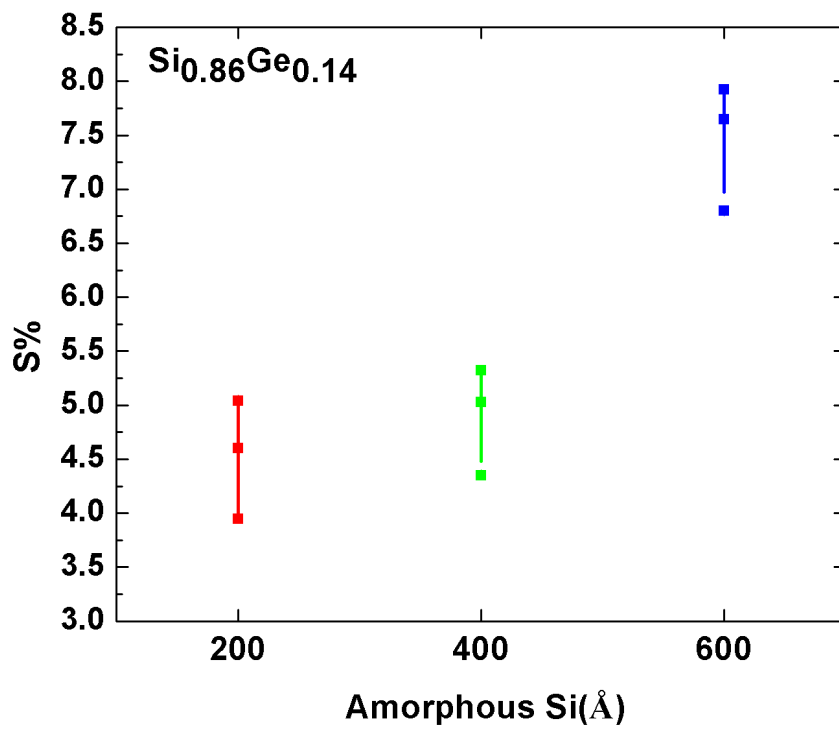


Fig.3- 21 The sensitivity of the different widths with Ge 14%

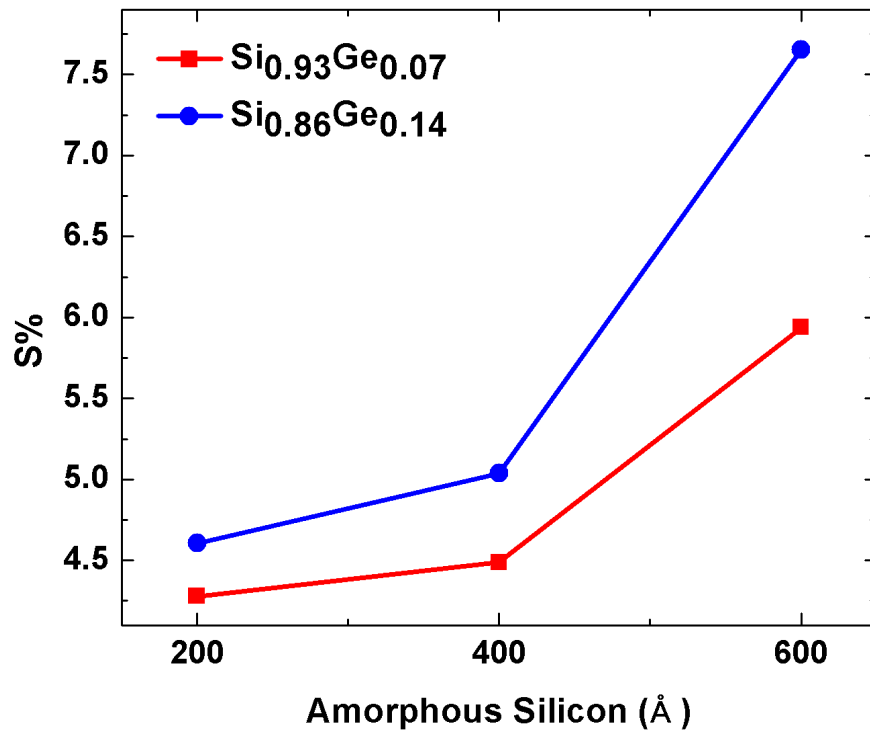


Fig.3- 22 The plot of sensitivity and the thickness of amorphous Si

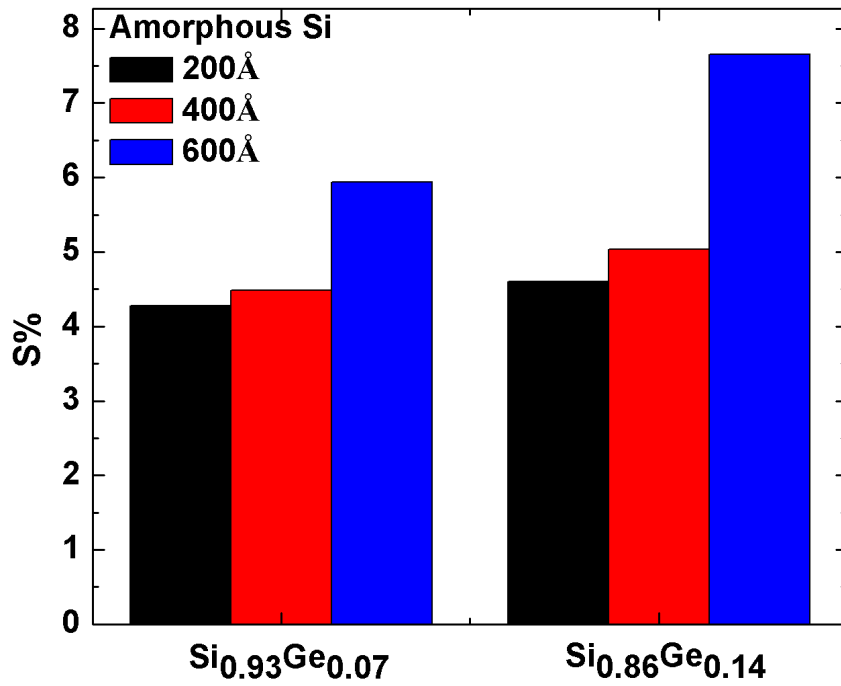


Fig.3- 23 The raise of sensitivity with different Ge densities

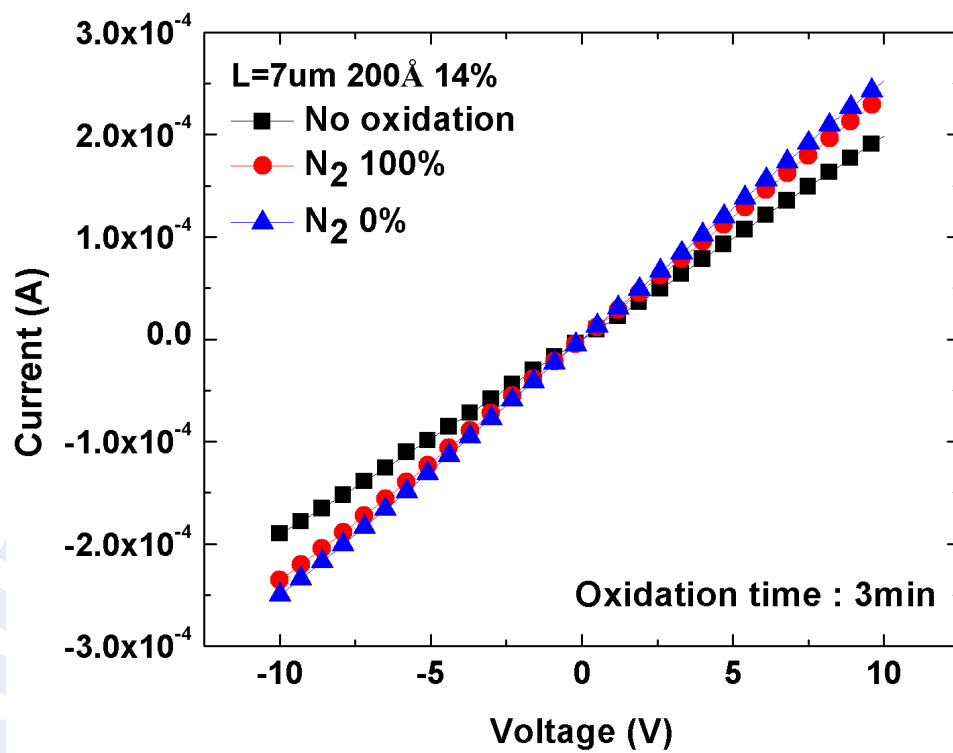


Fig.4- 1 I-V curve with oxidation on 200Å 14%

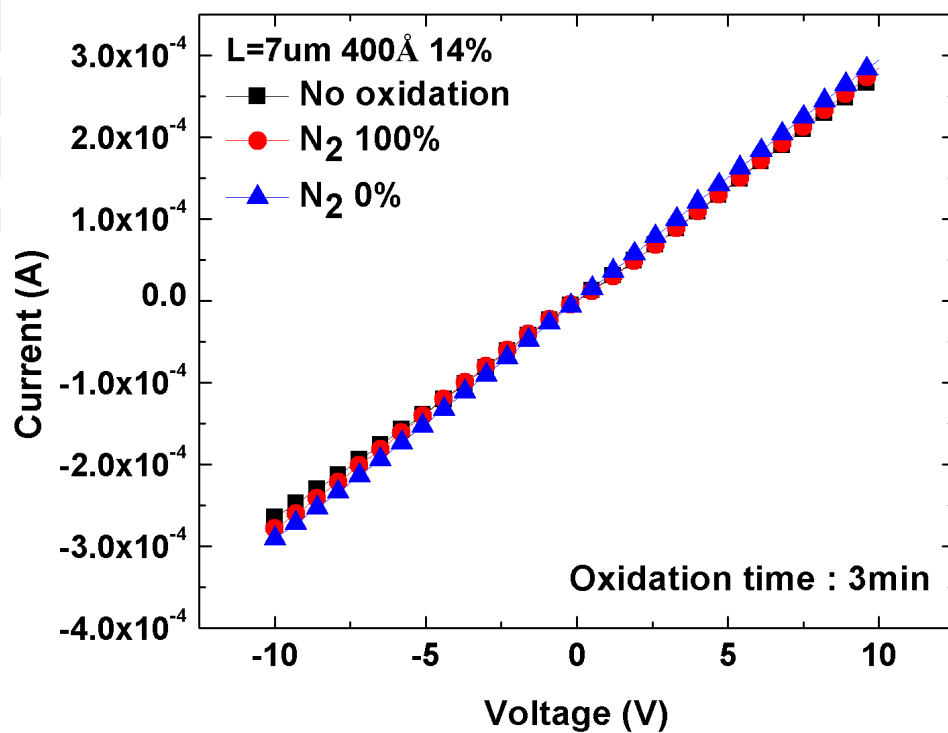


Fig.4- 2 I-V curve with oxidation on 400Å 14%

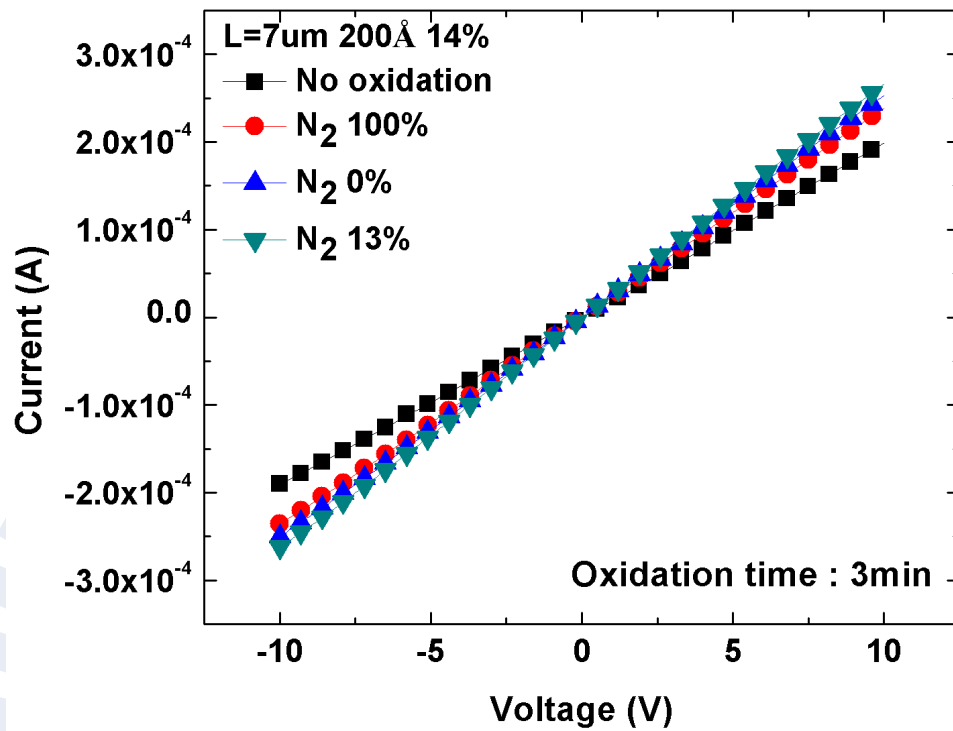


Fig.4- 3 I-V curve with oxidation on 200Å 14%

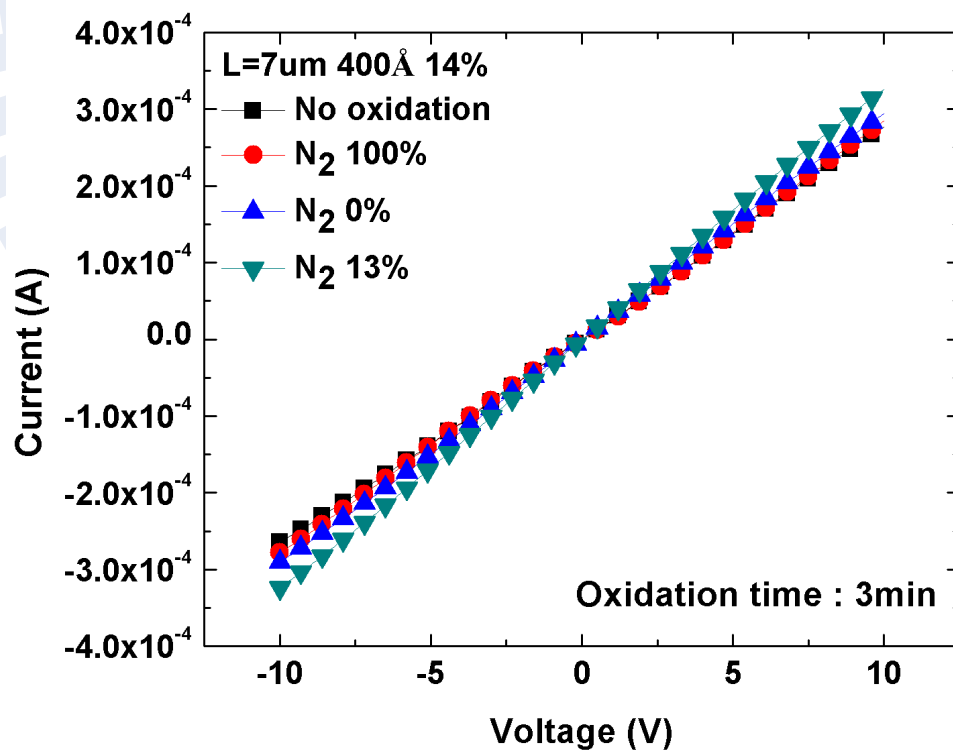


Fig.4- 4 I-V curve with oxidation on 400Å 14%

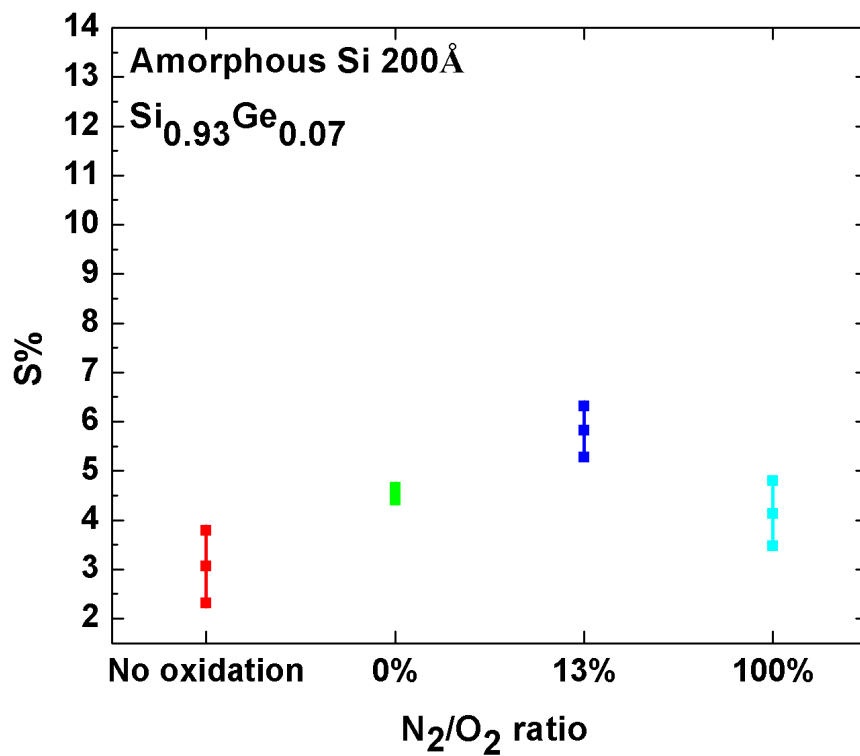


Fig.4- 5 The sensitivity of the treatment of oxidation on 200Å 7%

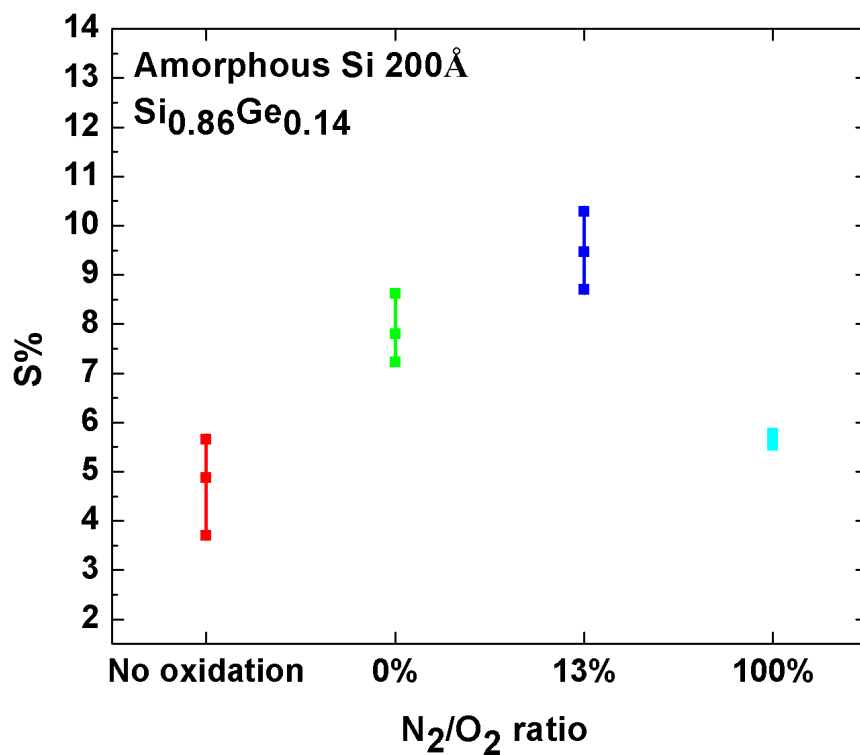


Fig.4- 6 The sensitivity of the treatment of oxidation on 200Å 14%

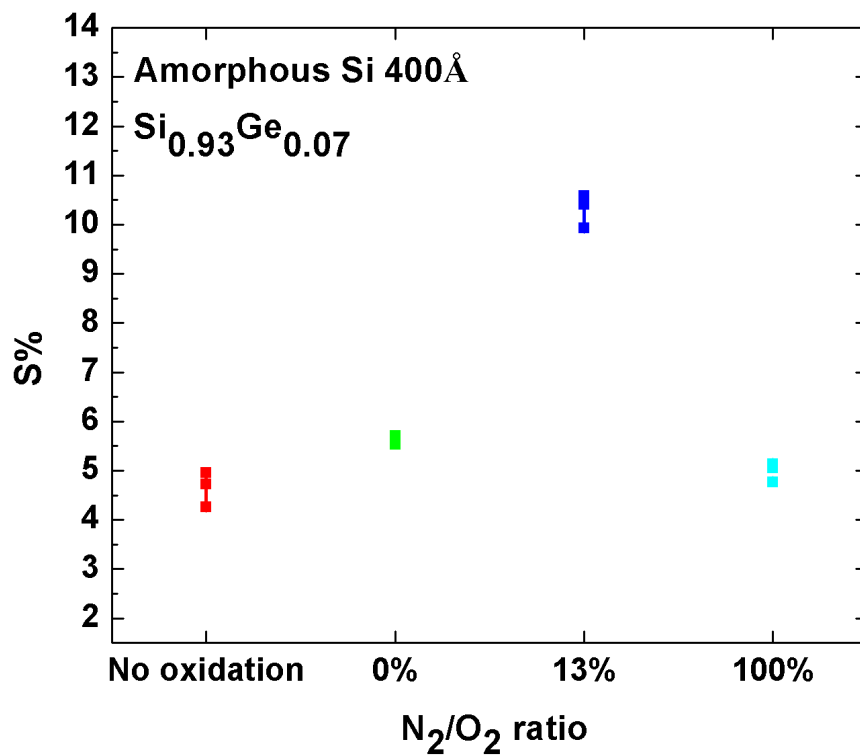


Fig.4- 7 The sensitivity of the treatment of oxidation on 400Å 7%

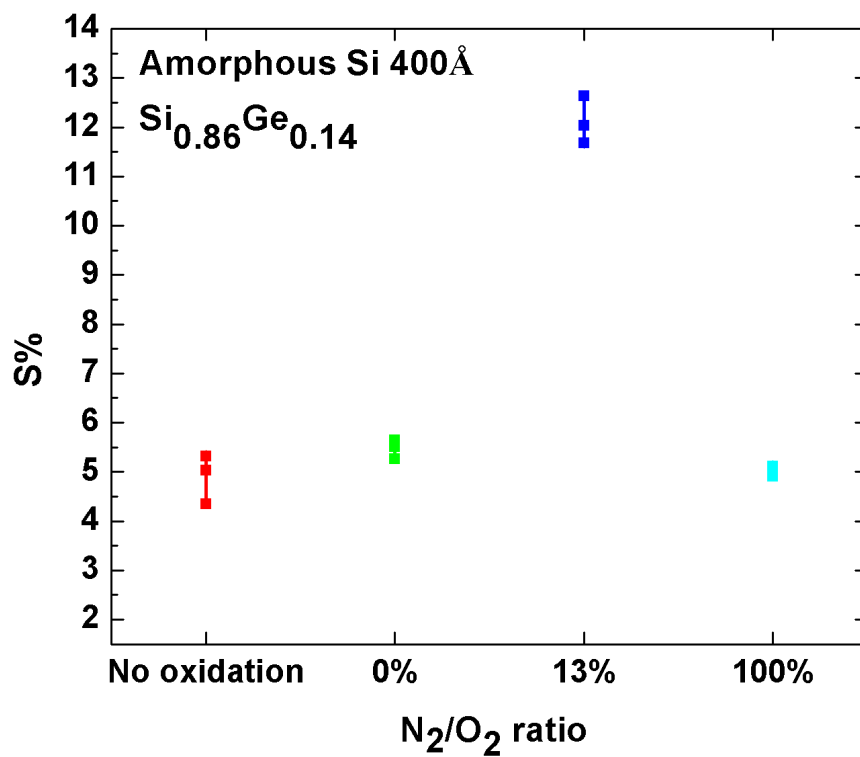


Fig.4- 8 The sensitivity of the treatment of oxidation on 400Å 14%

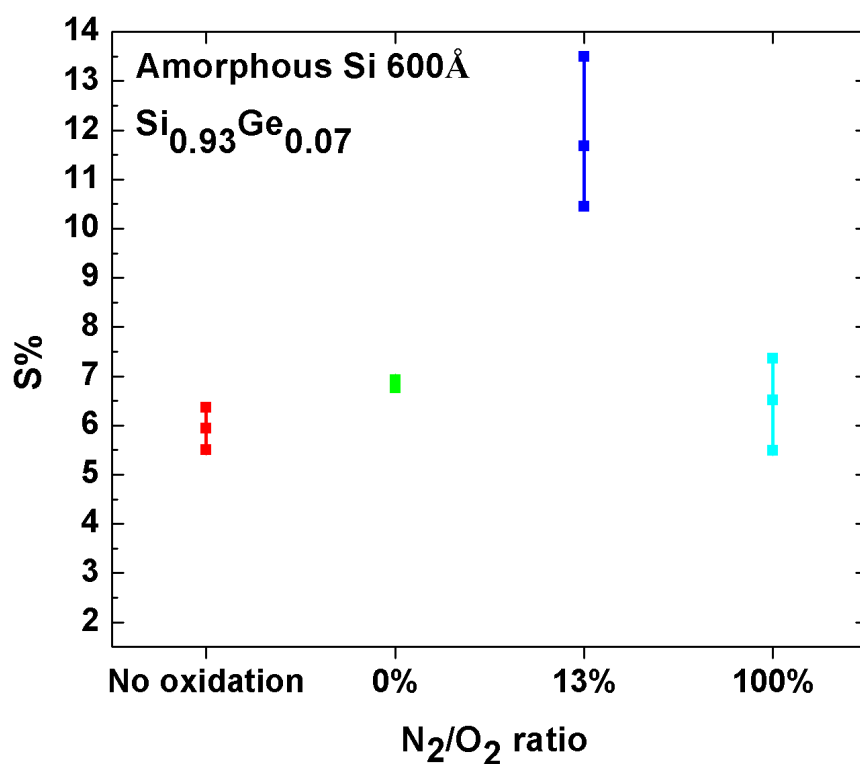


Fig.4- 9 The sensitivity of the treatment of oxidation on 600Å 7%

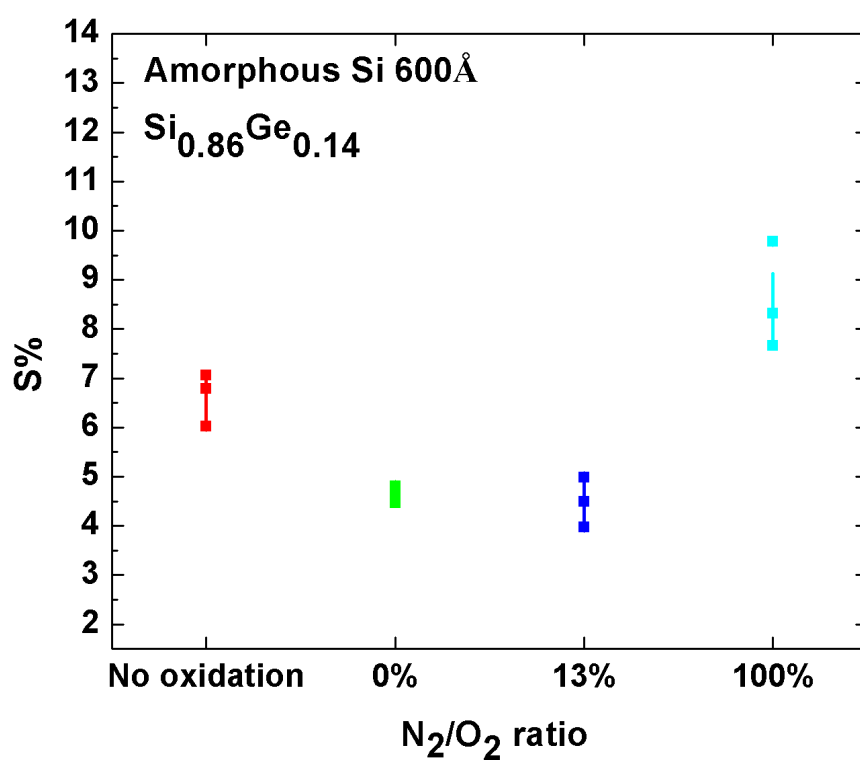


Fig.4- 10 The sensitivity of the treatment of oxidation on 600Å 14%

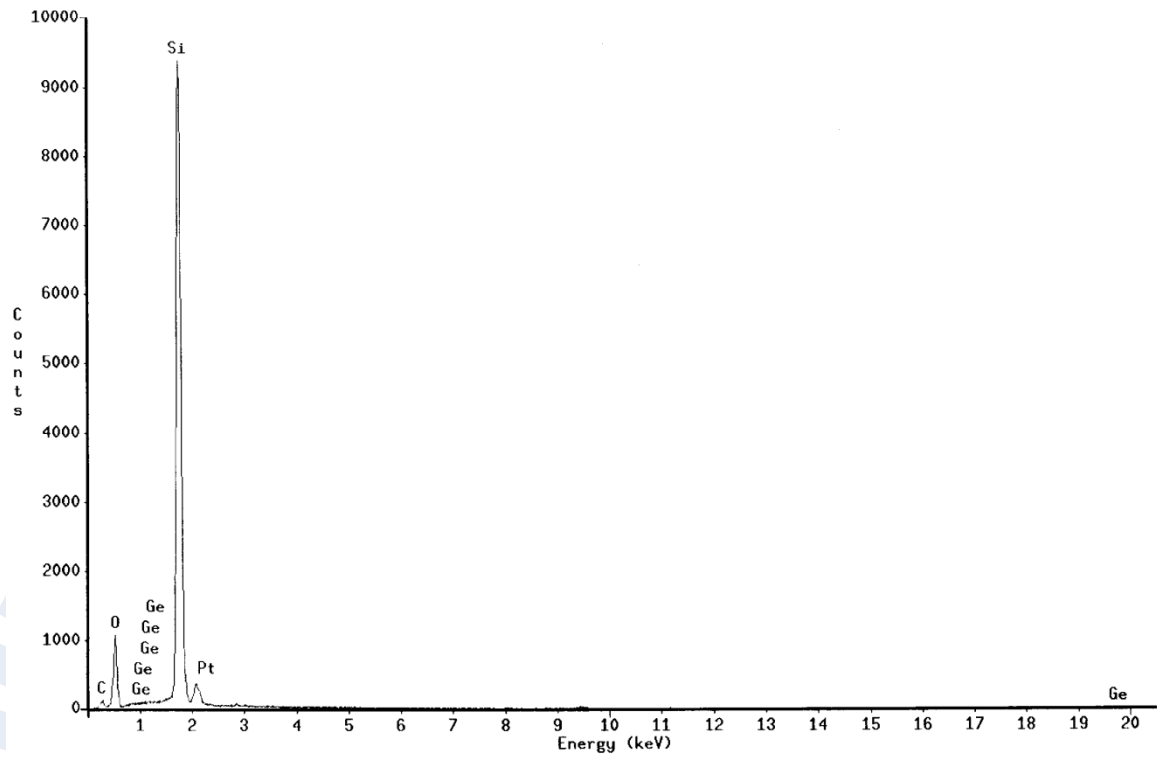


Fig.4- 11 The EDS analysis in 600Å 14%

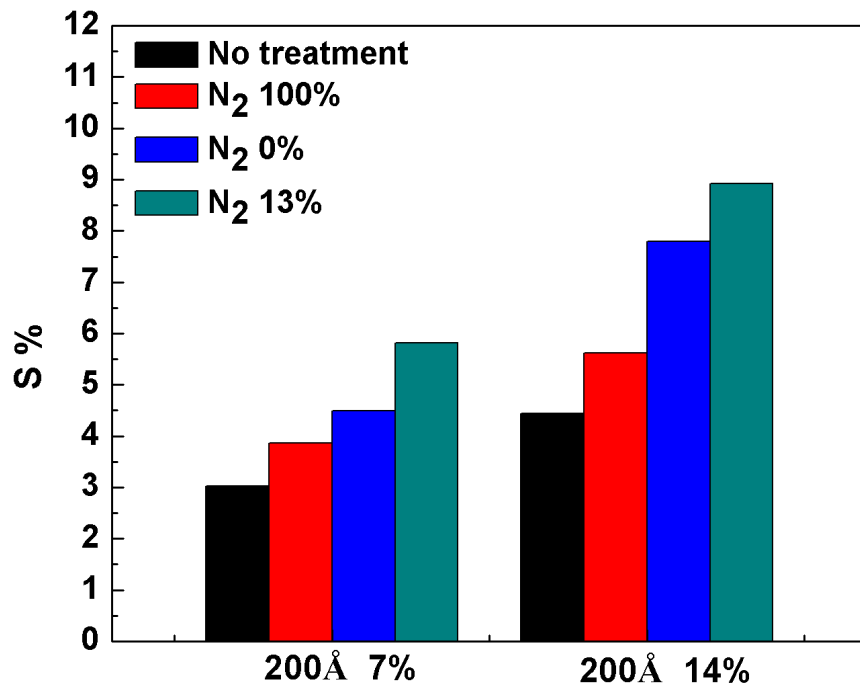


Fig.4- 12 The comparison between N<sub>2</sub> 100%, N<sub>2</sub> 0% and N<sub>2</sub> 13%

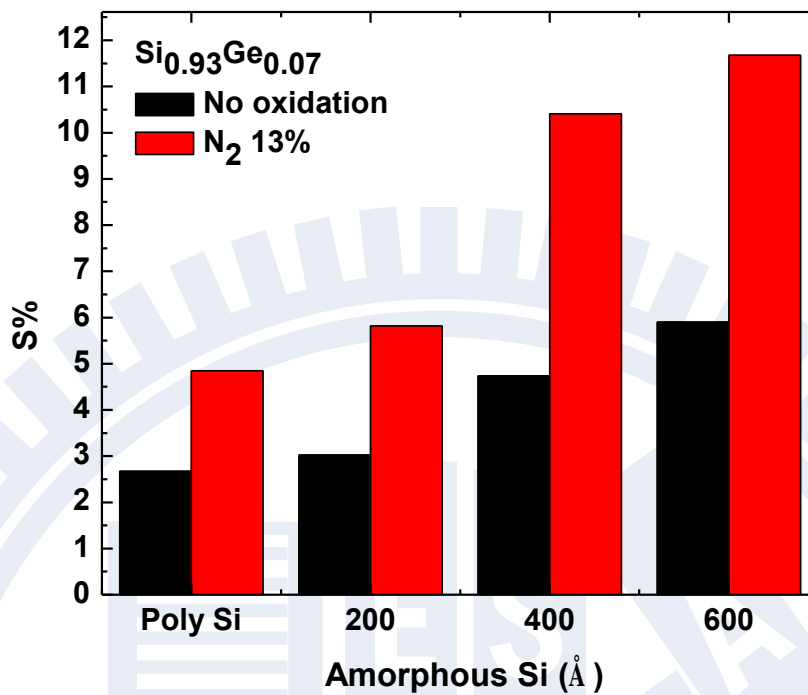


Fig.4- 13 The raise of sensitivity fixed on Si<sub>0.93</sub>Ge<sub>0.07</sub>

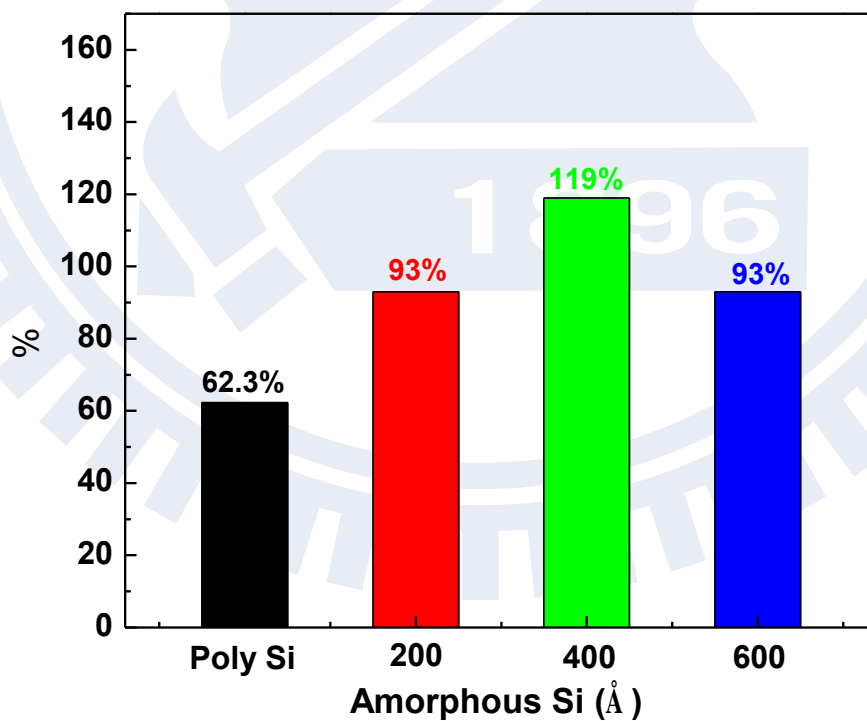


Fig.4- 14 The percentage change of Si<sub>0.93</sub>Ge<sub>0.07</sub> after APTMS modified

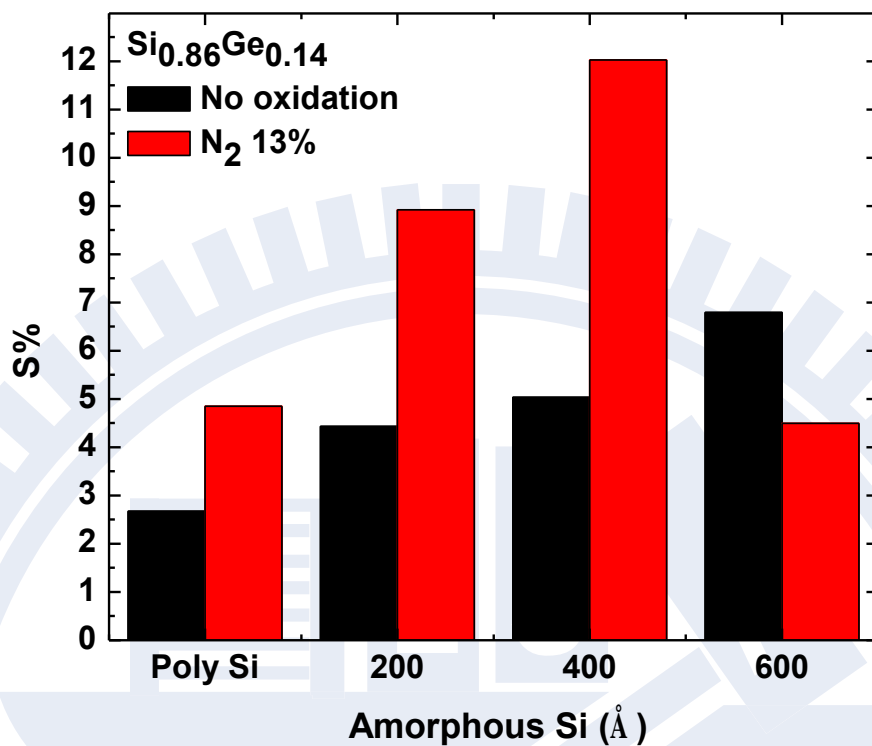


Fig.4- 15 The raise of sensitivity fixed on  $\text{Si}_{0.86}\text{Ge}_{0.14}$

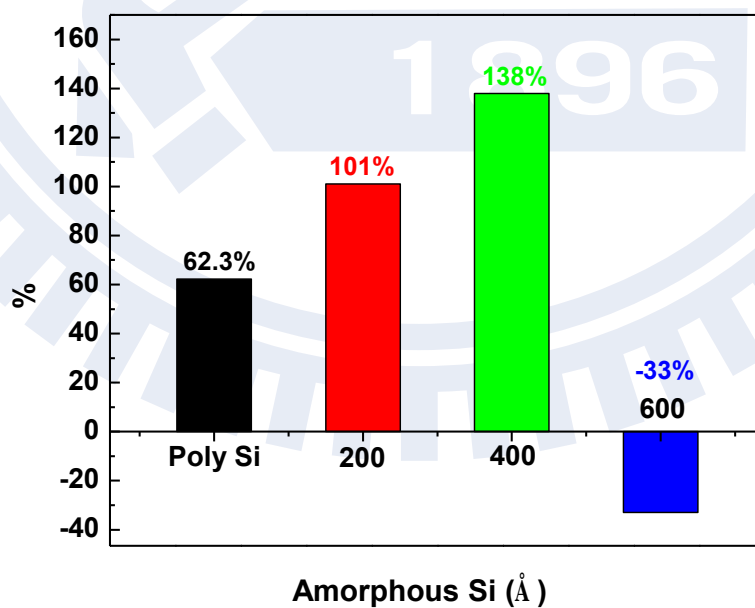


Fig.4- 16 The percentage change of  $\text{Si}_{0.86}\text{Ge}_{0.14}$  after APTMS modified

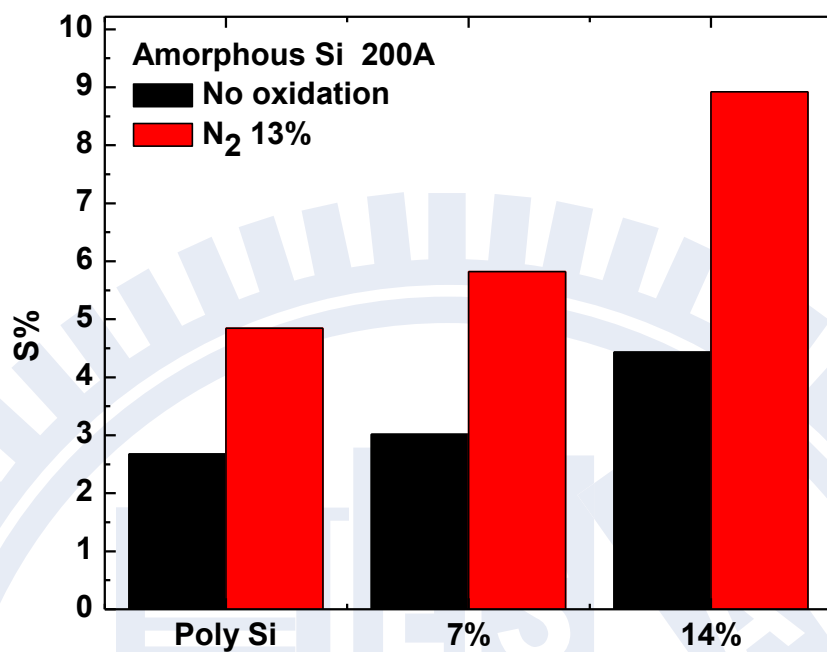


Fig.4- 17 The raise of sensitivity fixed on amorphous Si 200Å

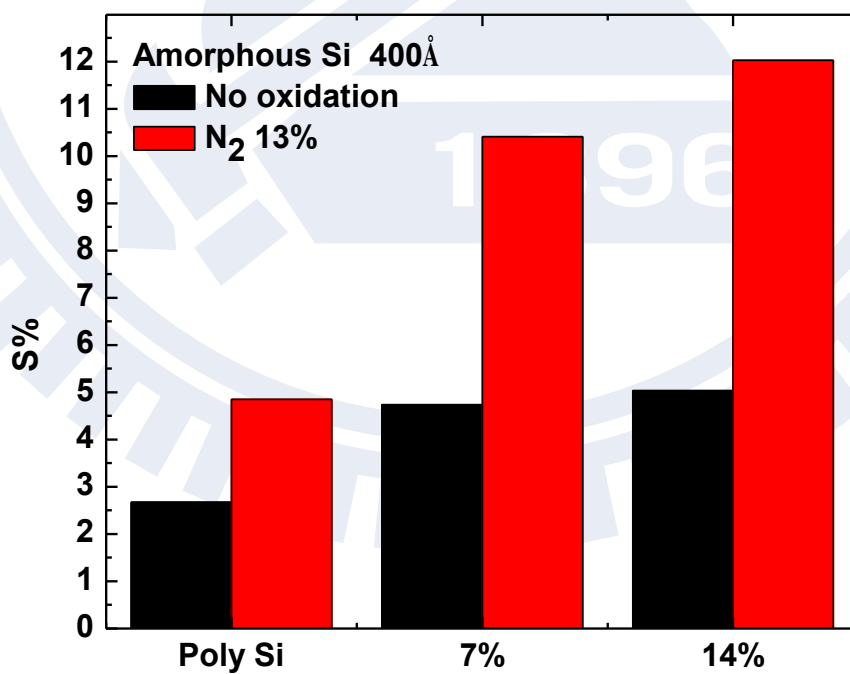


Fig.4- 18 The raise of sensitivity fixed on amorphous Si 400Å

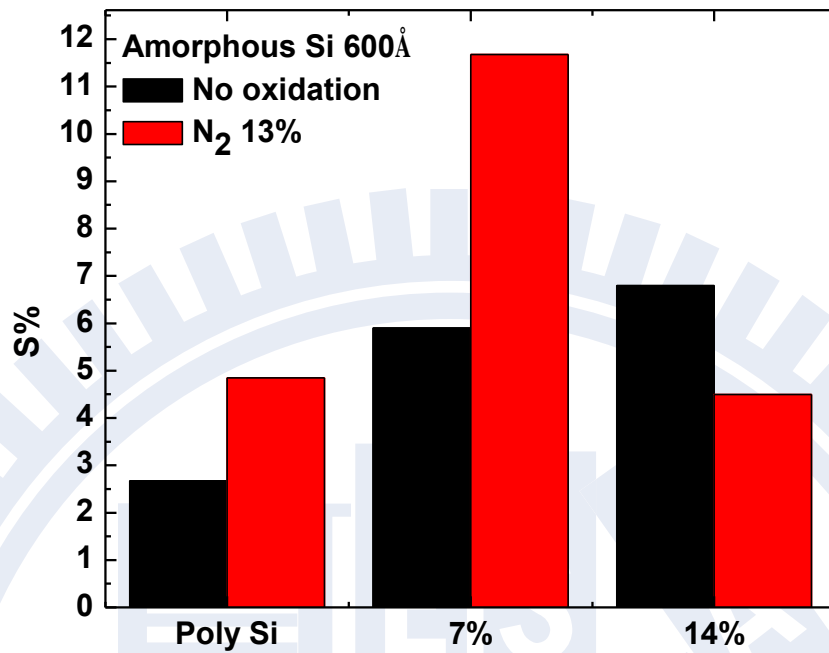


Fig.4- 19 The raise of sensitivity fixed on amorphous Si 600Å

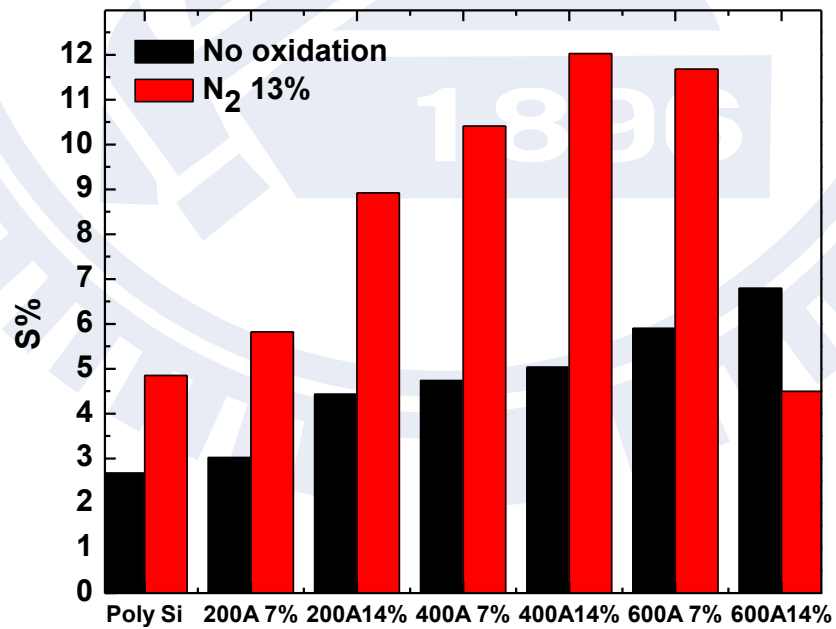


Fig.4- 20 The raise of sensitivity with all stacked structures

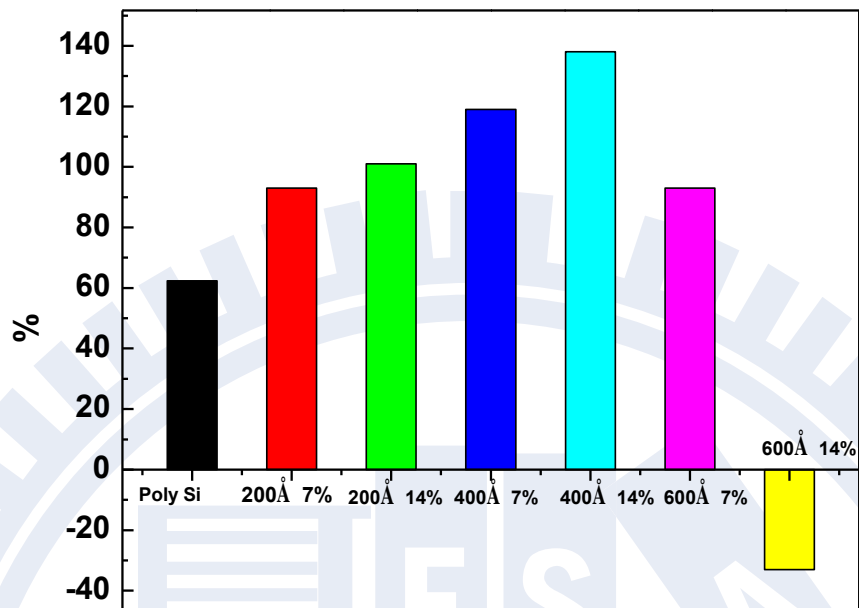


Fig.4- 21 The percentage change of all structures after APTMS modified

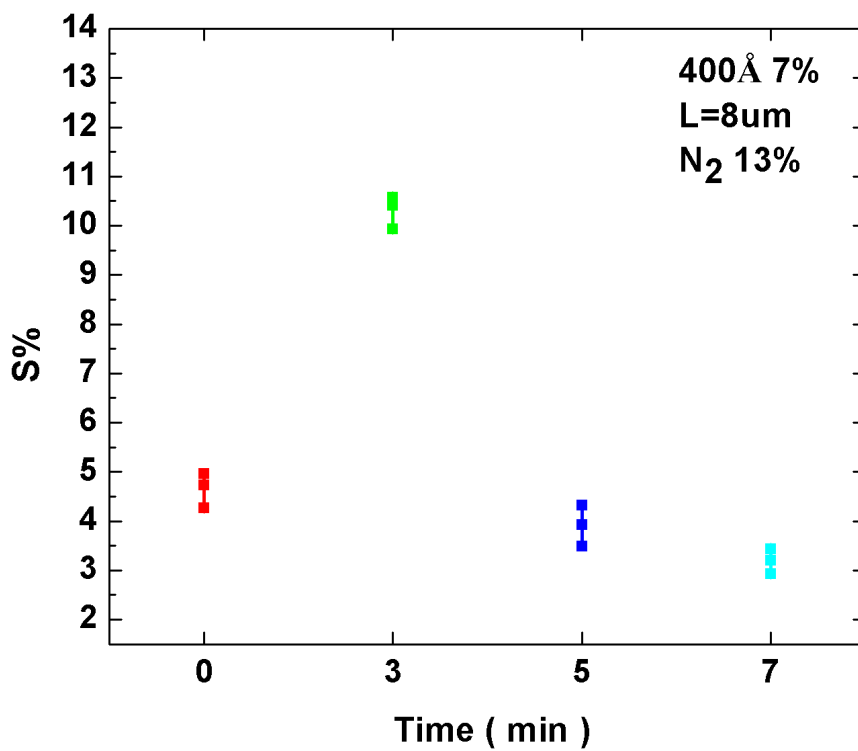


Fig.4- 22 The treatment of time on 400Å 7%

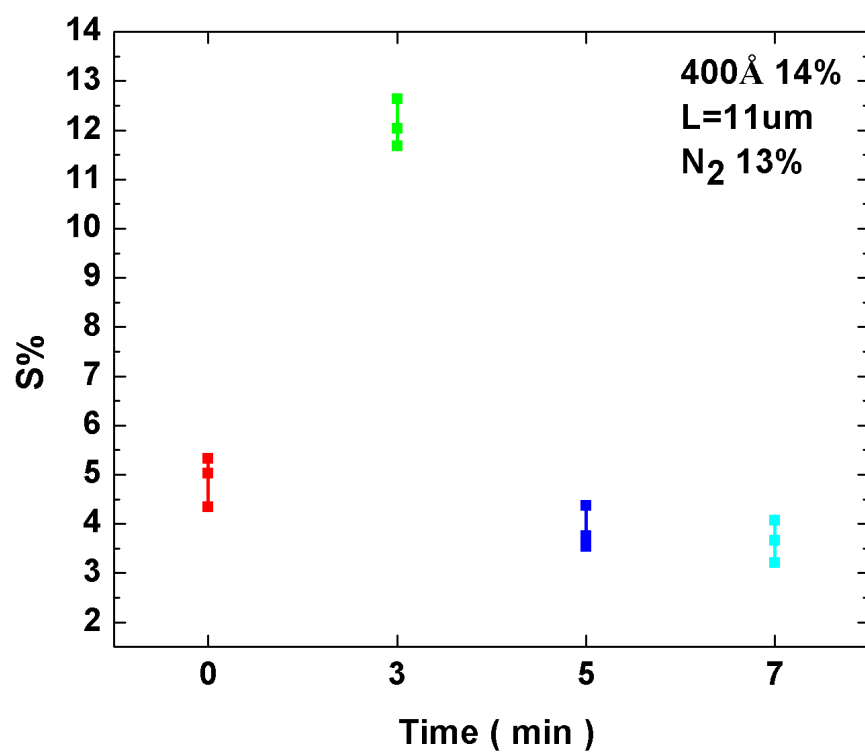


Fig.4- 23 The treatment of time on 400Å 14%

## Reference

- [1] Y. Cui, Q. Wei, H. Park and Charles M. Lieber , “Nanowire Nanosensors for Highly Sensitive and Selective Detection of Biological and Chemical Species,” *Science*, vol. 293, no. 5533, pp. 1289-1292, August 17, 2001.
- [2] G. Brambilla, F. Xu, and X. Feng, “Fabrication of optical fiber nanowires and their optical and mechanical characterization”, *Electronic Letters*, Vol 42, 8, 2006.
- [3] P. R. Nair, and M. A. Alam, “Performance limit of nanobiosensors,” *Applied Physics Letters*, vol. 88, no. 23, 2006.
- [4] Duan, C. Niu, V. Sahi, J. Chen, J. Parce, and S. Empedocles, “High-performance thin-film transistors using semiconductor nanowires and nanoribbons,” *Nature* 425, pp. 274-278, 2003.
- [5] A.M. Morales and C.M. Lieber, “A Laser Ablation Method for the Synthesis of Crystalline Semiconductor Nanowires,” *Science* 279, 208, 1998.
- [6] Zhaohui Zhong, Deli Wang, Yi Cui, Marc W. Bockrath, Charles M. Lieber, “Nanowire Crossbar Arrays as Address Decoders for Integrated Nanosystems,” *Science* Vol. 302. no. 5649, pp. 1377 – 1379, 2003.
- [7] G. Zheng, F. Patolsky, Y. Cui, W. U. Wang, C. M. Lieber, “Multiplexed electrical detection of cancer markers with nanowire sensor arrays,” *Nature Biotech.*, 2005

- [8] P. R. Nair, and M. A. Alam, "Performance limit of nanobiosensors," *Applied Physics Letters*, vol. 88, no. 23, 2006.
- [9] W. S. Shi, H. Y. Peng, and Y. F. Zheng, "Synthesis of Large Areas of Highly Oriented, Very Long Silicon Nanowires," *Advanced Materials*, vol. 12, no. 18, pp. 1343-1345, 2000.
- [10] Y. F. Zhang, Y. H. Tang, N. Wang et al., "One-dimensional growth mechanism of crystalline silicon nanowires," *Journal of Crystal Growth*, vol. 197, no. 1-2, pp. 136-140, 1999.
- [11] Jiangtao Hu, Teri Wang Odom, and Charles M. Lieber, "Chemistry and Physics in One Dimension: Synthesis and Properties of Nanowires and Nanotubes," *Acc. Chem. Res.*, 32 (5), pp. 435-445, 1999
- [12] Yiying Wu and Peidong Yang, "Direct Observation of Vapor-Liquid-Solid Nanowire Growth," *J. Am. Chem. Soc.*, 123 (13), pp. 3165-3166, 2001.
- [13] Z. Li, B. Rajendran and T. I. Kamins, "Silicon nanowires for sequence-specific DNA sensing: device fabrication and simulation," *Applied Physics a-Materials Science & Processing*, vol. 80, no. 6, pp. 1257-1263, Mar, 2005.
- [14] W. Xihua, C. Yu, and A. G. Katherine, "Silicon-based nanochannel glucose sensor," *Applied Physics Letters*, vol. 92, no. 1, pp. 013903, 2008.
- [15] Jing Wan, Shao-Ren Deng, Yifang Chen, Ejaz Huq, Ran Liu, Xin-Ping Qu, "Trilayer nanoimprint fabrication and simulation of the silicon nanowire sensor for gas detection," 2009 4th IEEE

International Conference on Nano/Micro Engineered and Molecular Systems, pp. 1013-1016, 2009.

- [16] H. C. Lin, M. H. Lee, C. J. Su, "A Simple and Low-Cost Method to Fabricate TFTs With Poly-Si Nanowire Channel," *Electron Device Letters, IEEE*, vol. 26, no. 9, pp. 643-645, 2005.
- [17] K. Dae-Hwan, S. Suk-Kang, K. Kyung-Rok, "Silicon single-electron transistors with sidewall depletion gates and their application to dynamic single-electron transistor logic," *Electron Devices, IEEE Transistors*, vol. 49, no. 4, pp. 627-635, 2002.
- [18] Z. Li, Y. Chen, X. Li, T. I. Kamins, K. Nauka, and R. S. Williams, "Sequence-Specific Label-Free DNA Sensors Based on Silicon Nanowires," *Nano Letters*, 4 (2), pp. 245–247, 2004.
- [19] Guozhen Shen, Po-Chiang Chen, Kounghmin Ryu and Chongwu Zhou, "Devices and chemical sensing applications of metal oxide nanowires," *J. mater. Chem.*, 19, pp.828-839, 2009.
- [20] Y. Cui, Q. Wei, H. Park, "Nanowire Nanosensors for Highly Sensitive and Selective Detection of Biological and Chemical Species," *Science*, vol. 293, no. 5533, pp. 1289-1292, August 17, 2001.
- [21] G. Zheng, F. Patolsky, Y. Cui, "Multiplexed electrical detection of cancer markers with nanowire sensor arrays," *Nat Biotech*, vol. 23, no. 10, pp. 1294-1301, 2005.
- [22] G. Zheng, F. Patolsky, Y. Cui, "Multiplexed electrical detection of cancer markers with nanowire sensor arrays," *Nat Biotech*, vol. 23, no. 10, pp. 1294-1301, 2005.

- [23] Z. Gao, A. Agarwal, A. D. Trigg, "Silicon Nanowire Arrays for Label-Free Detection of DNA," *Analytical Chemistry*, vol. 79, no. 9, pp. 3291-3297, 2007.
- [24] F. Patolsky, G. Zheng, O. Hayden, "Electrical detection of single viruses," *Proceedings of the National Academy of Sciences*, vol. 101, no. 39, pp. 14017-14022, 2004.
- [25] M. L. Y. Liu, "Growth of Aligned Square-Shaped SnO<sub>2</sub> Tube Arrays," *Advanced Functional Materials*, vol. 15, no. 1, pp. 57-62, 2005.
- [26] M. A.-H. Safaa, R. T. Al-Mofarji, and P. Klason, "Zinc oxide nanorods grown on two-dimensional macroporous periodic structures and plane Si as a pH sensor," *Journal of Applied Physics*, vol. 103, 2008.
- [27] J. Liu, X. Wang, Q. Peng, "Vanadium Pentoxide Nanobelts: Highly Selective and Stable Ethanol Sensor Materials," *Advanced Materials*, vol. 17, no. 6, pp. 764-767, 2005.
- [28] Y. Zhang, A. Kolmakov, Y. Lilach, "Electronic Control of Chemistry and Catalysis at the Surface of an Individual Tin Oxide Nanowire," *J. Phys. Chem. B*, vol. 109, no. 5, pp. 1923-1929, 2005.
- [29] M. A.-H. Safaa, R. T. Al-Mofarji, P. Klason, "Zinc oxide nanorods grown on two-dimensional macroporous periodic structures and plane Si as a pH sensor," *Journal of Applied Physics*, vol. 103, 2008.
- [30] A. Kolmakov, Y. Zhang, and G. Cheng, "Detection of CO and

- O<sub>2</sub> Using Tin Oxide Nanowire Sensors,” *Advanced Materials*, vol. 15, no 12, pp. 997-1000, 2003.
- [31] Y. Zhang, A. Kolmakov, and S. Chretien, “Control of Catalytic Reactions at the Surface of a Metal Oxide Nanowire by Manipulating Electron Density Inside It,” *Nano Letters*, vol. 4, no. 3, pp. 403-407, 2004.
- [32] B. J. Murray, E. C. Walter, and R. M. Penner, “Amine Vapor Sensing with Silver Mesowires,” *Nano Letters*, vol. 4, no. 4, pp. 665-670, 2004.
- [33] C. Z. Li, H. X. He, and A. Bogozzi, “Molecular detection based on conductance quantization of nanowires,” *Applied Physics Letters*, vol. 76, no. 10, pp. 1333-1335, 2000.
- [34] X. Wang, and C. S. Ozkan, “Multisegment nanowire sensors for the detection of DNA 77 molecules,” *Nano Letters*, vol. 8, no. 2, pp. 398-404, Feb, 2008.
- [35] B. W. Maynor, S. F. Filocamo, and M. W. Grinstaff, “Direct-Writing of Polymer Nanostructures: Poly(thiophene) Nanowires on Semiconducting and Insulating Surfaces,” *J. Am. Chem. Soc.*, vol. 124, no. 4, pp. 522-523, 2002.
- [36] H. X. He, C. Z. Li, and N. J. Tao, “Conductance of polymer nanowires fabricated by a combined electrodeposition and mechanical break junction method,” *Applied Physics Letters*, vol. 78, no. 6, pp. 811, 2001.
- [37] R. J. Christine Jerome, “Electrochemical Synthesis of Polypyrrole Nanowires,” *Angewandte Chemie International*

Edition, vol. 37, no. 18, pp. 2488-2490, 1998.

- [38] Z. Daihua, L. Chao, L. Xiaolei, "Doping dependent NH<sub>3</sub> sensing of indium oxide nanowires," *Applied Physics Letters*, vol. 83, no. 9, pp. 1845-1847, 2003.
- [39] D. Zhang, Z. Liu, C. Li, "Detection of NO<sub>2</sub> down to ppb Levels Using Individual and Multiple In<sub>2</sub>O<sub>3</sub> Nanowire Devices," *Nano Letters*, vol. 4, no. 10, pp. 1919-1924, 2004
- [40] A. S. Peter, D. N. Christopher, N. J. Thomas, "Electric-field assisted assembly and alignment of metallic nanowires," *Applied Physics Letters*, vol. 77, no. 9, pp. 1399-1401, 2000.
- [41] F. Favier, E. C. Walter, M. P. Zach, "Hydrogen Sensors and Switches from Electrodeposited Palladium Mesowire Arrays," *Science*, vol. 293, no. 5538, pp. 2227-2231, September 21, 2001.
- [42] Z. Li, B. Rajendran, T. I. Kamins, "Silicon nanowires for sequence-specific DNA sensing: device fabrication and simulation," *Applied Physics a-Materials Science & Processing*, vol. 80, no. 6, pp. 1257-1263, Mar, 2005.
- [43] I. Heller, A. M. Janssens, J. Mannik, "Identifying the Mechanism of Biosensing with Carbon Nanotube Transistors," *Nano Letters*, vol. 8, no. 2, pp. 591-595, 2008.
- [44] Y. Kun, W. Hui, Z. Kai, "Gold nanoparticle modified silicon nanowires as biosensors," *Nanotechnology*, no. 11, pp. S76, 2006.
- [45] H. K. Liou, P. Mei, U. Gennser, "Effects of Ge concentration on SiGe oxidation behavior," *Applied Physics Letters*, vol. 59, no.

10, pp. 1200-1202, 1991.

- [46] A. Tae-Hang, Y. In-Seok, and K. Tae-Kyun, "Effects of Ge Content on the Oxidation Behavior of Poly-SiGe Layers for Gate Electrode Application," *Journal of The Electrochemical Society*, vol. 148, no. 2, pp. G50-G54, 2001.
- [47] P. R. Nair, and M. A. Alam, "Design considerations of silicon nanowire biosensors," *IEEE Transactions Electron Devices*, vol. 54, no. 12, pp. 3400-3408, Dec, 2007.
- [48] F. K. LeGoues, R. Rosenberg, and T. Nguyen, "Oxidation studies of SiGe," *Journal of Applied Physics*, vol. 65, no. 4, pp. 1724-1728, 1989.
- [49] H. Tsutsu, W. J. Edwards, and D. G. Ast, "Oxidation of polycrystalline-SiGe alloys," *Applied Physics Letters*, vol. 64, no. 3, 17 January 1994.

## 簡 歷

姓 名：劉 重 顯

性 別：男

出生年月日：75 年 7 月 10 日

出 生 地：高 雄 市

住 址：高雄市林森一路 346 號

學 歷：

私立道明中學 (民國90年9月~民國93年6月)

國立彰化師範大學電機工程學系 (民國93年9月~民國97年6月)

國立交通大學電子研究所 (民國97年9月~民國99年9月)

碩士論文：

利用 Si/SiGe 堆疊式結構提升非均質矽鍺奈米線靈敏度之特性研究

The enhancement of the sensitivity for non-homogeneous SiGe nanowire  
by Si/SiGe stack structure